Integrated Master in Chemical Engineering

Modeling and Simulation of Water-Gas Shift Reactors: from Conventional Packed-Bed to Membrane Reactors

Master Thesis

by

Yaidelin Josefina Alves Manrique

Developed within the discipline of Dissertation

held in

Laboratory for Process, Environment and Energy Engineering (LEPAE)

Supervisor: **Prof. Luis Miguel Palma Madeira**

Universidade do Porto
Faculdade de Engenharia
FEUP

Department of Chemical Engineering

July 2010

Acknowledgments

First of all, I would like to express my special gratitude to my supervisor, Professor Luis M. Madeira, for giving me the greatest opportunity to participate in this field of research, for his support, confidence, and above all for his total availability, patience and instructions. I also want to thank Professor Adélio Mendes for his support during the laboratory experiments and to challenge me to achieve higher goals.

I would like to thank Eng. Diogo Mendes for his great contribution in this work, for his ideas, knowledge, support, patience, instructions and availability during the laboratory experiments, and motivation when things were not going well.

I want to thank to LEPAE for its technical support and staff, especially to Daniel, Paula and Vânia for giving me their support during my work in the laboratory.

Also, I would like to give a special thanks to my colleagues David, Ana, Isabel and Sílvio, for their constant motivation and support.

I am grateful to those who made all this possible, my family, for supporting me in every decision, and for their boundless confidence. I am here today only because of them. Thank you for everything.

Finally, I would like to have a "model" that could describe in the best way my gratefulness for everyone that one way or another had a contribution in this project. Unfortunately, today I do not have any "model" that could represent these feelings, then for now I can only say "*Thank you very much to all of you*".

Abstract

Nowadays, the green processes have an increasingly importance. In particular, emissions resulting from the use of hydrogen as fuel contain only water, one of the reasons why that component has a great potential to be the main energy carrier of the future. Therefore, it arises the interest to find an attractive way to produce and purify hydrogen, in an environmentally and economically sustainable way. Then, the main objective of this work was to address the water-gas shift (WGS) process, in particular to develop phenomenological models that can reproduce experimental results of CO conversion in a WGS reactor operating at low temperatures. The simulations were divided in two sections; in first place it was simulated the conversion obtained in a traditional packed-bed reactor, in which the maximum attainable reaction conversion is intrinsically limited by the equilibrium of the reversible reaction. Following, a membrane reactor was simulated (using a simple ideal model), aiming to shift the reaction by employing hydrogen-selective Pd-Ag membranes.

Firstly, different kinetics proposed in the literature (Langmuir-Hinshelwood, Redox and empirical – Power-law) were tested and compared against experimental data. It was found a better adherence by a composed kinetics in which the Langmuir-Hinshelwood rate equation is used for the temperature range 180 - 200 ºC, while for 230 – 300 ºC the Redox model applies.

Several packed-bed reactor models were then proposed and analyzed in detail, from a theoretical point of view. After comparing the simulations against experimental CO conversion data for different temperatures (in the range 150 – 300 ºC) and space time values, it was concluded that the heterogeneous model wherein it is considered axial dispersion and mass transfer resistances has a better fitting. This model revealed also good adherence for other experiments employing different feed compositions (CO and H_2O contents) and pressures.

Finally, it was seen that the membrane reactor has a better performance than a packed-bed reactor, allowing in certain conditions to overcome the thermodynamic equilibrium – the limit for traditional reactors.

Keywords: Modeling, Water-Gas Shift reaction, Kinetics, Packed-bed reactor, Pd-Ag membrane reactor.

Resumo

Actualmente, os processos verdes têm uma crescente importância. Em particular, as emissões resultantes do uso do hidrogénio como combustível só contém água, uma das razões pelas quais aquele composto é apontado como tendo grande potencial para ser uns dos principais transportadores de energia do futuro. Surge, portanto, o interesse de encontrar uma forma de produzir e purificar o hidrogénio, de forma ambiental e economicamente sustentável. Assim, o principal objectivo do presente trabalho foi a abordagem do processo *water-gas shift* (WGS), mais especificamente o desenvolvimento de modelos fenomenológicos que conseguissem reproduzir os resultados experimentais da conversão do CO para a operação do reactor WGS a baixas temperaturas. As simulações foram divididas em duas secções; em primeiro lugar foi simulada a conversão obtida no reactor tradicional de leito fixo, no qual a máxima conversão atingível está intrinsecamente limitada pelo equilíbrio da reacção. A seguir, foi simulado um reactor de membrana (usando um modelo simples e ideal), visando a sua utilização o deslocar a reacção no sentido dos produtos usando-se membranas de Pd-Ag selectivas ao hidrogénio.

Em primeiro lugar, foram testadas diferentes cinéticas propostas na literatura (Langmuir-Hinshelwood, Redox e empírica – Lei de Potência) e comparadas com dados obtidos experimentalmente. Verificou-se uma melhor adesão no uso do modelo cinético composto, no qual a equação de velocidade de Langmuir-Hinshelwood é usada para a gama de temperatura 180 - 200 ºC, enquanto que para o intervalo de 230 - 300 ºC aplica-se o modelo Redox.

Vários modelos para o reactor de leito fixo foram em seguida propostos e analisados em detalhe, do ponto de vista teórico. Depois de se compararem as simulações com os dados experimentais da conversão CO para diferentes temperaturas (na gama 150 - 300 ºC) e valores de tempo espacial, concluiu-se que o modelo heterogéneo no qual é considerada a dispersão axial e resistências à transferência de massa tem um melhor ajuste. Este modelo mostrou também uma boa aderência para diferentes composições de alimentação (variação no teor de CO o H_2O) e pressões.

Por último, verificou-se que o reactor de membrana tem um melhor desempenho do que o reactor de leito fixo, permitindo em determinadas condições superar o equilíbrio termodinâmico – o qual representa o limite para os reactores tradicionais.

Palavras-chave: Modelização, reacção de *Water-Gas Shift*, Cinética, Reactor de leito fixo, Membrana de Pd-Ag.

Table of Contents

1 Introduction 1

1.1 Background and Objectives 2

1.2 Outline 4

2 State of the Art 7

2.1 Water-Gas Shift Reaction 7

2.1.1 Industrial Process 7

2.1.2 Thermodynamic Considerations 8

2.1.3 Kinetics and Mechanism of the Reaction and Corresponding Models 10

2.2 Membrane Reactor 14

3 Phenomenological Models 17

3.1 Traditional Reactor 17

3.1.1 Pseudo-Homogeneous One-dimensional Models (Models 1 and 2) 17

3.1.2 Heterogeneous One-dimensional Models (Models 3 and 4) 21

3.1.3 Effect of the Feed Pressure 24

3.2 Membrane Reactor 25

4 Experimental Section 27

4.1 Experimental Setup 27

4.2 Catalyst Reduction 28

4.3 Experimental Test 28

5 Results and Discussion 31

5.1 Traditional Reactor 31

5.1.1 Evaluation of the Kinetics for the Low Temperature WGS Reaction 31

5.1.2 Evaluation of the WGS reactor performance by the different phenomenological models 35

5.1.3 Validation of the Phenomenological Models 40

5.2 Membrane Reactor 50

6 Conclusions and Future Work 53

7 References 55

List of Figures

Figure 1. Conventional two-stage process diagram of the WGS reaction unit (adapted from Mendes et al., 2010b). 7

Figure 2. Typical variations of CO-leves in HT and LT shift catalyst beds (adapted from Rhodes et al., 1995). 8

Figure 3. CO conversions in equilibrium for a typical reformate stream (inlet dry gas 7.21 % CO + 15.58 % CO_2 + 44.00 % H_2 + 33.21 % N_2) at various steam to dry gas (S/G) ratios. 10

Figure 4. Steps involved in reactions on a solid catalyst (adapted from Froment and Bischoff, 1990). 10

Figure 5. Schematic representation of the traditional reactor modeled. 17

Figure 6. Schematic representation of the reactor modeled in the pseudo-homogeneous models. 18

Figure 7. Schematic representations of the membrane reactor modeled in the heterogeneous models, considering separately the fluid and solid phases. 21

Figure 8. Schematic representation of the membrane reactor modeled. 25

Figure 9. Sketch of the experimental setup used (source Mendes et al., 2009). 27

Figure 10. Parity plots (theoretical vs. experimental CO conversion) using the phenomenological Model 1 with the kinetics models: a) LH1, b) Redox, c) Power-law rate equations, in the temperature range 180 to 300 ºC, and d) LH1 (180 - 200 ºC) and Redox (230 - 300 ºC). In all figures the dashed line represents an interval of ±10 % of error. 32

Figure 11. CO Conversion (experimental and theoretical) vs. space time (W_{cat}/F_{CO}^0) at different reaction temperatures using different kinetics model: a) LH1 (lower temperatures), b) Redox (higher temperatures). Points represent the experimental CO conversion, continuous line the CO conversion by Model 1, and dashed line equilibrium CO conversion. 34

Figure 12. Effect of the space time and temperature in the theoretical CO Conversion by Model 1 (see Table 5 for other operating parameters). 35

Figure 13. Different perspectives of the space time and temperature effect in the theoretical CO Conversion by Model 2 (see Table 5 for operating parameters). 36

Figure 14. Variation of the Peclet number with temperature and flow rate. Composition of gas mixture: 4.70 % CO, 34.78 % H_2O, 28.70 % H_2, 10.16 % CO_2, and 21.66 % N_2 (vol. %). 36

Figure 15. Variation of the mass transfer coefficient of CO in the mixture with temperature and flow rate. Composition of gas mixture: 4.70 % CO, 34.78 % H_2O, 28.70 % H_2, 10.16 % CO_2, and 21.66 % N_2 (vol. %). 37

Figure 16. Effect of the space time and temperature in the theoretical CO Conversion by Model 3 (see Table 5 for additional operating parameters). 38

Figure 17. Different perspectives of the space time and temperature effect in the theoretical CO Conversion by Model 4 (see Table 5 for additional operating parameters).....39

Figure 18. Effect of the space time and temperature in the theoretical CO Conversion by Models 1 and 3 (see Table 5 for additional operating parameters).....39

Figure 19. Different perspectives of the space time and temperature effect in the theoretical CO Conversion by Models 2 and 4 (see Table 5 for additional operating parameters). 40

Figure 20. Effect of the temperature on the CO conversion at different feed flow rate (a-c) and goodness of fit for the tested models (d). Feed composition: 4.70 % CO, 34.78 % H_2O, 28.70 % H_2, 10.16 % CO_2, 21.66 % N_2 (vol %), and Pressure 120 kPa. 42

Figure 21. Effect of the flow rate and temperature in the CO conversion. Points experimental CO conversion, continuous line CO conversion by Model 4, dashed line equilibrium CO conversion. 43

Figure 22. Effect of H_2O content in the CO conversion for different flow rate (a-c) and goodness of fit for the composition tested (d). Feed composition: ■16.90 % H_2O (mixture 4), ◆34.78 % H_2O (mixture 1) and ▲43.74 % H_2O (mixture 5) in all cases the rest of feed is: 4.70 % CO, 28.70 % H_2, 10.16 % CO_2, and the balance N_2 (vol. %). In all figures the point represent the experimental conversion, the continuous line represents the conversion for Model 4, and the dashed line the equilibrium. 44

Figure 23. Effect of the H_2O/CO ratio and temperature in the theoretical CO Conversion by Model 4, when changing the H_2O content in feed, keeping constant the rest of components (for a typical gas reforming, mixture 1 – see Table 4); Flow rate: 150 $mL_N \cdot min^{-1}$.....45

Figure 24. Effect of CO content in the CO conversion for different flow rate (a-c) and goodness of fit for the composition tested (d). Feed composition ■ 2.38 % CO (mixture 2), ◆ 4.70 % CO (mixture 1) and ▲ 9.42 % CO (mixture 3), in all cases the rest of feed is 34.78 % H_2O, 28.70 % H_2, 10.16 % CO_2, and the balance N_2 (vol. %). In all figures the point represent the experimental conversion, the continuous line represents the conversion for Model 4, and the dashed line the equilibrium. 46

Figure 25. Effect of the H_2O/CO ratio and temperature in the theoretical CO Conversion by Model 4, when change the CO content in feed, keeping constant the rest of component (for a typical gas reforming, mixture 1 – see Table 4) and the balance N_2. Flow rate: 150 $mL_N \cdot min^{-1}$ 47

Figure 26. Effect of the H_2O/CO ratio in the theoretical CO Conversion by Model 4. Flow rate: 150 $mL_N \cdot min^{-1}$. 48

Figure 27. Effect of the feed pressure in the CO conversion at different reaction temperatures and flow rates. In all figures the points represent the experimental conversion and the dashed line the equilibrium.....49

Figure 28. Parity plots (experimental vs. theoretical CO conversion) using the phenomenological Model 4. In both figures the dashed line represents an interval of ±10 % of error. 49

Figure 29. Effect of the reaction temperature in the CO conversion at different pressures and flow rates. In all figures the point represent the experimental conversion, the continuous line represents the conversion for Model 4 using the pressure scale-up factor, and the dashed lines the equilibrium.50

Figure 30. Comparison of the performance the TR and MR for the WGS reaction. Membrane thickness 60 μm.....51

Figure 31. Comparison of molar fraction to CO and H_2 inside the reaction chamber for the TR and MR. At 300 ºC and space time of 40 g·h·mol^{-1}. 52

Figure 32. Effect of the membrane thickness in the performance of a WGS MR.....52

List of Tables

Table 1. Parameters used for Langmuir-Hinshelwood and Redox rate equations (Mendes et al., 2010a). 13

Table 2. Different values reported in literature for the pre-exponential factor and activation energy (source: Tosti et al. (2006) and references therein). 16

Table 3. Different phenomenological models proposed. 24

Table 4. Different mixture compositions used in the reaction experiments (molar fraction). 29

Table 5. Operational parameters and reactor dimensions employed in the kinetic study. 31

Table 6. Operational parameters and reactor dimensions. 41

Notation and Glossary

A	cross section area of the tubular reactor	m^2
a_v	total external surface area of catalyst per unit volume	m^{-1}
$\Delta H_{298\mathrm{K}}$	reaction enthalpy at 298 K	$\mathrm{kJ \cdot mol}^{-1}$
C_i	concentration of species *i*	$\mathrm{mol \cdot m}^{-3}$
D	diffusion coefficient of the species in the membrane	$\mathrm{m}^2 \cdot \mathrm{s}^{-1}$
D_{ix}	dispersion coefficient in the axial direction	$\mathrm{m}^2 \cdot \mathrm{s}^{-1}$
E_a	activation energy	$\mathrm{kJ \cdot mol}^{-1}$
F^0	total feed flow rate	$\mathrm{mol \cdot s}^{-1}$
F_i^M	flux of permeated species	$\mathrm{mol \cdot m}^{-2} \cdot \mathrm{s}^{-1}$
F_{press}	Pressure scale-up factor	–
FO	comparison criteria for experimental and theoretical conversion	–
$J_{\mathrm{H_2}}$	hydrogen flux through membrane	$\mathrm{mol \cdot m}^{-2} \cdot \mathrm{s}^{-1}$
K_i	equilibrium adsorption constant of species *i*	Pa^{-1}
K_p	equilibrium constant for the WGS reaction	–
k	rate constant for the forward reaction	$\mathrm{mol \cdot g_{cat}^{-1} \cdot s^{-1} \cdot Pa^{-2}}$
$k_{f_{i,m}}$	mass transfer coefficient for the same species in the mixture	$\mathrm{m \cdot s}^1$
L	length of reactor	m
P	total pressure	Pa
$\mathrm{p_i}$	partial pressure of species *i*	Pa
$p_{\mathrm{H_2}}^{\mathrm{retentate}}$	hydrogen partial pressure on the retentate side	Pa
$p_{\mathrm{H_2}}^{\mathrm{permeate}}$	hydrogen partial pressure on the permeate side	Pa
Pe	permeability coefficient	$\mathrm{mol \cdot m}^{-1} \cdot \mathrm{s}^{-1} \cdot \mathrm{Pa}^{-0.5}$
Pe_m	Peclet number $\left(Pe_m = \frac{u_0 L}{\varepsilon D_{ax}}\right)$	–
$P_e{}^0$	pre-exponential factor	$\mathrm{mol \cdot m}^{-1} \cdot \mathrm{s}^{-1} \cdot \mathrm{Pa}^{-0.5}$
R	universal constant of ideal gas $\left(R = 8.314\ \mathrm{J \cdot mol^{-1} \cdot K^{-1}}\right)$	$\mathrm{J \cdot mol^{-1} \cdot K^{-1}}$
$-\mathrm{r_{CO}}$	rate of CO consumption reaction	$\mathrm{mol \cdot g_{cat} \cdot s}$
r^M	radius of the tubular reactor (membrane)	m
T	absolute temperature	K
u_0	superficial velocity	$\mathrm{m \cdot s}^{-1}$
u_i	interstitial velocity	$\mathrm{m \cdot s}^{-1}$
W_{cat}	mass of catalyst in the bed	$\mathrm{g_{cat}}$
W_{cat}/F^0	space time	$\mathrm{g \cdot s \cdot mol}^{-1}$
X_{CO}	carbon monoxide conversion	–
y_i	molar fraction of species i	–
$\bar{z}$	dimensionless position along the reactor axial direction	–
z	axial position along the reactor	m

Greek letters

β	factor of the reversible reaction $\left(\mathrm{p_{H_2}p_{CO_2}/p_{CO}p_{H_2O}}K_p\right)$	$-$
δ	membrane thickness	m
ε	bed void fraction	$-$
φ_i	molar flow of species *i* per unit area (flux)	$\mathrm{mol \cdot m^{-2} \cdot s^{-1}}$
ρ_p	particle density	$\mathrm{kg \cdot m^{-3}}$
ρ_b	bed density	$\mathrm{kg \cdot m^{-3}}$
ϑ_i	stoichiometric coefficient for species *i*	$-$

Subscripts or Superscripts

^{0}	refers to reactor feed conditions
b	Bulk
cal	calculated
eq	equilibrium
exp	experimental
i	CO, CO_2, H_2O and H_2
^{P}	Permeate side
^{R}	Retentate side
S	catalyst surface

List of Acronyms

CEM	*Controller Evaporator Mixer*
DAE	*Differential and Algebraic Equation*
FO	*Objective Function*
GC	*Gas Chromatography*
HTS	*High Temperature Shift*
LH	*Langmuir-Hinshelwood*
LTS	*Low Temperature Shift*
MFC	*Mass Flow Controller*
MFM	*Mass Flow Meter*
MR	*Membrane Reactor*
ODE	*Odinary Differential Equation*
R	*Redox Mechanism*
TCD	*Thermal Conductivity Detector*
TR	*Traditional Reactor*
WGS	*Water-Gas Shift*

1 Introduction

Hydrogen is one of the most important industrial commodities (Baade et al., 2001). It has a great potential to be the main energy carrier of the future, because this simplest element has the potential to supply all energy services practically without impact on the environment, both locally and globally (Padró and Keller, 2005). The emissions resulting from the use of hydrogen as fuel contain only water; therefore, the hydrogen combustion is not accompanied by harmful exhausts as methane or carbonic acid (Lukyanov et al., 2009). For this reason, in recent years, a lot of companies, academic institutions and government laboratories have attracted and ever-increasing attention to find an attractive way to produce and purify hydrogen, based mainly in the idea of sustainable development, environmentally and economically (Mendes et al., 2010b).

In nature, hydrogen is abundant, but it does not exist as a pure compound, only being possible to found it in a bound state. So, it can be produced from fossil energy sources (carbon, natural gas) or renewable energy sources (biomass or electrolysis of water). The energy per mass unit of hydrogen is higher than those of known organic fuels, this being 120.7 $MJ \cdot kg^{-1}$ for Hydrogen, 48 $MJ \cdot kg^{-1}$ for Methane, 42-44 $MJ \cdot kg^{-1}$ for Gasoline (C_6-C_{12}) (Padró and Keller, 2005). At atmospheric pressure and room temperature the specific density of H_2 is 0.089 kg m^{-3} (Lukyanov et al., 2009).

The main resource of hydrogen is gas natural (≥ 90 %) (Lukyanov et al., 2009). In the conversion of this hydrocarbon source into hydrogen there are three important processes: steam reforming, steam-oxygen conversion and partial oxidation. The reaction stoichiometry of the steam reforming is shown in equation (1) while equation (2) represents the partial oxidation (Ghenciu, 2002).

$$C_nH_m + n\,H_2O \leftrightharpoons n\,CO + \left(n + \frac{m}{2}\right) H_2 \qquad \Delta H_{298K} > 0 \qquad (1)$$

$$C_nH_m + n\,O_2 \leftrightharpoons n\,CO + \left(n + \frac{m}{2}\right) H_2 \qquad \Delta H_{298K} < 0 \qquad (2)$$

However, the streams of hydrogen produced from the above reactions contain significant amounts of CO, which it is adverse for the fuel cell catalyst because it poisons it; the CO-content must not be higher than 10 ppm (Boutikos and Nikolakis, 2010). One solution to reduce the CO concentration is the water-gas shift (WGS) reaction (3).

$$CO + H_2O \leftrightharpoons CO_2 + H_2 \qquad \Delta H_{298K} = -41.4\ kJ \cdot mol^{-1} \tag{3}$$

This reaction provides important advantages, because reduces the CO content at the same time that produces hydrogen. The WGS is an equilibrium-limited reaction, characterized by no variation in the number of moles; therefore, in the equilibrium, the effect of pressure does not affect the CO conversion.

One way to improve the performance of WGS reactors is provided by membranes, because with their use it becomes possible to remove one or two products from the reaction medium, in order to displace continually the equilibrium towards the formation of products (i.e. CO_2 and H_2). IUPAC defines membrane reactor as "*a device for simultaneously carrying out a reaction and membrane-based separation in the same physical enclosure"*; in other words, is one unit that offers the possibility to combine the reaction and separation process. This is of particular interest in the perspective of the process intensification strategy.

Therefore, membranes are great candidates for hydrogen purification. Besides, the usage of membrane reactors seems to be a promising technology, in particular Pd-membranes, because they allow the permeation of H_2 only. Thus it withdrawal from the reaction medium is promoted in order to reach higher yields. However, a great difficulty exists for the researchers in evaluating which process (catalysis or membranes) has a more relevance on membrane reactor development (Mendes et al., 2010b).

1.1 Background and Objectives

At the present, many experimental studies exist that attempted to seek the best performance of different catalysts in order to obtain a better conversion of CO in the WGS reaction for reforming streams. In particular Mendes et al. (2009) compared the performance of four different catalysts: Au/CeO_2, Au/TiO_2, CuO/Al_2O_3 and $CuO/ZnO/Al_2O_3$, in the temperature range 150 – 300 ºC. The authors studied the effect of the reaction products in the feed stream, and analyzed also the effects of the H_2O/CO concentration in the feed stream - to compare with the typical reformate composition (4.70 % CO + 34.78 % H_2O + 28.70 % H_2 +10.16 % CO_2 + 21.66 % N_2). They found that the increased concentration of water vapor has a positive effect on the CO conversion for the temperature range analyzed, and concluded that the selection of the best catalytic system is clearly dependent upon the range of temperature of interest. In this concern, the commercial $CuO/ZnO/Al_2O_3$ catalyst showed the best relation of activity/stability.

Then, based on this study, the same team of research decided to perform a kinetic study of the low-temperature WGS reaction, with the commercial catalyst $CuO/ZnO/Al_2O_3$ (at atmospheric pressure) (Mendes et al., 2010a). They found that Langmuir-Hinselwood and Redox models have a good fit to the experimental results, and the corresponding kinetic parameters have been determined by non-linear regression.

In the present work a composed kinetics will be proposed, validated against experimental data obtained by Mendes et al. (2010a), and compared with others present in the literature (Choi and Stenger, 2003). Then, a fixed bed reactor (in isothermal conditions) will be modeled using different approaches: i) one-dimensional pseudo-homogeneous models (*Ideal Model* – Model 1, *Ideal Model* + *Axial Dispersion* – Model 2) and ii) one-dimensional heterogeneous model (*Ideal Model* – Model 3, *Ideal Model with External Resistance* - Model 4). In this context, different experimental studies for the WGS with the $CuO/ZnO/Al_2O_3$ commercial catalyst will be done (with a particle diameter ~300 μm), employing conditions that guarantee applicability of the different models.

The results obtained for the different models tested will then be compared with experimental data and, after validation of the model(s), the effect of different parameters in the performance of the WGS reactor will be analyzed, namely the space time (W_{cat}/F_{CO}^{o}), temperature and Peclet Number (Pe_m).

After validation in the packed bed reactor, a model that describes the performance of a Pd-Ag membrane reactor for the water-gas shift reaction will be developed, and subsequently its performance will be compared with that of a conventional reactor. A parametric study will be performed, for the purpose of evaluating the influence of temperature, feed flow-rate and reaction pressure, on the performance of the membrane reactor. In this order of ideas, some variation of the physical characteristics of the membrane (e.g. thickness) will also be made, to verify its effect in the performance of the membrane/membrane reactor.

The main goal of this project is therefore to further understand the behavior and performance of integrated units related with both catalysis and membrane processes, experimentally and theoretically. In this way, after getting a phenomenological model that describes the experimental results for the WGS reaction at low temperature in a packed bed reactor, the performance of this unit when a membrane is included in the same system to displace the equilibrium-limited reaction towards the formation of the products will be analyzed.

1.2 Outline

The present work was divided in 6 chapters, each of them representing an important step towards the accomplishment of the proposed objectives. Firstly, the introduction contains a brief description of hydrogen importance as energy carrier, and in this context the water-gas shift (WGS) reaction is introduced as an important step in the H_2 production via steam reforming. After, the objectives proposed for this work have been addressed.

Following, in section 2 the state of art in this thematic was briefly described, focused in the WGS reaction and in its limitations by the thermodynamic equilibrium. In this concern the parameters that affect the equilibrium were analyzed. After, the some important kinetic and mechanistic studies related with the low-temperature (LT) WGS reaction were summarized, and finally, still in this section, is briefly described the membrane reactor (MR) technology, highlighting the parameters that have influence in the H_2 permeation through the Pd-Ag membranes.

Section 3 can be considered the heart of this study, because one of the main objectives was to determine a model with good adherence to experimental data obtained in a conventional packed-bed reactor, in a large range of operating conditions. So, in this section, different one-dimensional phenomenological models (pseudo-homogeneous and heterogeneous) have been described. In each model it was considered that the flux has a contribution by only convection or by a combination of diffusion and convection (axially-dispersed tubular reactor). For the heterogeneous models a mass transfer coefficient was included, to take into account the associated resistance in the film. The simple model used for the membrane reactor modelling was also described.

In section 4 was described the experimental setup used and the different operating conditions employed for experimental data collection. Besides, the protocol used for the catalyst reduction before use was also described.

Chapter 5 presents both the experimental and theoretical results obtained. Firstly, the composed kinetics for the LT WGS reaction was validated. Then, and for a better understanding of the parameters that have influence in the different models proposed in chapter 3, the results obtained by simulation for each model were compared. After that, and by comparison with some experimental data, it was determined which model has a better fitting; this model and subsequently compared with experimental data in other conditions (varying the feed composition, pressure, etc.). At the end of this chapter, some simulations with the MR are presented, and comparison is done with a conventional reactor, using the simplest model.

Finally, in chapter 6 were presented the main conclusions of this study and proposed some suggestions for future work.

2 State of the Art

2.1 Water-Gas Shift Reaction

At the end of the 19th century was for the first time reported in the literature the WGS-reaction (Mond and Langer, 1888). Since the beginning of 20th century, this reaction (3) has represented an important step in the industrial production of hydrogen for refinery hydro-processes, bulk storage and redistribution. It plays also a major role in the production of organic bulk chemicals such as methanol, ammonia, and alternative hydrocarbon fuels through Fischer–Tropsch synthesis (Ladebeck and Wang, 2003). Nowadays, the hydrogen production from synthesis gas has bring a huge interest, especially in terms of fuel cell applications, as a consequence of the growing concerns over environmental issues (Mendes et al., 2010b).

2.1.1 Industrial Process

Typically, the WGS reaction in industry can be conducted at two different temperature levels, where the effluent from the reformer system is transformed in two series adiabatic converters, such as in Figure 1. For each stage a specific catalyst is used, the selection depending of the reaction temperature. The Fe and Cu-based catalysts are the main classes of materials used in this reaction.

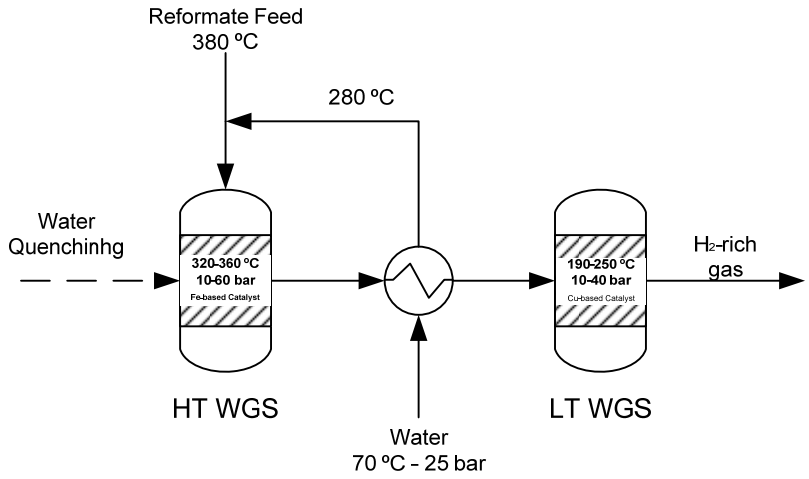

Figure 1. Conventional two-stage process diagram of the WGS reaction unit (adapted from Mendes et al., 2010b).

In the first stage, at "high temperature" (HT), fast CO consumption is favored. Thus, the Fe_2O_3/Cr_2O_3 catalyst is industrially used because it works well at operating temperatures around 320 – 450 ºC. Under these conditions it has an improved catalytic performance and selectivity. The product of this stage is carried to an inter-stage cooling system and then to the "lower temperature" (LT) shift unit, where is favored the approach to equilibrium conversions; generally, the Cu-based catalysts are used here. With this configuration, the enhancement obtained in the process allows reaching higher CO conversions and yields in the production of hydrogen. Thus, the major portion of the CO content is converted in the high temperature shift reactor, and in the low temperature unit is removed the remaining one. This approach is illustrated in Figure 2. In the LT stage the most used catalyst is a commercial copper/zinc oxide/alumina material ($CuO/ZnO/Al_2O_3$) (Rhodes et al., 1995). One problem with this type of catalyst is that the Cu crystallites are very susceptible to thermal sintering via surface migration, reducing the fully active catalyst life. Accordingly the thermal stability of the LT-WGS catalysts is inferior to that of the HT-WGS ones (Mendes et al., 2010b).

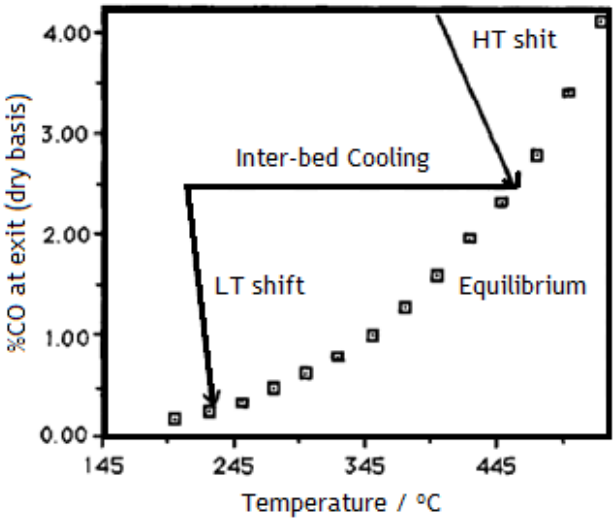

Figure 2. Typical variations of CO-leves in HT and LT shift catalyst beds (adapted from Rhodes et al., 1995).

2.1.2 Thermodynamic Considerations

Such as presented previously in equation (3), the WGS is a reversible exothermic reaction; then, higher CO conversions are favored at lower temperatures. This results from the decrease of the equilibrium constant with such a variable. Actually, for a temperature of 200 ºC the equilibrium constant is 43 times higher than at 500 ºC. The equilibrium constant (K_p) can be calculated by equation (4) (Mond and Langer, 1888), which is valid for a temperature range between 38.8 - 300 ºC.

$$K_p = \exp\left(\frac{4577.8}{T} - 4.33\right) \quad (4)$$

The effect of the total pressure in a WGS reactor performance is only noticed up to the equilibrium, by increasing the reaction rate. So, this variable has a positive effect in the CO conversion. However, in accordance with Le Chatelier's principle, when pressure is applied to a system at equilibrium it will adjust to minimize this increase (Rhodes et al., 1995). Therefore, in the equilibrium, the pressure has no effect in the WGS reaction, because the number of moles of reactants and products in the gas-phase at any axial position in a fixed-bed reactor (or instant in a batch operation) is not determined by the relative position of the forward and reverse reactions. In other words, the number of moles is constant while the reaction occurs.

In the equilibrium, the CO-conversion is only a function of temperature and feed composition. By solving equation (5) is possible to obtain the CO-conversion in the equilibrium $\left(X_{CO,eq}\right)$, only knowing the reaction temperature and the mole fraction for all species at reactor inlet (assuming ideal gas behavior and that CO is the limiting reagent; the same equation also applies for a batch reactor, but now the conditions refer to the initial instant).

$$K_p = \frac{\left(\frac{y^o_{CO_2}}{y^o_{CO}} + X_{CO,eq}\right)\left(\frac{y^o_{H_2}}{y^o_{CO}} + X_{CO,eq}\right)}{\left(\frac{y^o_{H_2O}}{y^o_{CO}} - X_{CO,eq}\right)\left(1 - X_{CO,eq}\right)} \quad (5)$$

As shown in equation (5), the feed/initial molar fraction of the different species *i* (y_i^o) have influence in the equilibrium conversion. In a particular case, the effect of the water content for a typical reformate stream (inlet dry-gas 7.21 % CO + 15.58 % CO_2 + 44.00 % H_2 + 33.21 % N_2) is represented in Figure 3. It is possible to observe that an increase in the temperature (over 200 ºC) has an adverse effect in the conversion, being the conversion higher when the water content increases (higher steam to dry gas, S/G, ratios).

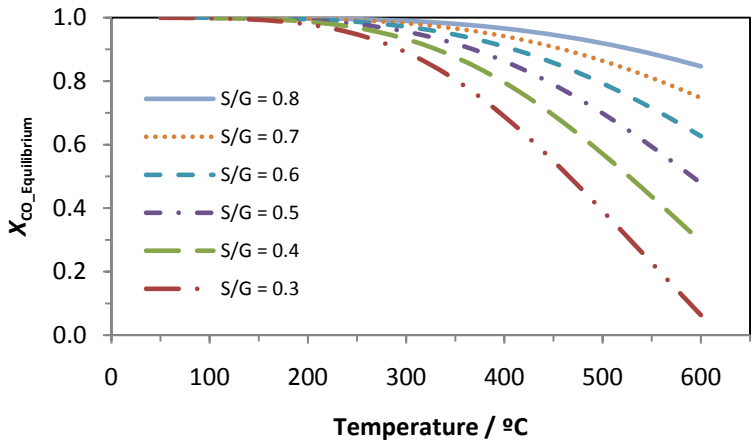

Figure 3. CO conversions in equilibrium for a typical reformate stream (inlet dry gas 7.21 % CO + 15.58 % CO_2 + 44.00 % H_2 + 33.21 % N_2) at various steam to dry gas (S/G) ratios.

Therefore, for reaching a higher CO-conversion is better to have the greatest steam/dry-gas relationship and low temperatures; however, the kinetics is almost instantaneous at very high temperatures and as result of the WGS reaction being exothermic, the process has an inherent temperature increase during the reaction. Besides, higher S/G ratios imply higher costs in the final separation and previous water vaporization. All these issues should therefore be taken into consideration and balanced in industrial practice.

2.1.3 Kinetics and Mechanism of the Reaction and Corresponding Models

In all heterogeneous catalytic reactions the observed rate of reaction may include effects of the rates of transport processes in addition to intrinsic reaction rate. In fact, the mechanism of this type of reactions involves seven consecutive steps (Froment and Bischoff, 1990), and for a simple irreversible reaction of the type $A \xrightarrow{cat} R$, this mechanism is presented in Figure 4.

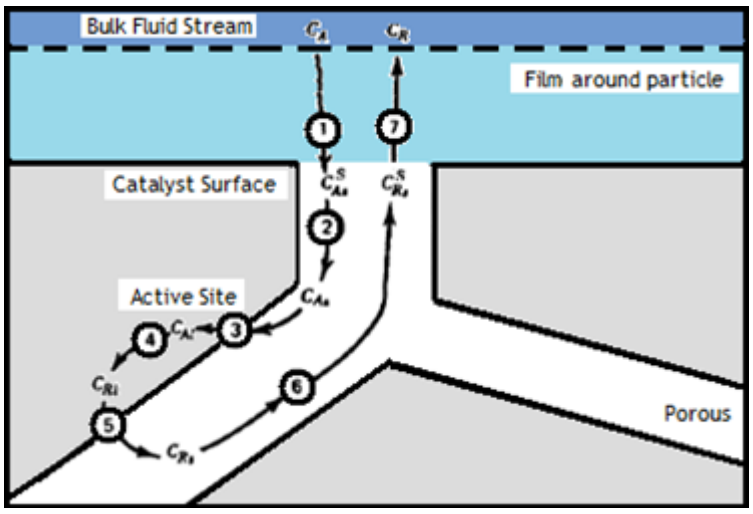

Figure 4. Steps involved in reactions on a solid catalyst (adapted from Froment and Bischoff, 1990).

In first place, it will be considered the gradient of concentration and transport of reagents. Since they are consumed by reaction inside the particle, there is a spontaneous tendency for reagents to move from the bulk gas to the interior of the particle (external and internal diffusion), firstly from the main fluid stream to the catalyst pellet surface (step 1), and then by some mode of diffusion through the pore structure of the particle (step 2). These two steps do not involve any chemical change, only a physical process where the reactants are brought through the main fluid stream to the active site in the catalyst. Then, the reactants are adsorbed on the catalyst site (step 3), and subsequently occurs the chemical reaction in the surface between adsorbed atoms or molecules (step 4). The last step in the catalyst site is the desorption of products adsorbed (step 5), and finally the products move through the interior catalyst pores back to the particle surface (step 6) and from here until the main fluid stream (bulk – step 7). So, the observed reaction rate will be often different of the real/intrinsic rate of reaction, because one or more of these steps may have an important influence. Therefore, the heterogeneous reaction can depend on the adsorption of reactant(s) onto the surfaces, or on the desorption of product(s) back into the fluid stream; it can be affected by pore diffusion resistance, or film diffusion resistance. When the reaction rate is governed by a truly chemical step, the rate is unaffected by a better stirring (in batch reactor) and is accurately proportional to catalyst weight or to the concentration of the active component (Bond, 1974). It is also independent of the catalyst particle size.

In the framework of mechanisms illustrated through Figure 4, it is assumed that all processes are in equilibrium, except one that is rate-determining. The rate expressions derived from various postulated mechanisms are in this case of the following form (Levenspiel, 1999):

$$\text{rate of reaction} = \frac{(\text{kinetic term})(\text{driving-force or displacement from equilibrium term})}{(\text{resistance term})^n} \qquad (6)$$

where *n* is the number of active sites involved in the rate-determining step. The WGS is a catalytic reaction that involves only four species, but in the literature there is yet not full agreement concerning the reaction mechanism (Mendes et al., 2010b). Nevertheless, two types are principally distinguished: Langmuir-Hinshelwood and Regenerative (Redox) mechanisms. According with Rhodes et al. (1995), for the low temperature shift reaction over copper/zinc oxide/alumina catalysts both mechanisms are possible, i.e., either could proceed on the catalyst surface, while for the high temperature shift reaction catalyzed over iron oxide/chromium oxide, the experimental evidence supports a regenerative mechanism.

The Langmuir-Hinshelwood mechanism most often proposed for the WGS reaction (also known as associative mechanisms LH1 - equations (7) to (11)) considers that reactants adsorbed on the catalyst surface form an intermediate which instantaneously reacts to form the products in the surface, and these products will finally be desorbed. In this mechanism, a surface reaction of molecularly adsorbed reactants (equation (9)) is the rate-determining step (Ayastuy et al., 2004).

$$\mathrm{CO_{(g)}} + \mathrm{Z} \leftrightharpoons \mathrm{CO_{(ads)}} - \mathrm{Z} \tag{7}$$

$$\mathrm{H_2O_{(g)}} + \mathrm{Z} \leftrightharpoons \mathrm{H_2O_{(ads)}} - \mathrm{Z} \tag{8}$$

$$\mathrm{CO_{(ads)}} - \mathrm{Z} + \mathrm{H_2O_{(ads)}} - \mathrm{Z} \leftrightharpoons \mathrm{CO_{2(ads)}} - \mathrm{Z} + \mathrm{H_{2(ads)}} - \mathrm{Z} \tag{9}$$

$$\mathrm{CO_{2(ads)}} - \mathrm{Z} \leftrightharpoons \mathrm{CO_{2(g)}} + \mathrm{Z} \tag{10}$$

$$\mathrm{H_{2(ads)}} - \mathrm{Z} \leftrightharpoons \mathrm{H_{2(g)}} + \mathrm{Z} \tag{11}$$

The equation rate for this LH1 mechanism is given by the following equation:

$$-r_{\mathrm{CO}} = \frac{k\left(p_{\mathrm{CO}}p_{\mathrm{H_2O}} - \frac{p_{\mathrm{CO_2}}p_{\mathrm{H_2}}}{K_p}\right)}{\left(1 + K_{\mathrm{CO}}p_{\mathrm{CO}} + K_{\mathrm{H_2O}}p_{\mathrm{H_2O}} + K_{\mathrm{H_2}}p_{\mathrm{H_2}} + K_{\mathrm{CO_2}}p_{\mathrm{CO_2}}\right)^2} \tag{12}$$

where, k is the rate constant for the forward reaction, K_p is the equilibrium constant (calculated by equation (4)), K_i is the equilibrium adsorption constant for species *i* and p_i is the corresponding partial pressure.

The Redox mechanism is valid if the cyclic reduction-oxidation reactions on the catalyst surface are applicable (Rhodes et al., 1995). Water adsorbs and dissociates on reduced sites of the catalyst surface to produce hydrogen while oxidizing an active site s, and in the following step CO is oxidized to CO_2 on this oxidized sites (Choi and Stenger, 2003). This mechanism is represented by equations (13) to (14).

$$\mathrm{H_2O} + \mathrm{s} \leftrightharpoons \mathrm{H_2} + \mathrm{O \cdot s} \tag{13}$$

$$\mathrm{CO} + \mathrm{O \cdot s} \leftrightharpoons \mathrm{CO_2} + \mathrm{s} \tag{14}$$

If rate control occurs by the reduction of oxidized copper (equation (14)), then the rate equation derived for this model is (Ayastuy et al., 2004):

$$-r_{CO} = \frac{k\left(p_{H_2O} - \frac{p_{CO_2} p_{H_2}}{p_{CO}\, K_p}\right)}{1 + K_{CO_2} p_{CO_2} / p_{CO}} \tag{15}$$

The parameters for each equation can be obtained by fitting experimental CO rate data (e.g., obtained at different contact times). In such experiments it must be guaranteed the absence of any mass and heat resistances, both internal and external, so that the rate observed will be the intrinsic reaction rate. As the main purpose of this research work is not to determine the mechanism and kinetics of the LT WGS reaction, the Langmuir-Hinshelwood (LH1) and Redox kinetic parameters proposed by Mendes et al. (2010a) will be used – Table 1.

Table 1. Parameters used for Langmuir-Hinshelwood and Redox rate equations (Mendes et al., 2010a).

Langmuir-Hinshelwood (LH1)	**Redox (R)**
$-r_{CO} = \frac{k\left(p_{CO} p_{H_2O} - \frac{p_{CO_2} p_{H_2}}{K_p}\right)}{\left(1 + K_{CO} p_{CO} + K_{H_2O} p_{H_2O} + K_{H_2} p_{H_2} + K_{CO_2} p_{CO_2}\right)^2}$	$-r_{CO} = \frac{k\left(p_{H_2O} - \frac{p_{CO_2} p_{H_2}}{p_{CO}\, K_p}\right)}{1 + K_{CO_2} p_{CO_2} / p_{CO}}$
$453\ \mathrm{K} < T < 488\ \mathrm{K}$	$503\ \mathrm{K} < T < 573\ \mathrm{K}$
$k = 1.188\ exp\left(-\frac{36658}{R\,T}\right)$ [mol·g$_{cat}^{-1}$·h^{-1}·Pa^{-2}]	$k = 1.841x10^{-3}\ exp\left(-\frac{6710}{R\,T}\right)$ [mol·g$_{cat}^{-1}$·h^{-1}·Pa^{-1}]
$K_{CO} = 2.283x10^{-24}\ exp\left(-\frac{45996}{R\,T}\right)$ [Pa^{-1}]	$K_{CO_2} = 6.343x10^{-1}\ exp\left(-\frac{19459}{R\,T}\right)$
$K_{H_2O} = 1.957x10^{-28}\ exp\left(-\frac{79963}{R\,T}\right)$ [Pa^{-1}]	
$K_{CO_2} = 5.419x10^{-4}\ exp\left(-\frac{16474}{R\,T}\right)$ [Pa^{-1}]	
$K_{H_2} = 2.349x10^{-4}\ exp\left(-\frac{13279}{R\,T}\right)$ [Pa^{-1}]	where $-r_{CO}$ is given in $\mathrm{mol \cdot g^{-1} \cdot h^1}$

Nevertheless, in this study it will be also considered the use of an empirical Power-Law rate equation (equation (16)), because the design and optimization of an industrial reactor requires high computational efforts that can be facilitated by the used of this type of simpler rate equations (Ayastuy et al., 2004):

$$-r_{CO} = k p_{CO}^{a} p_{H_2O}^{b} (1 - \beta) \tag{16}$$

The parameters *a*, *b* and the kinetic rate constant for this power-law kinetics are the following (Choi and Stenger, 2003), for temperature range 473 to 573 K:

$$a = b = 1$$

$$k = 2.236x10^{-5} exp\left(-\frac{47400}{R\,T}\right) \left[\text{mol}\cdot\text{g}_{\text{cat}}^{-1}\cdot\text{hr}^{-1}\cdot\text{Pa}^{-2}\right]$$

These kinetics were all obtained at nearly atmospheric pressure. However, if the process is applied at high pressure, as required in industrial practice, the reaction rates can be vastly over-predicted by as much as three orders of magnitude (Adams and Barton, 2009). However, empirical pressure scale-up correlations can be used to apply a kinetic equation derived at low pressure to higher pressures, for instance with the following relation (Adams and Barton, 2009):

$$-r_{\text{CO}}|_P = F_{press}(-r_{\text{CO}}|_{P=101x10^3\,Pa}) \tag{17}$$

where F_{press} is a pressure scale-up factor, which can be calculated by equation (18) (Singh and Saraf, 1980):

$$F_{press} = P^{(0.5-P/250)}; \quad P < 30 \text{ bar} \tag{18}$$

where the pressure in given in bar.

2.2 Membrane Reactor

Until now, the WGS-reaction has been described, which is limited by the equilibrium, and is for this reason that membrane reactors (MR) are becoming increasingly interesting; because they provide a selective extraction of one or more products from the reaction mixture through the membrane, so that the reaction is continually shifted towards the product(s). Then, a membrane reactor can have an important role in enhancing the performance when compared with the traditional reactors (TRs). It is then possible to achieve better performances at the same operating conditions as in the TR, and the capital costs can be reduced due to the combination of reaction and separation in only one system (Mendes et al., 2010b).

Separation through porous membranes is based on kinetic gas principles, as a consequence of differences in the sorption characteristics and diffusion rates of the components of a mixture in the membrane (Rautenbach and Albrecht, 1989). To explain the permeation through dense membranes, like the ones used here, it is used the solution-diffusion model (the simplest one), in which is assumed that the gas at the high pressure side of the membrane dissolves in the membrane and diffuses down a concentration gradient to the low pressure side, where the gas is desorbed. Then, the combination of Henry's law (solubility) and Fick's law (diffusion) leads to the following equation for the flux (J) of the permeating species (Membrane Technology in the chemical industry, 2001):

$$J = \frac{D \cdot S \cdot \Delta p}{\delta} = \frac{Pe \cdot \Delta p}{\delta} \tag{19}$$

where D is the diffusion coefficient of the species in the membrane (kinetic term), S is the gas solubility (a thermodynamic term), Δp is the pressure difference between the high and low pressure side, δ is the membrane thickness and Pe is the so-called permeability coefficient.

In this study it was only considered the use of Pd-Ag membranes (inorganic), since they have attracted the interest of many researchers due to their capability to separate and produce ultra-pure hydrogen from gaseous mixture without requiring a further separation/purification unit (Mendes et al., 2010b). This means that the membrane is infinitively selective towards hydrogen.

Such as represented in equation (19), and by application of the Sieverts' law, the hydrogen flux through Pd and Pd-alloy membranes can be illustrated by the following equations (Mendes et al., 2010b):

$$J_{\mathrm{H_2}} = \frac{P_e}{\delta}\left[\left(p_{\mathrm{H_2}}^{\mathrm{retentate}}\right)^n - \left(p_{\mathrm{H_2}}^{\mathrm{permeate}}\right)^n\right] \tag{20}$$

where $p_{\mathrm{H_2}}^{\mathrm{retentate}}$ stands for the hydrogen partial pressure on the retentate side, $p_{\mathrm{H_2}}^{\mathrm{permeate}}$ for the hydrogen partial pressure on the permeate side, δ is the membrane thickness and $n = 0.5$ (whenever the hydrogen diffusion through the metal film is the rate-limiting step and hydrogen atoms form an ideal solution in the membrane).

The relation of the permeability with the temperature is described by the Arrhenius law, as show in equation (21):

$$P_e = P_e{}^0 exp\left(-\frac{E_a}{R\,T}\right) \tag{21}$$

where E_a represents the activation energy for permeation and $P_e{}^0$ the pre-exponential factor. Then, the flux through the membrane increases when the thickness decreases. The same tendency it obtained with the increase in temperature, because the process is thermally activated.

By experimental tests of permeability through a Pd-Ag membrane (23 wt.% of Ag), Pereira (2008) obtained a value of 3.86×10^{-6} $mol \cdot m^{-1} \cdot s^{-1} \cdot Pa^{-0.5}$ for the pre-exponential factor, while the activation energy determined was 19.94 $kJ \cdot mol^{-1}$. According to the author, the values obtained for both parameters are within the ranges reported in literature, as shown in Table 2. These values will therefore be used in the simulation of the membrane reactor (chapter 3.2).

Table 2. Different values reported in literature for the pre-exponential factor and activation energy (source Tosti et al. (2006) and references therein).

$P_e{}^0 / (\mathrm{mol \cdot m^{-1} \cdot s^{-1} \cdot Pa^{-0.5}})$	$E_a / (\mathrm{kJ \cdot mol^{-1}})$	Reference
6.64×10^{-8}	11.24	(Tosti et al., 2006)
5.25×10^{-7}	33.31	(Basile et al., 2005)
2.44×10^{-6}	29.73	(Basile et al., 2001)
6.93×10^{-7}	15.70	(Koffler et al., 1969)
1.20×10^{-7}	12.48	(Itoh and Xu, 1993)

3 Phenomenological Models

The development of phenomenological models that can reproduce experimental result is of great relevance in the exploration of reactor performance and design. In this work, the simulations were divided in two sections; in first place it was only considered the reaction where the products remain in the reactor section, i.e. it was simulated the conversion obtained in a traditional packed-bed reactor (TR), in which the maximum attainable reaction conversion is intrinsically limited by the equilibrium. Following the membrane reactor (MR) was simulated, where besides the chemical reaction it was considered the permeation of one product of the reaction through the wall (hydrogen-selective membrane).

3.1 Traditional Reactor

In this type of reactor (Figure 5), the maximum conversion obtained for the WGS reaction is the equilibrium-conversion, because the products obtained are not removed. Different models will be considered, and their inherent complexity is different, depending on the assumption made, which might be related with the experimental conditions employed (e.g., if flow pattern differs from ideal plug-flow, axial dispersion has to be accounted for; if external resistances are not negligible, a mass transfer equation has to be considered; etc.). In the following sections the models considered in this work will be described, and the inherent hypothesis described.

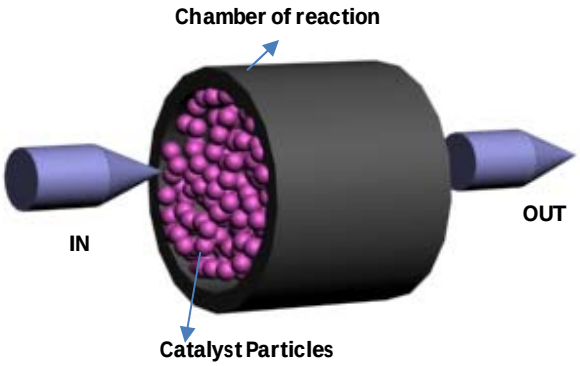

Figure 5. Schematic representation of the traditional reactor modeled.

3.1.1 Pseudo-Homogeneous One-dimensional Models (Models 1 and 2)

The pseudo-homogeneous models do not account explicitly for the presence of catalyst. Therefore, they consider there is not any gradient, both in terms of temperature and concentration between the main stream and the catalyst surface (i.e., external resistances

are considered to be negligible). The concentration and temperatures gradients only occur in the axial direction (Froment and Bischoff, 1990).

The two pseudo-homogeneous models proposed in this section only consider one-dimension, so the radial dispersion is negligible, they only consider transport by plug flow in the axial direction and do not take into account temperatures gradients in the axial direction (i.e. isothermal operation is considered to be valid); the other main assumptions are the following:

1. Gases have an ideal behavior;
2. Negligible pressure drop across the bed;
3. Reaction takes place only on the catalyst surface;
4. Negligible mass and heat-transfer resistances between surface catalyst and bulk gas phase and within the catalyst particle (external and internal limitations).

In Figure 6 are presented a scheme of the reactor, and as this model is a pseudo-homogeneous the balance are doing considerer no difference between the fluid and solid phase.

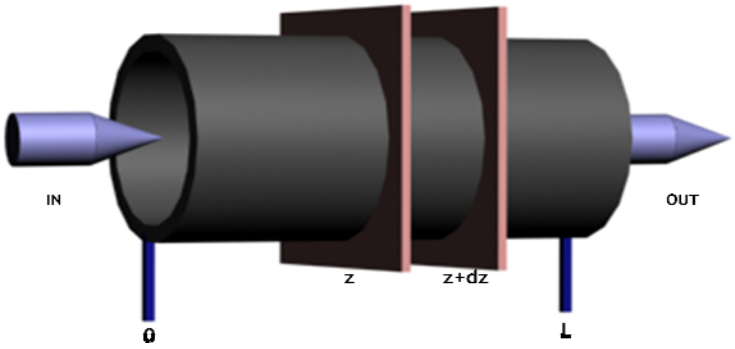

Figure 6. Schematic representation of the reactor modeled in the pseudo-homogeneous models.

According to the Figure 6, the mass conservation equation may thus be written for steady state, resulting for the axial position *z* and respecting to a reactor element with length dz:

$$(\varepsilon A)\varphi_i|_z = (\varepsilon A)\varphi_i|_{z+dz} + (\vartheta_i r_{\mathrm{CO}})\rho_p(1-\varepsilon)A\mathrm{d}z \qquad (22)$$

where ε represents the bed void bed fraction, A is the cross section area of the tubular reactor, φ_i is the molar flow of species *i* per unit area (or molar flux), ϑ_i is the stoichiometric coefficient for species *i* (taken negative for reagents and positive for products), $-r_{\mathrm{CO}}$ is the

rate of consumption reaction of CO (always the limiting reactant in this study), and ρ_p is the particle density.

In the limit, when $\mathrm{d}z \rightarrow 0$, the following differential equation is obtained for each species *i*:

$$\varepsilon \frac{\mathrm{d}\varphi|_i}{\mathrm{d}z} = -(\vartheta_i r_{\mathrm{CO}})\rho_b \tag{23}$$

where ρ_b in the bed density.

3.1.1.1 Ideal Model (Model 1)

In this ideal model, the flow has only a convective contribution, i.e.:

$$\varphi_i = u_i C_i \tag{24}$$

where u_i stands for the interstitial velocity and C_i for the concentration of species *i*.

Then, substituting equation (24) into equation (23), along with the dimensionless parameters $y_i = \frac{p_i}{P_t}, \mathrm{and}\ ; \bar{z} = \frac{z}{L}$, the following first-order differential equation is obtained (see Appendix 1):

$$\frac{\mathrm{d}y_i}{\mathrm{d}\bar{z}} = -\left(\vartheta_i r_{\mathrm{CO}(f(y_i,P_t,T))}\right)\frac{W_{cat}}{F^0} \tag{25}$$

which needs one condition to be solved. The corresponding boundary condition at inlet is $y_i|_{\bar{z}=0} = y_i^0$, where $\mathrm{y_i}$ is the molar fraction of species *i*, p_i is the corresponding partial pressure while P_t is the total pressure, $\bar{z}$ is the dimensionless position (input=0 and output=1), L is the reactor length, and W_{cat}/F^0 represents the space time (W_{cat} is the mass of catalyst in the bed and F^0 is the total feed flow rate).

This model is characterized by the presence of only one parameter, the space time $(\mathrm{W_{cat}/F^0})$. To solve numerically the system of first-order differential equations the Matlab software package was used, via a 4th order Runga-Kutta method. For this the *ODE45* function was used, inside other function developmet a way to get the molar fraction for different space time, pressure and temperatures. Finally, the molar fraction at the reactor outlet was converted to conversion (see Appendix 1).

3.1.1.2 Model with Axial Mixing (Model 2)

In this case it is considered that the flux has a contribution by both convection and diffusion:

$$\varphi_i = u_i C_i - D_{ix} \frac{\mathrm{d}C_i}{\mathrm{d}z} \tag{26}$$

where D_{ix} is the dispersion coefficient in the axial direction. After substituting equation (26) in equation (23), and introducing the same dimensionless parameters as above, the following equation is obtained (see Appendix 1):

$$\frac{\mathrm{d}^2 y_i}{\mathrm{d}\bar{z}^2} = Pe_m \left(\frac{\mathrm{d}y_i}{\mathrm{d}\bar{z}} + \left(\vartheta_i \, r_{\mathrm{CO}(f(y_i, P_t, T))} \right) \frac{W_{cat}}{F^0} \right) \tag{27}$$

Because this is a second-order differential equation, two boundary conditions are required. The Danckwerts' boundary condition at inlet was used: $y_i|_{\bar{z}=0^-} = y_i|_{\bar{z}=0^+} - \frac{1}{Pe_m} \frac{\mathrm{d}y_i}{\mathrm{d}\bar{z}}\Big|_{\bar{z}=0}$, while in the outlet of reactor the commonly employed condition was adopted: $\frac{\mathrm{d}y_i}{\mathrm{d}\bar{z}}\Big|_{\bar{z}=1} = 0$, because there is no reaction.

In this model a new parameter appears, the dimensionless Peclet number ($Pe_m = \frac{u_o L}{\varepsilon \, D_{ix}}$). When $Pe_m \to \infty$**,** the flow pattern approaches the hypothesis of ideal plug-flow; this is therefore a particular case in which Model 2 becomes Model 1:

$$\begin{aligned} \frac{1}{Pe_m} \frac{\mathrm{d}^2 y_i}{\mathrm{d}\bar{z}} &= \frac{\mathrm{d}y_i}{\mathrm{d}\bar{z}} + \left(\vartheta_i \, r_{\mathrm{CO}(f(y_i, P_t, T))} \right) \frac{W_{cat}}{F^0} \\ 0 &= \frac{\mathrm{d}y_i}{\mathrm{d}\bar{z}} + \left(\vartheta_i \, r_{\mathrm{CO}(f(y_i, P_t, T))} \right) \frac{W_{cat}}{F^0} \end{aligned} \tag{28}$$

The problem to solve this numerically was in the fact that the boundary conditions were defined in different positions, one in the inlet and the other at the outlet. For this reason an iterative process (shooting method) was implemented, as explained in Appendix 1. In this iterative process the Matlab software was used, and to solve numerically the second-order differential equations they were converted into systems of first-order differential equations. The function *ODE15s* was used (see Appendix 1), because even the problem is stiff a solution can be obtained. Equal to the previous case, a function was developed through which it was

possible to obtain the molar fractions for different space times, pressures and temperatures. Finally, the molar fraction at the outlet was converted to conversion.

3.1.2 Heterogeneous One-dimensional Models (Models 3 and 4)

For the heterogeneous models the presence of catalyst is explicitly accounted, so that the conservation equations are written separately for fluid and catalyst. In Figure 7 is presented a scheme of the reactor.

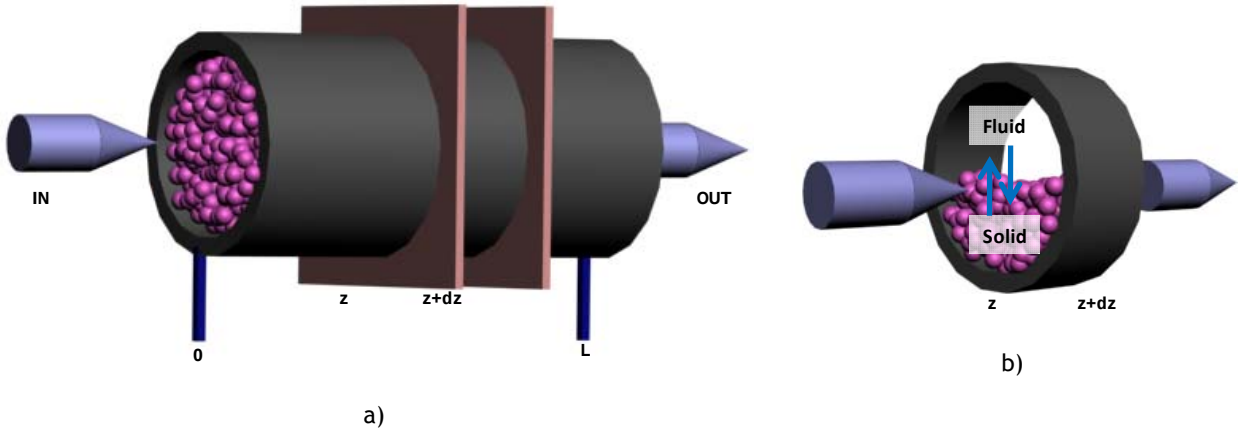

Figure 7. Schematic representations of the membrane reactor modeled in the heterogeneous models, considering separately the fluid and solid phases.

The models proposed in this section, as in the previous one, consider one-dimension, i.e. transport is only considered in the axial direction. The main assumptions for models 3 and 4 are the following:

1. Gases have an ideal behavior;
2. There are no temperature gradients (isothermal operation);
3. Negligible pressure drop across the bed;
4. Reaction takes place only on the surface of the catalyst;
5. Negligible heat-transfer resistance between surface catalyst and bulk (external limitations);
6. Negligible mass and heat-transfer resistances within the catalyst particle (internal limitations).

The big difference between the pseudo-homogeneous and the heterogeneous models is that only in the later it is possible to consider the resistances (mass and/or heat-transfer) that can exist around and/or inside the catalyst particles (see Figure 7). Although this effect is mostly a physical phenomenon, it can have a major influence on the reactor performance.

3.1.2.1 Model accounting for interfacial gradients (Model 3)

This basic heterogeneous model, as in Model 1, only considers transport by plug flow, but distinguishes between conditions in the fluid and on the solid. The steady-state equations may be written for each part and for a given species *i* as follows:

For the Fluid:

$$u_o \frac{\mathrm{d}C_i}{\mathrm{d}z} + k_{f_{i,m}} a_v \left(C_{i\_b} - C_{i\_s}\right) = 0 \tag{29}$$

For the Solid:

$$k_{f_{i,m}} a_v \left(C_{i\_b} - C_{i\_s}\right) = \left(\vartheta_i r_{\mathrm{CO}(f(C_s,T,P_t))}\right)\rho_b \tag{30}$$

where u_o stands for the superficial velocity, C_{i_b} and C_{i_s} are the concentration of species *i* in the bulk and catalyst surface, respectively, a_v is the total external surface area of catalyst per unit volume, and $k_{f_{i,m}}$ is the mass transfer coefficient for the same species in the mixture. By introducing the dimensionless parameters above mentioned ($y_i = \frac{P_i}{P_t}$; $\bar{z} = \frac{z}{L}$), it is possible to obtain the following equations that describe Model 3 (see Appendix 1):

For the Fluid:

$$\frac{\mathrm{d}y_{i\_b}}{\mathrm{d}\bar{z}} = -k_{f_{i,m}} a_v \left(y_{i\_b} - y_{i\_s}\right) \tag{31}$$

For the Solid:

$$k_{f_{i,m}} a_v \left(y_{i\_b} - y_{i\_s}\right) = \vartheta_i r_{\mathrm{CO}(f(C_s,T,P_t))} \frac{W_{cat}}{F^0} \tag{32}$$

In this case the system is again composed by first-order differential equations, and so it is necessary to know one boundary condition. This condition is similar to that used in Model 1, because the molar fraction of each species is known at the inlet of reactor, i.e.: $y_{i\_b}\big|_{\bar{z}=0} = y_i^0$**,** where y_{i_b} is the molar fraction of species *i* in the bulk, y_{i_s} is the molar fraction of that species in the catalyst surface and $k_{f_{i,m}}$ is the mass transfer coefficient.

As presented in equations (31) and (32), Model 3 requires the simultaneous resolution of several differential and algebraic equations (DAEs). If the kinetics were simple, which is not the case as shown below, it would be possible to explicitly write the value of the molar fraction on the catalyst surface - equation (32) replace it in equation (31) and solve the problem, as in the case of Model 1. The method of solution used in this model was detailed in the Appendix 1.

3.1.2.2 Model accounting for interfacial gradients with Axial Mixing (Model 4)

The only different between models 3 and 4 is in the fluid phase, because in both models the mass transfer resistances within the catalyst particles are negligible (the reasons for this approach are based in a previous study of Pereira (2008), where the author verified the absence of internal resistances because the conversion was constant for particle sizes in the range 180 - 500 μm). For Model 4, as in Model 2, it was considered that the flux has a contribution by both convection and diffusion, and therefore the steady-state equations are as follows:

For the Fluid:

$$u_o \frac{\mathrm{d}C_{i\_b}}{\mathrm{d}z} - \varepsilon D_{ix} \frac{\mathrm{d}^2 C_{i\_b}}{\mathrm{d}z^2} + k_{f_{i,m}} a_v \left(C_{i\_b} - C_{i\_s}\right) = 0 \tag{33}$$

For the Solid:

$$k_{f_{i,m}} a_v \left(C_{i\_b} - C_{i\_s}\right) = \left(\vartheta_i r_{\mathrm{CO}(f(C_s,T,P_t))}\right)\rho_b \tag{34}$$

By introducing the same dimensionless parameters, it is possible to obtain the following equations that describe Model 4:

For the Fluid:

$$\frac{\mathrm{d}^2 y_{i\_b}}{\mathrm{d}\bar{z}^2} = Pe_m \left(\frac{\mathrm{d}y_{i\_b}}{\mathrm{d}\bar{z}} + k_{f_{i,m}} a_v \left(y_{i\_b} - y_{i\_s}\right) \right) \tag{35}$$

For the Solid:

$$k_{f_{i,m}} a_v \left(y_{i\_b} - y_{i\_s}\right) = \vartheta_i r_{\mathrm{CO}(f(C_s,T,P_t))} \frac{W_{cat}}{F^0} \tag{36}$$

As in Model 2, in this one appears the dimensionless Peclet number ($Pe_m = \frac{u_o L}{\varepsilon\, D_{ix}}$). For this model two boundary conditions are required. The first condition, as in Model 2, is given by the Danckwerts' boundary condition: $y_{i\_b}\big|_{\bar{z}=0^-} = y_{i\_b}\big|_{\bar{z}=0^+} - \frac{1}{Pe_m}\frac{\mathrm{d}y_{i\_b}}{\mathrm{d}x}\Big|_{\bar{z}=0}$, while at the outlet,

where there is no reaction: $\left.\frac{\mathrm{d}y_{i\_b}}{\mathrm{d}x}\right|_{\bar{z}=1} = 0$. It is important to note that these conditions are in the fluid phase, i.e. in the bulk. To solve this problem a combination of the strategy used in Models 2 and 3 was used (see Appendix 1).

As a summary, in Table 3 are shown the conditions and equations of each model proposed previously.

Table 3. Different phenomenological models proposed.

	Pseudo-Homogeneous	**Heterogeneous**
Flow contribution	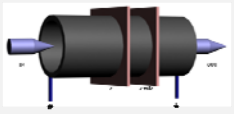	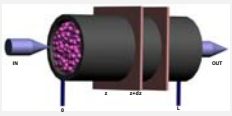
	MODEL1	**MODEL3**
Convective $\varphi_i = u_i C_i$	$\frac{\mathrm{d}y_i}{\mathrm{d}\bar{z}} = -\left(\vartheta_i r_{\mathrm{CO}(f(y_i,P_t,T))}\right)\frac{W_{cat}}{F^0}$ BC: $y_i\|_{\bar{z}=0} = y_i^0$	$\frac{\mathrm{d}y_{i\_b}}{\mathrm{d}\bar{z}} = -k_{f_{i,m}} a_v \left(y_{i\_b} - y_{i\_s}\right)$ BC: $y_{i\_b}\|_{\bar{z}=0} = y_i^0$ $k_{f_{i,m}} a_v \left(y_{i\_b} - y_{i\_s}\right) = \vartheta_i r_{\mathrm{CO}(f(C_s,T,P_t))}\frac{W_{cat}}{F^0}$
	MODEL2	**MODEL4**
Convective + Diffusive $\varphi_i = u_i C_i - D_{ix}\frac{\mathrm{d}C_i}{\mathrm{d}z}$	$\frac{\mathrm{d}^2 y_i}{\mathrm{d}\bar{z}^2} = Pe_m\left(\frac{\mathrm{d}y_i}{\mathrm{d}\bar{z}} + \left(\vartheta_i\, r_{\mathrm{CO}(f(P_t,T))}\right)\frac{W_{cat}}{F^0}\right)$ BC: $y_i\|_{\bar{z}=0^-} = y_i\|_{\bar{z}=0^+} - \frac{1}{Pe_m}\left.\frac{\mathrm{d}y_i}{\mathrm{d}\bar{z}}\right\|_{\bar{z}=0}$ and $\left.\frac{\mathrm{d}y_i}{\mathrm{d}\bar{z}}\right\|_{\bar{z}=1} = 0$	$\frac{\mathrm{d}^2 y_{i\_b}}{\mathrm{d}\bar{z}^2} = Pe_m\left(\frac{\mathrm{d}y_{i\_b}}{\mathrm{d}\bar{z}} + k_{f_{i,m}} a_v\left(y_{i\_b} - y_{i\_s}\right)\right)$ BC: $y_{i\_b}\|_{\bar{z}=0^-} = y_{i\_b}\|_{\bar{z}=0^+} - \frac{1}{Pe_m}\left.\frac{\mathrm{d}y_{i\_b}}{\mathrm{d}\bar{z}}\right\|_{\bar{z}=0}$ and $\left.\frac{\mathrm{d}y_{i\_b}}{\mathrm{d}\bar{z}}\right\|_{\bar{z}=1} = 0$ $k_{f_{i,m}} a_v\left(y_{i\_b} - y_{i\_s}\right) = -r_{\mathrm{CO}(f(C_s,T,P_t))}\frac{W_{cat}}{F^0}$

3.1.3 Effect of the Feed Pressure

The effect of the pressure will be considered by introducing the factor of pressure scale-up in the kinetics for each model. In the particular case, for Model 1 the new equation would be the following:

$$\frac{\mathrm{d}y_i}{\mathrm{d}\bar{z}} = -\left(\vartheta_i r_{\mathrm{CO}(f(y_i,T,P=101kPA))} F_{press}\right)\frac{W_{cat}}{F^0} \tag{37}$$

where F_{press} is the pressure scale-up factor, given by equation (18).

3.2 Membrane Reactor

In this section it was assumed a pseudo-homogeneous one-dimensional model (so the radial dispersion is negligible) for a membrane reactor with the geometry of tube-and-shell as presented in Figure 8.

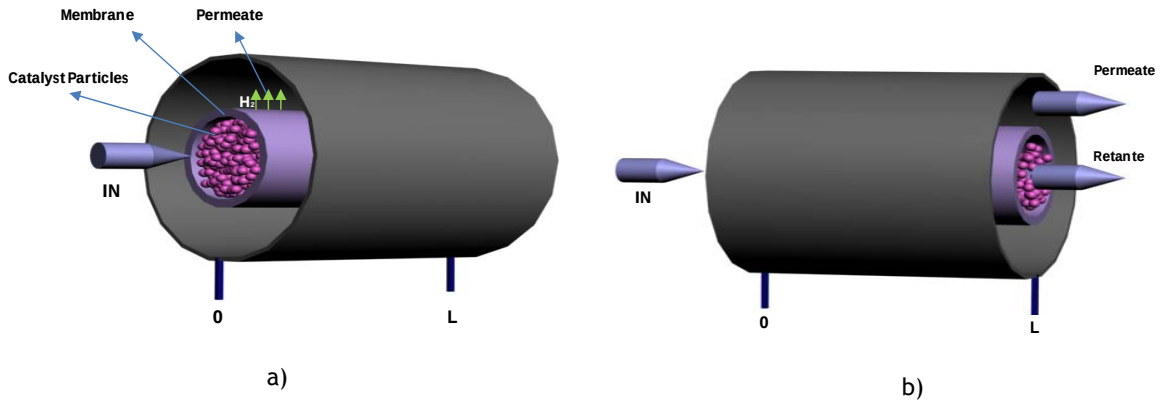

Figure 8. Schematic representation of the membrane reactor modeled.

The main assumptions are the following:

1. Gases have an ideal behavior;
2. Isothermal operation is considered to be valid;
3. Negligible pressure drop across the bed;
4. Only is considered the transport by plug flow in the axial direction for both sections, retentate and permeate;
5. Only hydrogen permeates through the membrane, and this permeation is proportional to the difference in the partial pressure of hydrogen between the tube and shell side;
6. Reaction takes place only on the catalyst surface;
7. Negligible mass and heat-transfer resistances between surface catalyst and bulk gas phase and within the catalyst particle (external and internal limitations).

According to Figure 8, the mass conservation equation may thus be written for steady state, resulting for the axial position *z* and respecting to a reactor element with length *dz*:

$$(\varepsilon_b^R A^R)\varphi_i^R|_z = (\varepsilon_b^R A^R)\varphi_i^R|_{z+dz} - \varepsilon_b^R 2\pi r^M F_i^M \mathrm{d}z + (\vartheta_i r_{\mathrm{CO}})\rho_p(1-\varepsilon_b^R)A^R \mathrm{d}z \quad (38)$$

where ε_b^R represents the bed void bed fraction in the retentate side, A^R is the cross section area of the tubular reactor, ${\varphi_i}^R$ is the molar flow of species *i* per unit area (or molar flux) in the retentate, r^M is the ratio of the tubular reactor, F_i^M is the flow of permeate of species *i* (in this particular case is only considered H_2 permeation through the membrane).

Considering the ideal model, in which the flow has only a convective contribution (equation (24)), the mass balance for each species becomes (see Appendix 1):

$$\frac{\mathrm{d}p_i}{\mathrm{d}z} = -\frac{p_i}{u_o}\frac{\mathrm{d}u_o}{\mathrm{d}z} + (\vartheta_i r_{\mathrm{CO}})\frac{\rho_b}{u_o} - \frac{\varepsilon_b^R 2\pi r^M F_i^M}{u_o A^R} \tag{39}$$

which needs one boundary condition to be solved, which is defined at the inlet: $p_i|_{z=0} = p_i^0$, and $u_o|_{z=0} = u_o^0$, where p_i is the partial pressure of species *i*, and u_o is the superficial velocity.

The molar flow of hydrogen through the membrane was based in equation (20), using the permeation parameters defined in section 2.2. It was considered that the hydrogen partial pressure in the permeation chamber is null.

The overall mass balance in the reaction (retentate) chamber is:

$$\frac{\mathrm{d}u_0}{\mathrm{d}z} = -\frac{u_o}{P}\frac{\mathrm{d}P}{\mathrm{d}z} + \sum(\vartheta_i r_{\mathrm{CO}})\frac{\rho_b}{u_o} - \sum\frac{\varepsilon_b^R 2\pi r^M F_i^M}{u_o A^R} \tag{40}$$

Assuming constant pressure in the reaction side, and because only H_2 permeates, the overall mass balance becomes as follows:

$$\frac{\mathrm{d}u_0}{\mathrm{d}z} = -\frac{\varepsilon_b^R 2\pi r^M F_{\mathrm{H_2}}^M}{u_o A^R} \tag{41}$$

4 Experimental Section

4.1 Experimental Setup

The experiments were carried out using a packed-bed reactor operating isothermally, which was encased in an electric oven (Memmert, type UNE200), controlled by a programmable temperature controller. The material of the reactor was stainless steel, which was loaded with 250 mg of $CuO/ZnO/Al_2O_3$ catalyst (300 μm-diameter particles), supported by two fritted Teflon disks to avoid the catalyst powder dispersion over the pipes. A schematic of the experimental setup is presented in Figure 9.

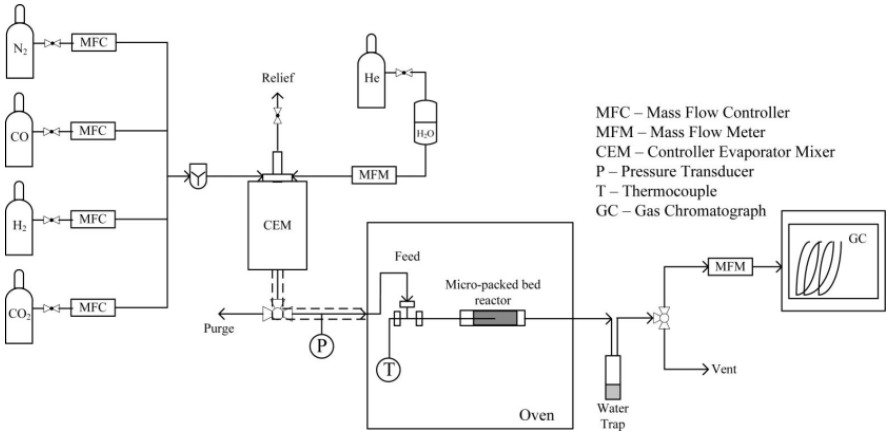

Figure 9. Sketch of the experimental setup used (source Mendes et al., 2009).

As shown in Figure 9, the feed section consists in four independent gas lines with individual mass flow controllers (MFCs) and one liquid line of deionized water that was metered, vaporized, and mixed in a controller evaporator mixer (CEM, Bronkorst) with the other gases. All the pipes and valves along the water feed stream till the entrance of the reactor were heated to 115 ºC using a thermal resistance to prevent the condensation of water. The analysis of effluent gas was performed by gas chromatography (Dani 1000 GC) after water condensation. The reactor outlet stream was thus cooled making it passing through a "water trap", where all content of water was removed; the dry-gas products were then analyzed in an online gas chromatograph in which were detect and quantified the N_2, CO, and CO_2 using a chromatographic column (Supelco Carboxen 1010 plot, from Sigma-Aldrich, 30 m × 0.32 mm), with He as the carrier gas (1 $mL_N \cdot min^{-1}$), and a TCD (Valco thermal conductivity detector). The temperature program that was defined for the analysis in the GC consisted in the first 7.5 min of an isothermal operation at 35 ºC, followed by heating with a rate of 10 $ºC \cdot min^{-1}$ from

35 to 80 ºC, and then keeping the sample at 80 ºC for 8 min. Because hydrogen has a thermal conductivity close to that of helium, it is difficult to measure its composition by GC. Therefore, the hydrogen composition in the dry-gas was calculated from the mass balance (difference from 100 %, dry basis), which is required for mass flow rate corrections. The carbon and the nitrogen molar balance relative errors were typically lower than 5 %.

4.2 Catalyst Reduction

The catalyst used in this work was the commercial material $CuO/ZnO/Al_2O_3$ (from REB Research & Consulting). The reduction protocol applied was based on literature information to ensure complete metal oxide reduction, without sintering (Mendes et al., 2009). The catalyst was activated in situ with a mixed gas flow of H_2/N_2 measured by means of mass flow controllers. The reduction process started with a heating of the catalyst from room temperature to 80 ºC at 12 ºC·min^{-1} in nitrogen with a total flow rate of 90 mL_N·min^{-1}, and for one hour the temperature was maintained at 80 ºC; this was followed by the reduction mixture (5 vol. % H_2/N_2) feed, and then the catalysts was heated at 5 ºC·min^{-1} from 80 to 230 ºC and maintained at this temperature for 4 h. After this reduction, the catalyst was cooled or heated to the reaction temperature and flushed with N_2, before the reaction mixture was admitted to the catalytic bed.

4.3 Experimental Test

In this work, it was proceeded differently from the methodology employed to determine the kinetics of the reaction (Mendes et al., 2010a). When a kinetic study is made it must be guaranteed the absence of internal or external resistances, in order to be equal the observed and the real reaction rate (intrinsic kinetic conditions). However, in this work conditions closer to "real" operation will be employed. Therefore, the experiments can in some conditions be carried out in the presence of external (and eventually internal) resistances; so, the various models proposed and described in previous sections have to be validated.

According with the experimental study of Pereira (2008), it was guaranteed that there is the possibility of occurring resistances to mass transfer in the film around the particles for superficial velocities lower than 0.094 m·s^{-1}. In the same study it was concluded that the CO conversion is independent of the catalyst particle size for diameters between 180 and 500 μm; so, the internal resistances to mass transfer can be considered negligible in the present work (i.e., there are no intra-particle diffusion limitations for the samples used - 300 μm diameter particles).

The experiments were carried out in a stainless steel reactor with 6 mm of internal diameter. After the reduction of the commercial catalyst ($CuO/ZnO/Al_2O_3$) following the protocol mentioned above, the reaction was started by introducing the gases in the reactor feed according to the five different mixtures reported below (see Table 4); each mixture composition was tested at three different volumetric flow rates (40, 80 and 150 $mL_N \cdot min^{-1}$). The temperature range of operation was from 150 to 300 ºC. The principal reaction mixture (mixture 1) consisted in a typical reforming gas mixture with 4.70 % CO, 34.78 % H_2O, 28.70 % H_2, 10.16 % CO_2, and 21.66 % N_2 (vol.%). Then, changes in the content of CO or H_2O have been done, maintaining fixed the composition of CO_2 and H_2, for evaluation their effect in the performance of the WGS-reactor (mixtures 1 to 3 show the effect of the carbon monoxide content in the feed while mixtures 1, 4 and 5 the effect of water). All these experiments were performed at atmospheric pressure.

Table 4. Different mixture compositions used in the reaction experiments (molar fraction).

Mixture	Species				
	CO	H_2O	CO_2	H_2	N_2
1	4.70	34.78	10.16	28.70	21.66
2	2.38	34.78	10.16	28.70	23.98
3	9.42	34.78	10.16	28.70	16.94
4	4.70	16.90	10.16	28.70	39.54
5	4.70	43.74	10.16	28.70	12.70

In the second part of the experimental section, it was intended to evaluate the effect of the feed pressure in the CO conversion; so, additional experiments were conducted at pressures ~300 and ~600 kPa for one reactive mixture (Mixture 1), for the same temperature range and volumetric flow rates.

5 Results and Discussion

5.1 Traditional Reactor

5.1.1 Evaluation of the Kinetics for the Low Temperature WGS Reaction

In accordance with the literature (Figueiredo et al., 2007), in order to determine the kinetics from experimental data the operating conditions have to ensure the total absence of any type of resistance for mass and heat transfer, both internally and externally. In this order of ideas, in the work of Mendes et al. (2010a) a packed-bed reactor was used to determine the kinetic data of the WGS reaction at low-temperature over a $CuO/ZnO/Al_2O_3$ catalyst. In Table 5 are described the conditions used in such a work, which guaranteed the applicability of the plug-flow model (neglecting axial dispersion and wall effects in gas-solid operation) and the possibility of neglecting pressure drop, in addition to any resistances to mass or heat transfer. The authors varied the mass of catalyst to determine the conversion at different space time values, W_{cat}/F_{CO}^{o} (keeping constant the flow rate in the feed).

Table 5. Operational parameters and reactor dimensions employed in the kinetic study.

Operational parameters	
Temperature range [K]	453.15 – 573.15
Feed Pressure [kPa]	~120
Mass of Catalyst [mg]	70 – 2400
Feed composition	4.70 % CO, 34.78 % H_2O, 10.16 % CO_2, 28.70 % H_2, 21.66 % N_2
Flow Rate in the Feed [$mL_N \cdot min^{-1}$]	270
Reactor dimensions	
Length [cm]	5
Diameter [cm]	0.775

As the experimental data obtained in that work (Mendes et al., 2010a) guarantees the absence of any type of resistance, for either mass and/or heat transfer, it is possible to obtain the theoretical conversion for the same conditions using Model 1 (see section 3.1.1.1), in which are taken the above-mentioned assumptions (neglecting axial dispersion, etc.). For simulation three different kinetics rate equations were considered: Langmuir-Hinshelwood (LH1), Redox and Empirical (Power-Law), as described in section 2.1.3. For the range of temperatures in this study (180 – 300 ºC), the purpose is to determine which kinetic model has a better fit for the experimental data.

Figure 10 show the parity plots for the theoretical vs. experimental CO conversion (according to Model 1). The criteria used to compare the results obtained in all kinetic models was the following: $FO = \sum_{i=1}^{N}\left(X_{CO}^{exp} - X_{CO}^{cal}\right)^2$.

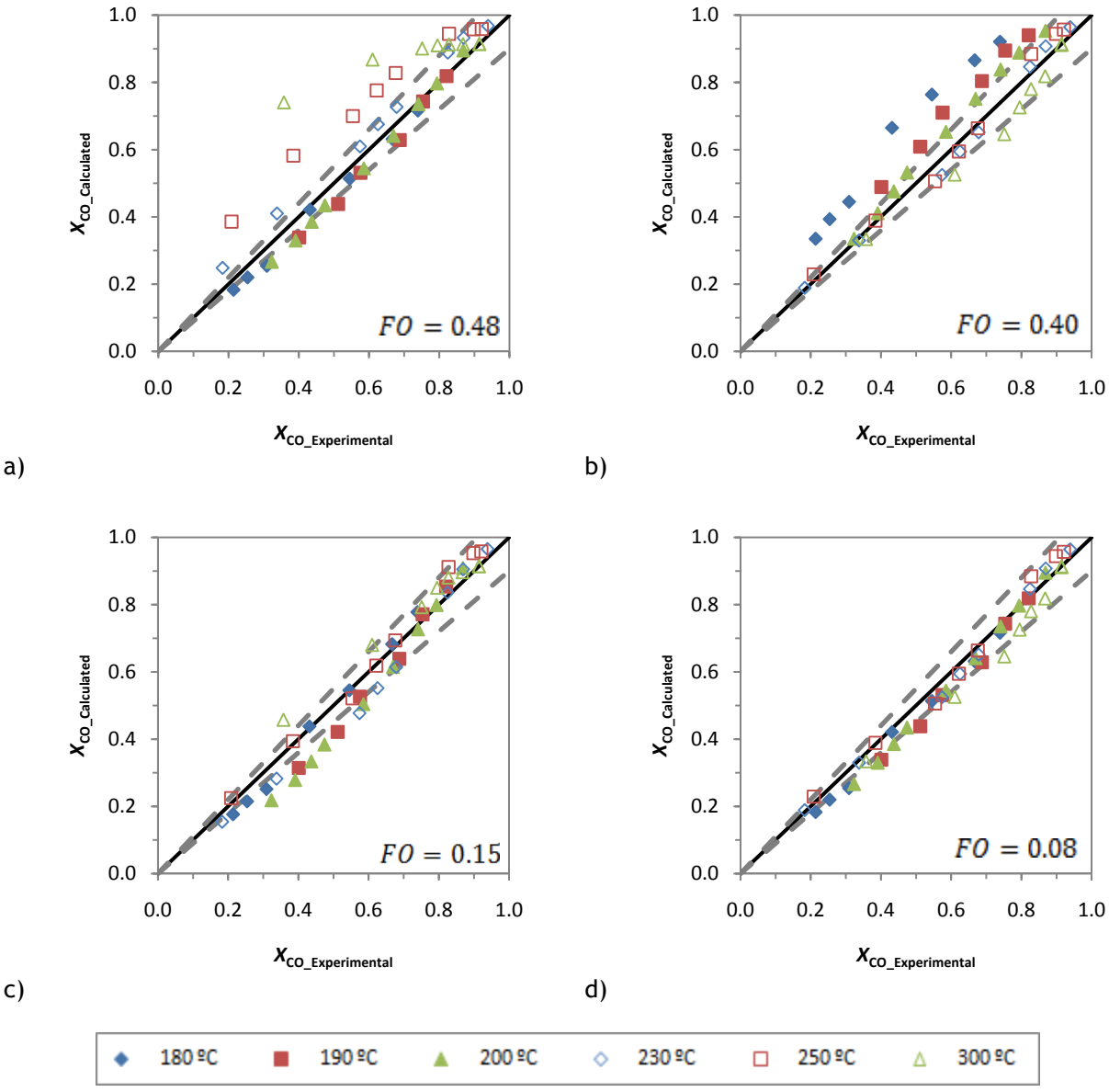

Figure 10. Parity plots (theoretical vs. experimental CO conversion) using the phenomenological **Model 1** with the kinetics models: a) LH1, b) Redox, c) Power-law rate equations, in the temperature range 180 to 300 °C, and d) LH1 (180 - 200 °C) and Redox (230 - 300 °C). In all figures the dashed line represents an interval of ±10 % of error.

When the LH1 kinetic model is used (Figure 10 a), the theoretical CO conversion has a good fit with the experimental data at temperatures lower that 230 °C. When the temperature increases the conversion increases too (for the same space time), however, the predicted conversion is much higher than that obtained experimentally. When the Redox model is applied, a similar plot is observed, with an overall better fit. In addition, it is noteworthy that in this case the goodness-of-fit is better for temperatures above 200 °C than at lower

temperatures (below this temperature the theoretical CO conversion is higher than that obtained experimentally).

For the whole temperature range (180 - 300 ºC) the kinetic model that offers the best fit to the experimental data is the empirical one, of the Power-Law type (Figure 10 c), with $FO = 0.15$. However, in the work done by Mendes et al. (2010a) the authors proposed the use of two kinetic models (LH1 and Redox) for the temperature range adopted in the study, i.e., the Langmuir-Hinshelwood 1 kinetics for a temperature range of 180 to 200 ºC, while for the interval between 230 to 300 ºC must be used the Redox model. So, in Figure 10 d) this restriction was assumed, obtaining the best fit tried for the experimental data, where $FO = 0.08$.

Until now, it was only referred which kinetic rate equations provided the best fitting by comparing the theoretical conversion with the experimental data, but it is also important to illustrate the effect of the space time and temperature in the conversion. As expected, at higher temperatures the reaction rate increases, resulting in major CO conversion levels, as can be seen in Figure 11. Nevertheless, this is only true while not in the equilibrium condition; such as described in previous sections, the equilibrium conversion decreases with increasing temperatures, and this fact can be clearly seen in Figure 11 b) for the temperatures of 230, 250 and 300 ºC. Consequently, the carbon monoxide conversion at 300 ºC is always higher than the conversion obtained at 250 ºC, when the system is not in the equilibrium (for 300 ºC this means a space time < ~25 - 30 $g_{cat}\cdot h\cdot mol_{CO}^{-1}$), but for space times above this values and at 300 ºC the system is in the equilibrium; so, an increase in the space time does not have any influence in the conversion, which is lower than that obtained at 250 ºC (and obviously at 230 ºC too).

Equal to the effect of temperature, the space time always favors the conversion (because either the mass of catalyst or the residence time is increased, for the same feed flow rate or amount of catalyst, respectively), regardless of the reaction temperature, although when one gets the equilibrium condition this parameter has no effect on the CO conversion (Figure 11).

Figure 11 also clearly shows the good adherence, with the experimental data, of the composed kinetic model described above, i.e., using the LH1 formulation in the lowest temperatures and the Redox for the highest temperatures.

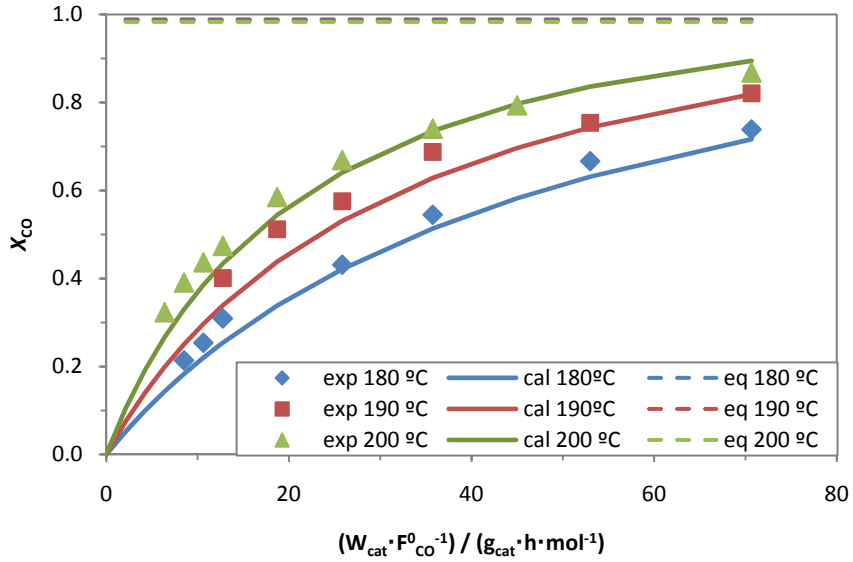

a)

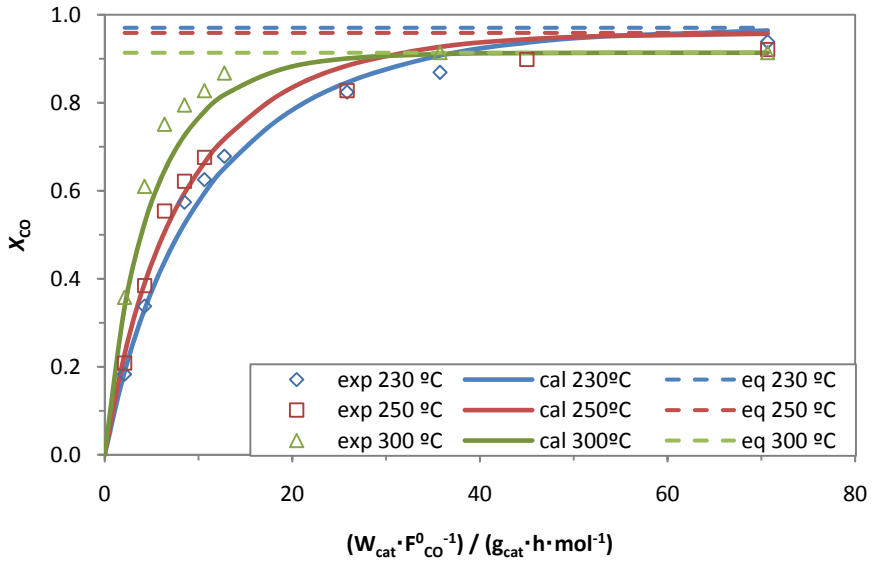

b)

Figure 11. CO Conversion (experimental and theoretical) vs. space time ($W_{cat}/F_{CO}{}^0$) at different reaction temperatures using different kinetics model: a) LH1 (lower temperatures), b) Redox (higher temperatures). Points represent the experimental CO conversion, continuous line the CO conversion by **Model 1,** and dashed line equilibrium CO conversion.

In conclusion, in this section the proposed composed kinetics was validated. In the next section, the performance of a packed-bed WGS reactor obtained by the different phenomenological models described in section 3.1 will be compared. This will allow also better understanding which parameters affect each model, and how they account for the overall CO conversion (i.e., how sensitive is the reactor performance towards changes in each operating condition). The range of conditions used in the simulations are those shown in Table 5, but the flow rate is not kept constant (it was varied in the range 1 – 270 $mL_N\cdot min^{-1}$).

5.1.2 Evaluation of the WGS reactor performance by the different phenomenological models

5.1.2.1 MODEL 1

After validating Model 1 and the composed kinetics, for the conditions proposed in the study of Mendes et al. (2010a) (see Table 5), in Figure 12 is represent a 3D graphical plot in which is possible to observe the effect of temperature and space time in the conversion, comparing it with the equilibrium value (the maximum conversion obtained in the traditional reactor). As expected the conversion increases with the increase in either temperature or space time, approaching the equilibrium conversion limit, which decreases with a temperature raise. The increase in conversion due to an increase in temperature may be explained by the fact of increasing the kinetic rate constant $\left(k = A_0 exp\left(-{}^{E}/_{R\,T}\right)\right)$; then the reaction rate is higher. About the increase with the space time, it is a consequence of the largest residence time/mass of catalyst.

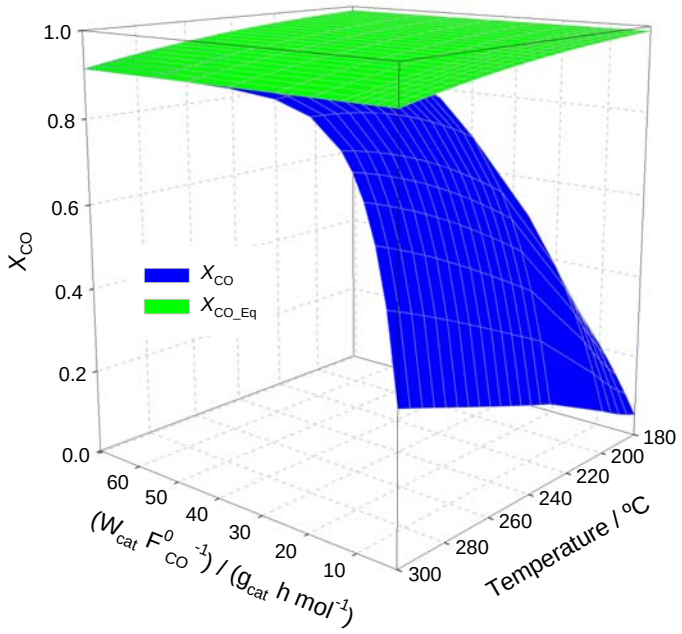

Figure 12. Effect of the space time and temperature in the theoretical CO Conversion by **Model 1** (see Table 5 for other operating parameters).

5.1.2.2 MODEL 2

In the case of Model 1, the variation in the flow rate is not relevant in the conversion attained whenever keeping constant the $W_{cat}/F_{CO}{}^{0}$ value. To better observe this effect it is necessary to introduce a new parameter, that "links" the effect of fluid flow rate with the diffusion rate (Peclet number). In Model 2 it was considered that the flow has a convective and a diffusive

contribution (equation (26)), and therefore this parameter appears in equation (27). In Figure 13 is shown that an increase in the flow rate (Pe_m increases too, because $Pe_m \propto q_0$), for the same space time, leads to an increase in the conversion, because the diffusive effect becomes negligible (so reactor performance approaches the plug-flow).

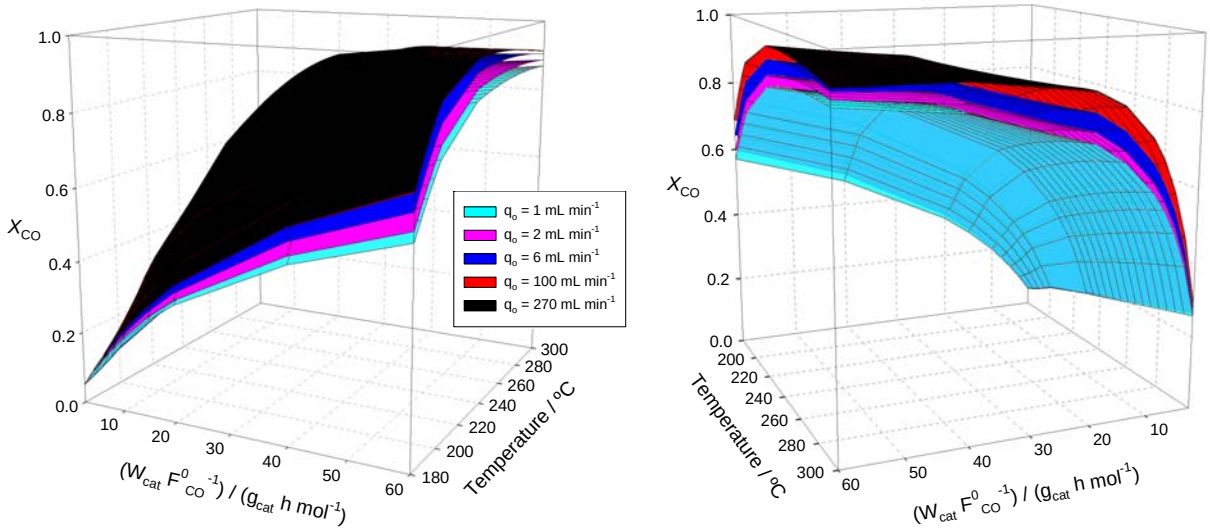

Figure 13. Different perspectives of the space time and temperature effect in the theoretical CO Conversion by **Model 2** (see Table 5 for operating parameters).

For this particular case study, the curves in Figure 13 used the flow rate for describing the CO conversion, and not the Peclet Number ($Pe_m = u_0\ L/\varepsilon\ D_{ax}$). This fact is consequence of Pe_m changing not only with the flow rate but also with the temperature and composition (see Appendix 2). The variation of the Peclet number is represented in Figure 14, for the feed composition.

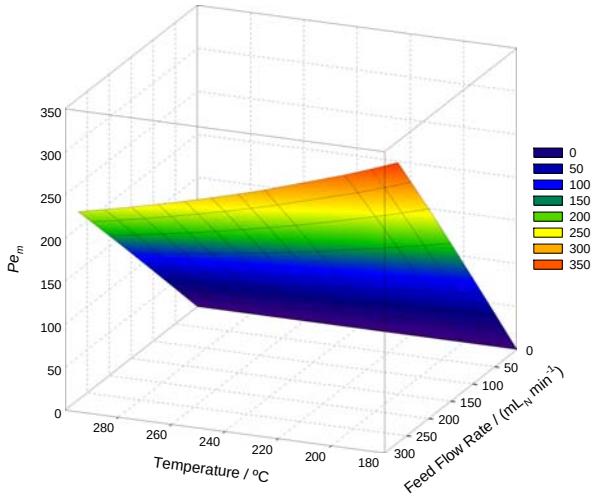

Figure 14. Variation of the Peclet number with temperature and flow rate. Composition of gas mixture: 4.70 % CO, 34.78 % H_2O, 28.70 % H_2, 10.16 % CO_2, and 21.66 % N_2 (vol. %).

It is noteworthy that, for a flow rate of 270 $mL_N \cdot min^{-1}$ (the value used when obtaining the kinetic data), the minimum value for Pe_m is 218, validating the fact of assuming ideal plug-flow (Model 1) in section 5.1.1.

5.1.2.3 MODEL 3

As described in section 3.1.2.1, this model is similar to Model 1 (plug-flow), but considers also the solid phase, thus requiring an extra parameter to account for the mass transfer resistance. Again, when changing the flow rate (but keeping constant the space time) no important effect in the conversion was noticed (data not shown). The variation of the mass transfer coefficient for CO in the mixture is represented in Figure 15. For the same temperature the mass transfer coefficient increases with an increase in the feed flow rate (see Appendix 2), and as a consequence the difference between the CO conversion results from Models 1 and 3 decreases. Nevertheless, even for the smallest flow rate the effect is nearly negligible *($\Delta X_{CO} < 2\ \%$)*.

It is important to note, and as shown in Figure 15, that the temperature has almost no effect on the mass transfer coefficient. According to the literature (*Perry's chemical engineers' handbook*, 1997), that parameters depends only on the Reynolds number and on the Schmidt number (see Appendix 2). As the Schmidt number for a gas is approximately independent of temperature, then the principal effect of temperature arises from changes in the gas viscosity. For normally encountered temperature ranges, these effects will be small owing to the fractional powers involved in Reynolds number terms (*Perry's chemical engineers' handbook*, 1997).

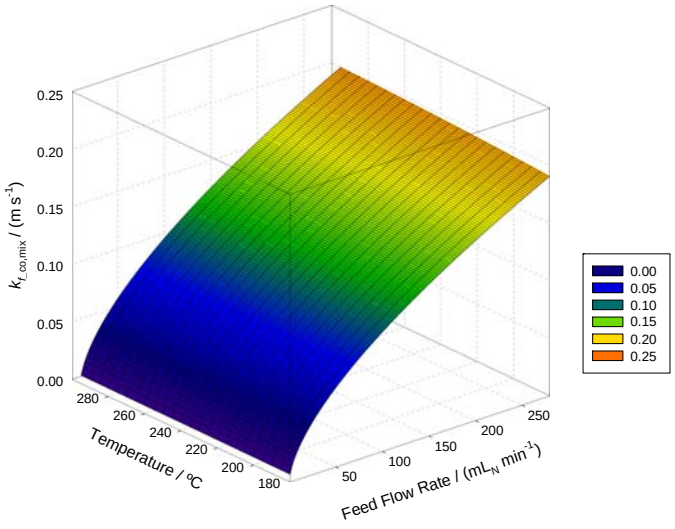

Figure 15. Variation of the mass transfer coefficient of CO in the mixture with temperature and flow rate. Composition of gas mixture: 4.70 % CO, 34.78 % H_2O, 28.70 % H_2, 10.16 % CO_2, and 21.66 % N_2 (vol. %).

Figure 16 represents the variation in the CO conversion, when the temperature and space time are changed. The trends are equal to those reported in Figure 12 (Model 1), i.e., the conversion increases with an increase in both space time and temperature, but the conversion for this model is lower that obtained in Model 1, which is as consequence of including a resistance to mass transfer, as shown later on section 5.1.2.5.

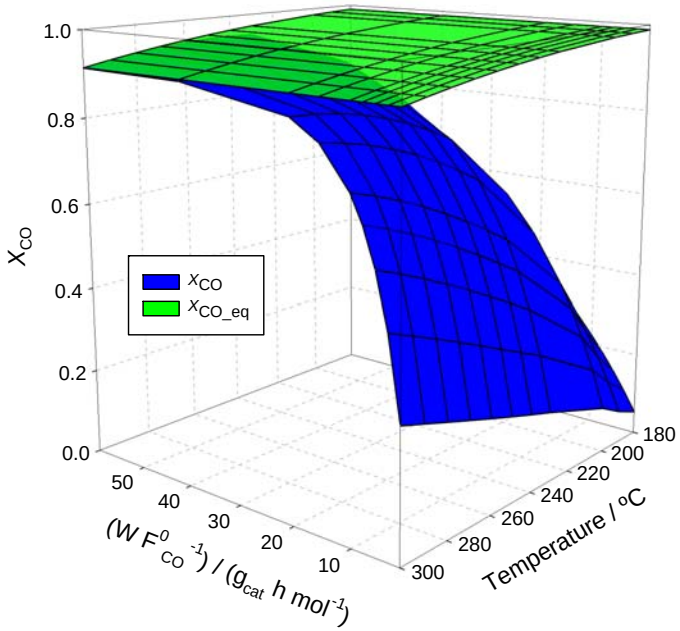

Figure 16. Effect of the space time and temperature in the theoretical CO Conversion by **Model 3** (see Table 5 for additional operating parameters).

5.1.2.4 MODEL 4

Now, similarly to Figure 13 (Model 2), in Figure 17 is represented the CO conversion for Model 4 as a function of the space time and temperature. This model considers and axially-dispersed plug flow pattern and external resistances to mass transfer. In general the behavior of both figures are similar, with the difference that Model 4 considers the resistance in the film around the particle. Consequently, a variation in the feed flow rate has here a greater effect on the conversion, especially for lower flow rates, because it affects not only the Peclet number but also the mass transfer coefficient. Again, for a constant space time (and temperature), the reactor performance is improved for higher flow rates, because flow pattern approaches plug-flow and mass transfer resistances are decreased.

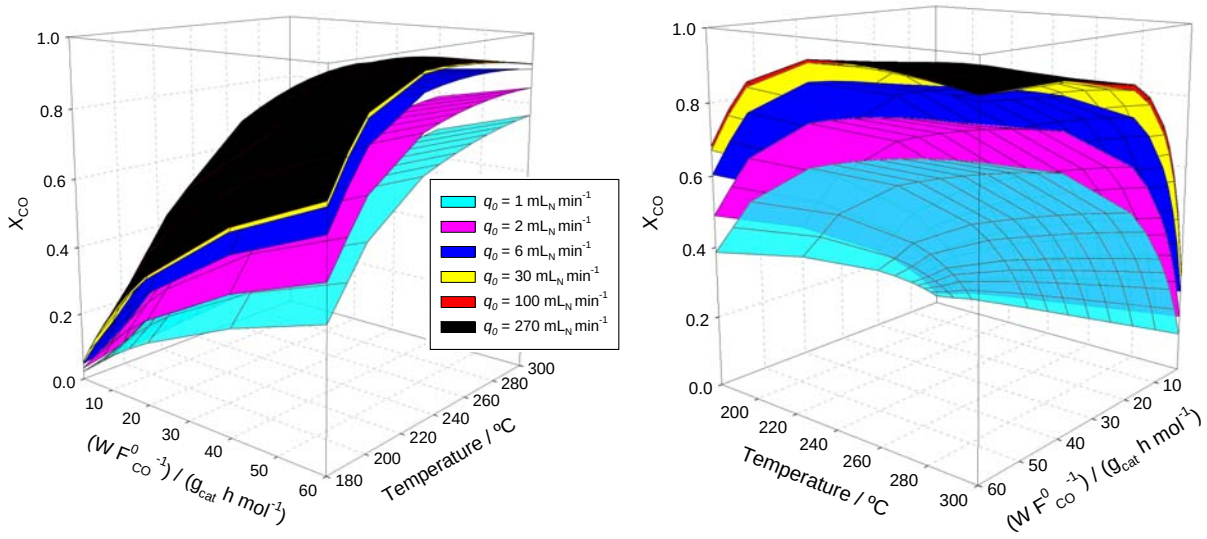

Figure 17. Different perspectives of the space time and temperature effect in the theoretical CO Conversion by **Model 4** (see Table 5 for additional operating parameters).

5.1.2.5 Comparison of the models

Comparing all phenomenological models, it is possible to highlight some similitude between them, for example Models 1 and 3 represent the simplest models, in which is not considered any axial diffusion. As a consequence, the theoretical conversion is not (Model 1) or almost not (Model 3) dependent upon the flow rate (as mentioned before), if $W_{cat}/F_{CO}{}^0$ is kept constant. Figure 18 shows that the conversion obtained by Model 1 is a little bit higher than that obtained by Model 3, but the difference is marginal ($\Delta X_{\mathrm{CO}} = X_{\mathrm{CO_{Model1}}} - X_{\mathrm{CO_{Model3}}} < 2\ \%$). In both cases, when the space time and temperature increase the conversion is approaching the equilibrium value.

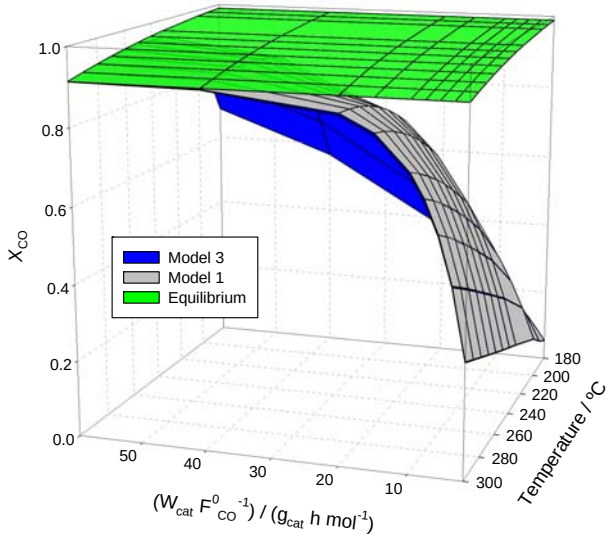

Figure 18. Effect of the space time and temperature in the theoretical CO Conversion by **Models 1 and 3** (see Table 5 for additional operating parameters).

In the case of Models 2 and 4, both consider the dimensionless Peclet number (Pe_m), the first simulating a pseudo-homogeneous system while the latter considers heterogeneous conditions. In Figure 19 is represented the CO conversion for these models for two different flow rates. In any case, Model 2 predicts always a better performance, because external mass transfer resistance does not exist. It is noteworthy that when the flow rate is lower the difference between the results for the two models is bigger; this is a consequence of being more relevant the effects of the external mass-transfer resistance.

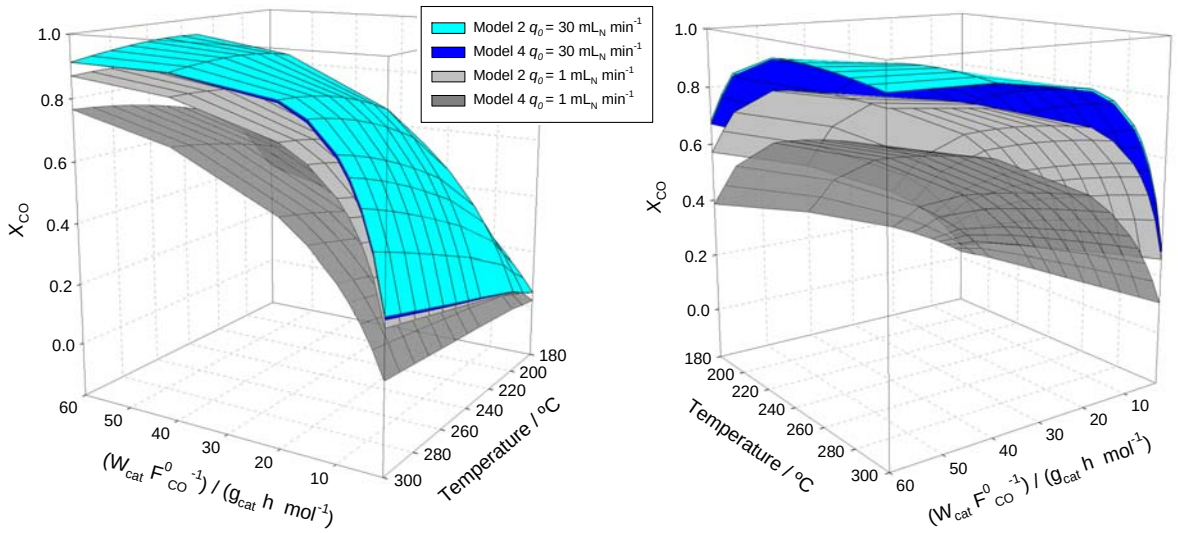

Figure 19. Different perspectives of the space time and temperature effect in the theoretical CO Conversion by **Models 2 and 4** (see Table 5 for additional operating parameters).

After studying the response of the different phenomenological models to the different operating conditions, particularly the effect of the feed flow rate in the performance of WGS reactor, arises the necessity to validate this models. Then, in the next sections experimental data are reported, in which was varied the flow rate and pressure for a typical steam reforming composition. The CO or H_2O-content in feed was also varied, and the result compared with model predictions.

5.1.3 Validation of the Phenomenological Models

The goal of this study was to validate which model(s) has(have) a better performance, when compared with experimental data, even when the WGS reactor is not operating in the ideal conditions or it is not possible to suppose all resistances (internal and external) negligible.

In this section, the feed flow rate, pressure and the feed composition will be changed to evaluate the effect of the different reactant concentrations. The operating conditions are described in Table 6.

Table 6. Operational parameters and reactor dimensions.

Operational parameters	
Temperature range [K]	453.15 – 573.15
Feed Pressure [kPa]	~120; ~300 and ~600
Mass of Catalyst [mg]	250
Feed composition	Mixture 1 to 5 (see Table 4)
Flow Rate in the Feed [$mL_N \cdot min^{-1}$]	40 - 80 - 150
Reactor dimensions	
Diameter [cm]	0.60

5.1.3.1 Effect of the flow rate and temperature

In this section it is reported the results of experimental data obtained when a feed composition consisted in a typical reforming gas mixture (Mixture 1 - Table 4) is used, but for different feed flow rates (40, 80 and 150 $mL_N \cdot min^{-1}$) with the same mass of catalyst (250 mg), i.e., for different space times.

The CO conversions were predicted using all phenomenological models proposed (see section 3.1), with the objective of finding the model that had the better performance when compared with the experimental result. The composed kinetic model that was described previously in section 5.1.1 will be used, in which LH1 is employed for the lowest temperatures and the Redox model for the highest temperatures.

In Figure 20 a, b and c) are represented, for the different flow rates, the experimental CO conversions and the conversions obtained theoretically, for each phenomenological model (Models 1 to 4). For a better visualization of the goodness-of-fit, in Figure 20 d) is illustrated the result of the criteria mentioned above, putting into evidence that the best fit was proportionated by Model 4, for all experimental data.

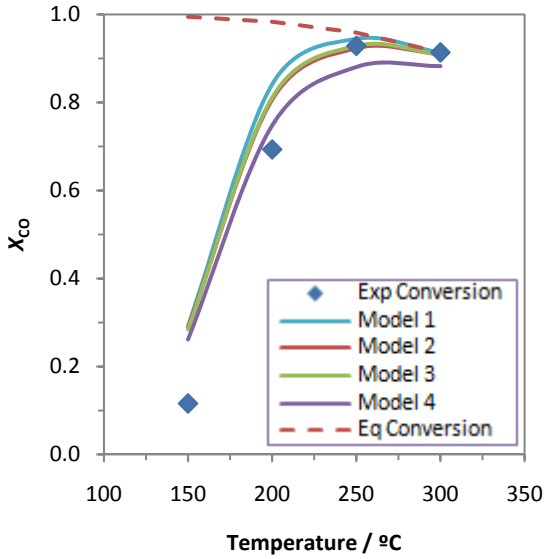

a) Flow Rate: 40 $mL_N \cdot min^{-1}$

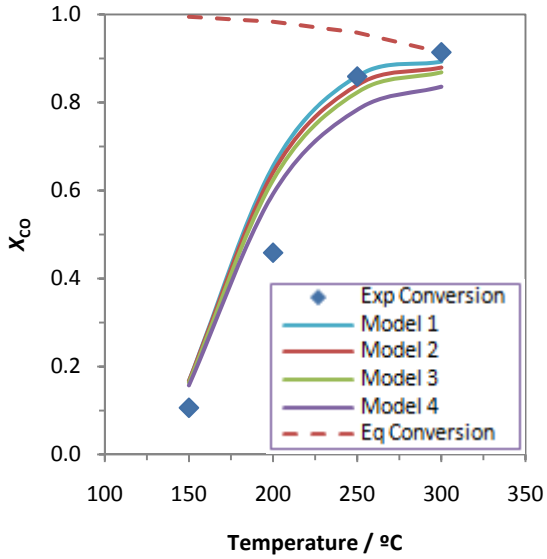

b) Flow Rate: 80 $mL_N \cdot min^{-1}$

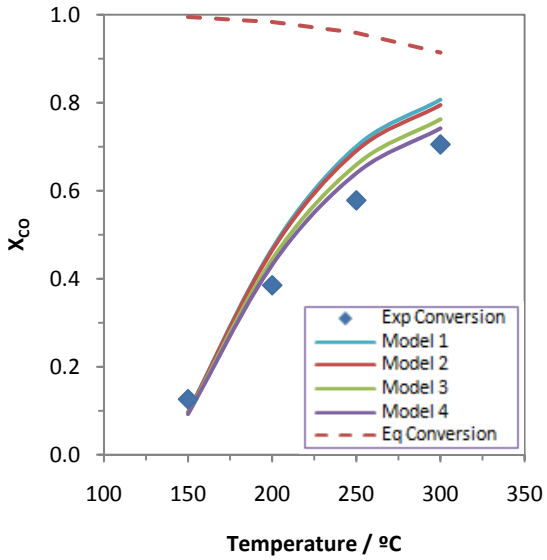

c) Flow Rate: 150 $mL_N \cdot min^{-1}$

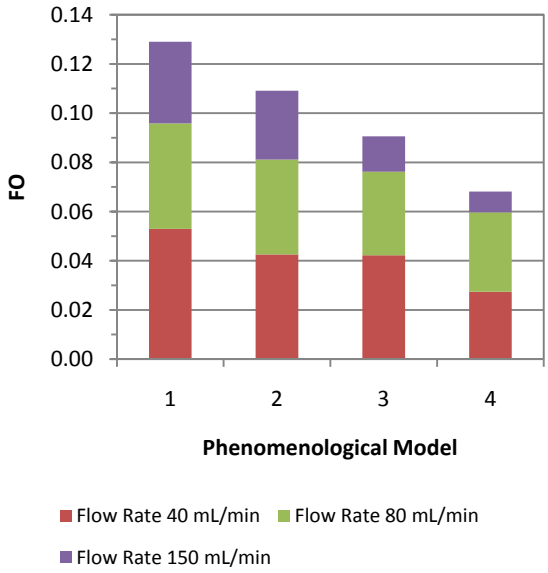

d) Comparison objective function for the four models

Figure 20. Effect of the temperature on the CO conversion at different feed flow rate (a-c) and goodness of fit for the tested models (d). Feed composition: 4.70 % CO, 34.78 % H_2O, 28.70 % H_2, 10.16 % CO_2, 21.66 % N_2 (vol %), and Pressure 120 kPa.

It important to highlight that the kinetics used are only valid for the temperature range between 180 - 300 ºC; then, this is probably the reason why the largest deviation between the experimental data and theoretical predictions occur at 150 ºC (Figure 20 a-c) . Nevertheless, all models respond well, with the same behavior of experimental data when changing either the temperature or the feed flow rate.

Figure 21 shows the effect in the CO conversion when the space time (W_{cat}/F_{CO}^{0}) is changed, i.e. when the flow rate changes for the same mass of catalyst, and the results obtained for Model 4. For the same temperature and mass of catalyst, if the flow rate increases the residence time of the fluid elements in the reactor decrease and consequently a decrease in conversion occurs. The model predicts reasonably well the trends, in a large range of carbon monoxide conversion data (from ca. 10 to 90 %).

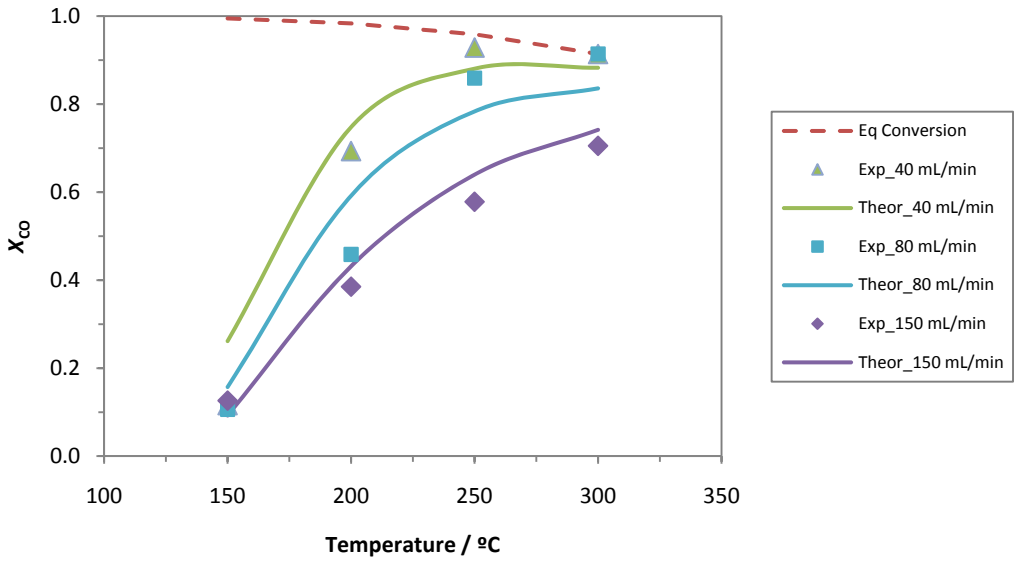

Figure 21. Effect of the flow rate and temperature in the CO conversion. Points experimental CO conversion, continuous line CO conversion by Model 4, dashed line equilibrium CO conversion.

In the next sections changes were made in the water vapor and CO content in feed, maintaining fixed the composition of CO_2, H_2 and balance with N_2, with the objective of verifying the performance of the WGS reactor and the results obtained by the proposed model (Model 4).

5.1.3.2 Effect of the H_2O content in the feed.

In Figure 22, it is possible to see that an increase in the water vapor content in the feed has a positive effect in the conversion (in all temperature range 150 – 300 ºC). This fact is in agreement with the positive reaction order with respect to water obtained in power law rates (Mendes et al., 2009). Besides, the trends also follow the thermodynamic predictions (cf. dashed lines), as a consequence of the Le Chatelier's principle.

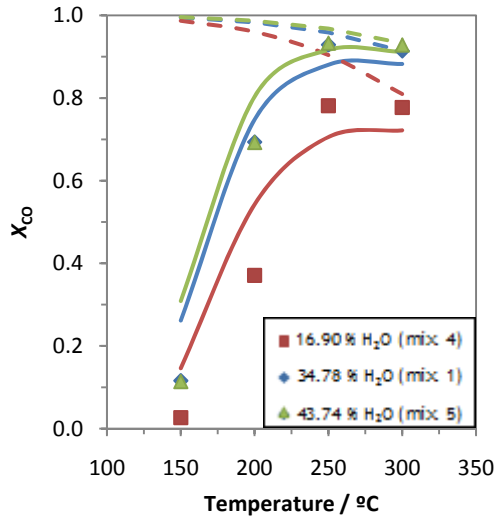

a) Flow Rate: 40 $mL_N \cdot min^{-1}$

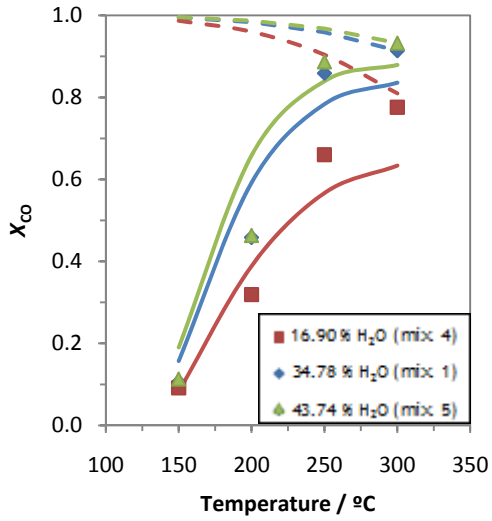

b) Flow Rate: 80 $mL_N \cdot min^{-1}$

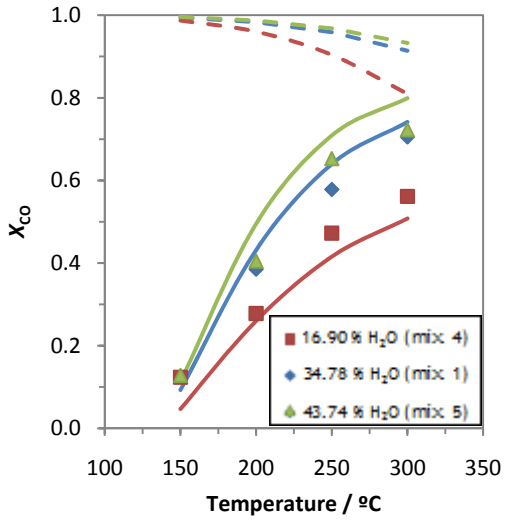

c) Flow Rate: 150 $mL_N \cdot min^{-1}$

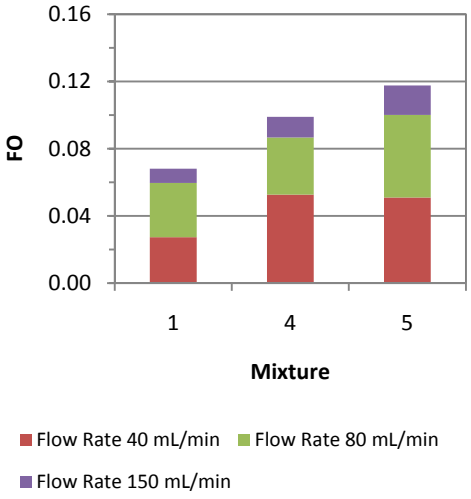

d) Comparison objective function for 3 mixtures

Figure 22. Effect of H_2O content in the CO conversion for different flow rate (a-c) and goodness of fit for the composition tested (d). Feed composition: ■16.90 % H_2O (mixture 4), ◆34.78 % H_2O (mixture 1) and ▲43.74 % H_2O (mixture 5) in all cases the rest of feed is: 4.70 % CO, 28.70 % H_2, 10.16 % CO_2, and the balance N_2 (vol. %). In all figures the point represent the experimental conversion, the continuous line represents the conversion for **Model 4**, and the dashed line the equilibrium.

In the simulations the best fit were reached for mixture 1 (34.78 % of H_2O – Fig. 17 d), possibly because this was the composition for which the kinetic model used was developed and optimized. Nevertheless, the results of the simulation have in general a good description of the experimental behavior. It is important to highlight that, when the flow rate increases (for the same mass of catalyst), a decrease in the space time, so the conversion must also decrease, as show in Figure 22 a, b and c.

Figure 23 shows the CO conversion for Model 4, with the variation of both temperature and H_2O/CO ratio (when the CO-content was fixed). As shown previously, by increasing the content of water vapor or temperature the conversion increases too, by in the range studied is still far from the thermodynamic limit. Here, the use of a membrane reactor came be very useful.

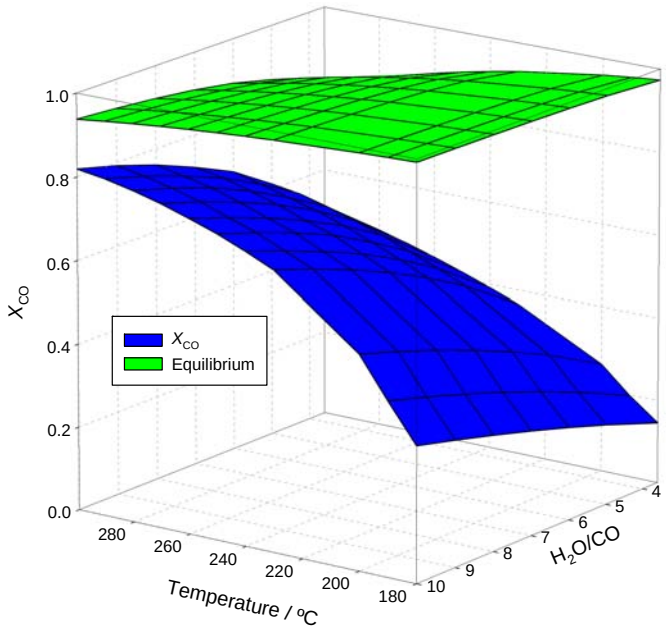

Figure 23. Effect of the H_2O/CO ratio and temperature in the theoretical CO Conversion by **Model 4,** when changing the H_2O content in feed, keeping constant the rest of components (for a typical gas reforming, mixture 1 – see Table 4); Flow rate: 150 $mL_N \cdot min^{-1}$.

5.1.3.3 Effect of the CO content in the feed

In this case the content of water vapor was kept constant while changing the CO content in the feed; the results are represented in Figure 24. The performances in the WGS reaction, at least at temperatures up to 250 ºC, have apparently a behavior that seems to contradict the predictions by the Le Chatelier's principle, because a decrease of the CO content in the feed produces an increase in the performance. Nevertheless, this behavior was also observed in other experimental works (Amadeo and Laborde, 1995; Mendes et al., 2009).The reason for this negative effect at lower temperatures was explained by Mendes et al. (2009) as being a consequence of intermediate species formed during the reaction (in the associative mechanism). Then, once the CO concentration increases, the formation of intermediate species also increases, and the coverage of this species over the catalyst surface increases. Therefore, a blocking effect of the active sites by the reaction intermediates occurs, being more severe at lower temperatures. However, for higher temperatures, and depending on the feed flow rate and composition, it seems that this trend is reversed, tending to follow the

thermodynamic predictions (i.e., for higher CO contents in the feed a higher conversion is obtained). In addition, the phenomenological model proposed has a good description of this unexpected behavior.

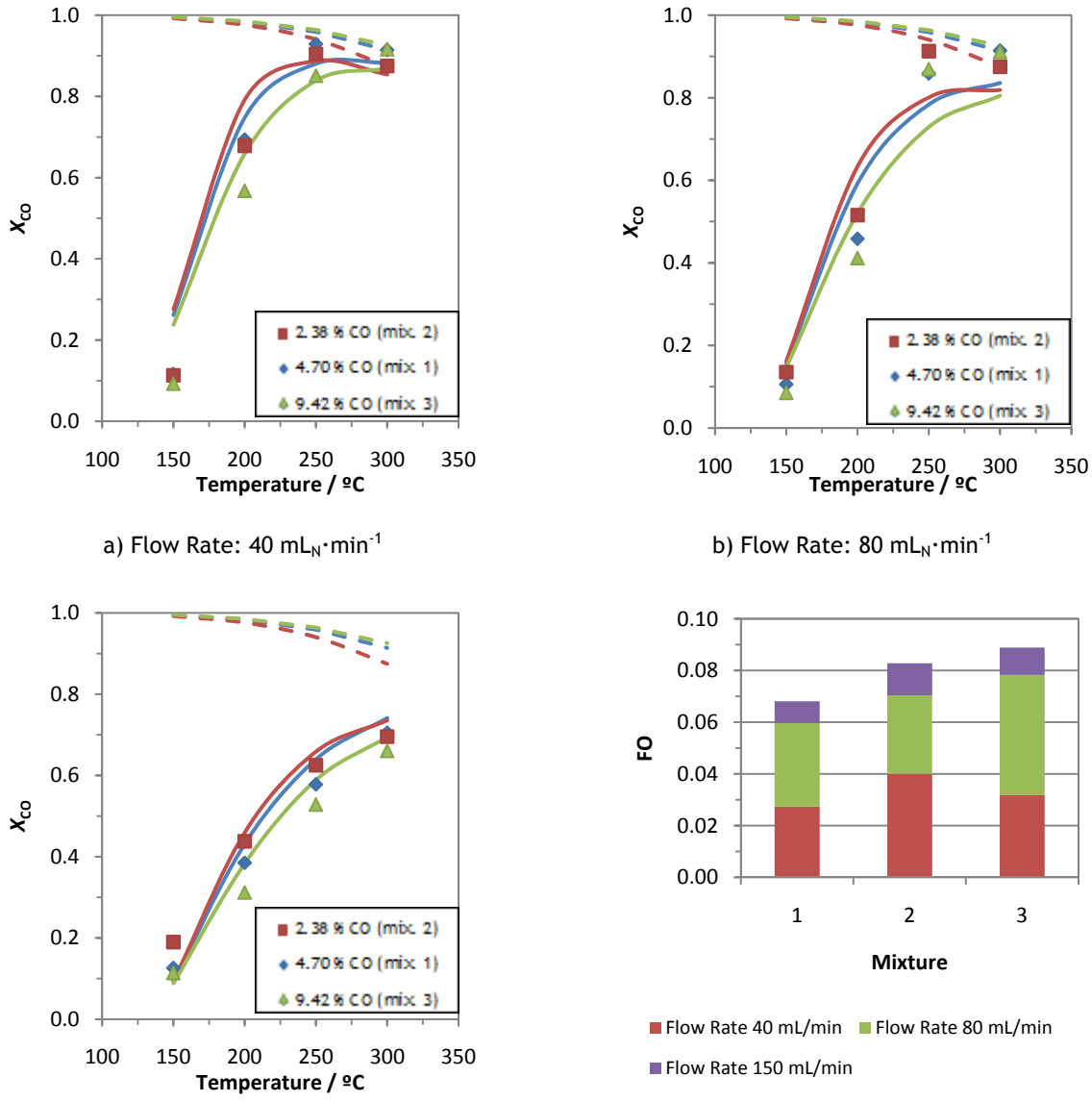

a) Flow Rate: 40 $mL_N \cdot min^{-1}$

b) Flow Rate: 80 $mL_N \cdot min^{-1}$

c) Flow Rate: 150 $mL_N \cdot min^{-1}$

d) Comparison objective function for 3 mixtures

Figure 24. Effect of CO content in the CO conversion for different flow rate (a-c) and goodness of fit for the composition tested (d). Feed composition ■ 2.38 % CO (mixture 2), ◆ 4.70 % CO (mixture 1) and ▲ 9.42 % CO (mixture 3), in all cases the rest of feed is 34.78 % H_2O, 28.70 % H_2, 10.16 % CO_2, and the balance N_2 (vol. %). In all figures the point represent the experimental conversion, the continuous line represents the conversion for **Model 4**, and the dashed line the equilibrium.

Figure 25 shows the CO conversion for Model 4, with the variation of both temperature and H_2O/CO ratio (when the H_2O content was fixed, for a flow rate of 150 $mL_N \cdot min^{-1}$). When there is an increment in the temperature the conversion also increases, because it is below the

thermodynamic limit. Regarding the effect of the H_2O/CO ratio, as shown above the conversion also increases with this parameter (lower CO contents in the feed).

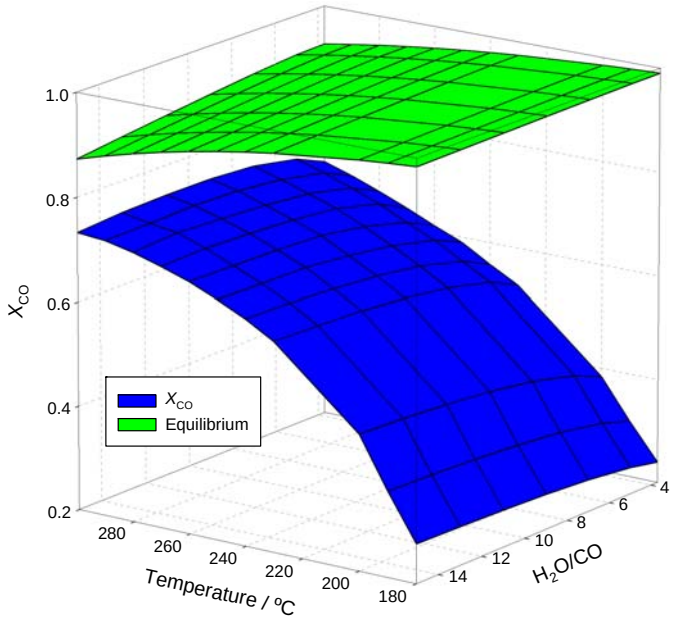

Figure 25. Effect of the H_2O/CO ratio and temperature in the theoretical CO Conversion by **Model 4,** when change the CO content in feed, keeping constant the rest of component (for a typical gas reforming, mixture 1 – see Table 4) and the balance N_2. Flow rate: 150 $mL_N \cdot min^{-1}$

Although the increase in the H_2O/CO ratio has a positive effect in the CO conversion, the response is different when it is changed the CO or the H_2O content in the feed. In Figure 26 is represented, for a flow rate of 150 $mL_N \cdot min^{-1}$, the CO conversion obtained in each case (content of CO or H_2O constant). This follows the thermodynamics predictions when the water content is changed (shift effect). But in case the H_2O content in the feed does not change, the reactor performance shows the opposite trend, leading to smaller CO conversions for lower H_2O/CO ratios – i.e., higher CO concentrations. In this case the kinetics or mechanistic effects prevail, as explained above (the intermediate species formed during the reaction block the active sites, being this effect more notorious for higher carbon monoxide concentrations).

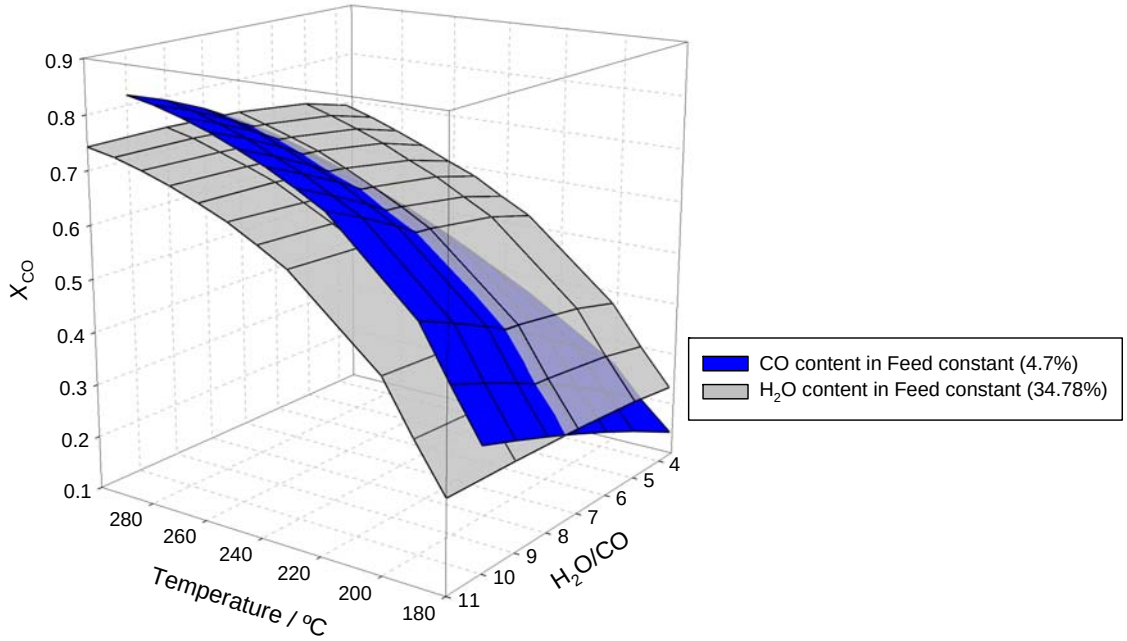

Figure 26. Effect of the H_2O/CO ratio in the theoretical CO Conversion by **Model 4.** Flow rate: 150 $mL_N \cdot min^{-1}$.

5.1.3.4 Effect of the Feed Pressure

In this section are reported the results obtained when the feed pressure was varied (~120; ~300 and ~600 kPa). for the typical reforming gas mixture (mixture 1 – see Table 4), and two flow rates (40 and 150 $mL_N \cdot min^{-1}$).

It is clearly seen from Figure 27 that, when the pressure increases (and regardless the flow rate), the CO conversion increases proportionally too, at least at low temperatures. This result was somehow expected because an increment in the feed pressure leads to an increase in the rate of reaction, and as consequence a better performance of the reactor is obtained. The same result is noticed when the temperature increases, if still far from the equilibrium conditions.

The increasing performance with the feed pressure brings the consequence that, for the same temperature, it is possible to obtain the same conversion with different space times and pressures. For example Figure 27 a) (flow rate = 40 $mL_N \cdot min^{-1}$) and for a temperature of 200 ºC at atmospheric pressure, a conversion of ~69 % is obtained; when the flow rate is 150 $mL_N \cdot min^{-1}$ (i.e. the space time decreases by a factor of 3.75, because the mass of catalyst is the same), Figure 27 b) shows that for the same temperature a pressure of ~300 kPa is required to attain approximately the same conversion level.

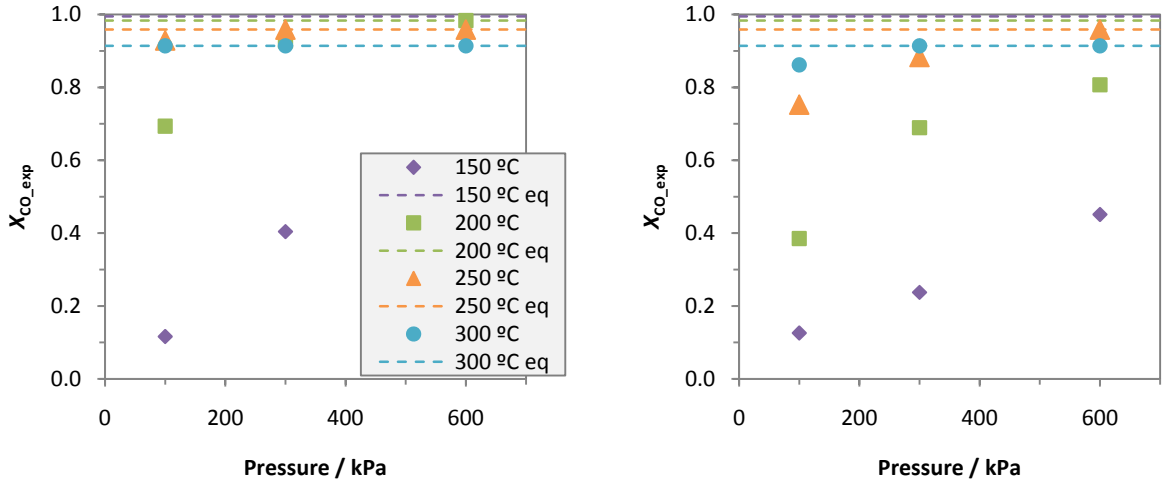

a) Flow Rate: 40 $mL_N \cdot min^{-1}$

b) Flow Rate: 150 $mL_N \cdot min^{-1}$

Figure 27. Effect of the feed pressure in the CO conversion at different reaction temperatures and flow rates. In all figures the points represent the experimental conversion and the dashed line the equilibrium.

Figure 28 shows the parity plot for the experimental data and the result obtained considering the pressure scale-up factor (see section 3.1.3). It is possible to be observed that when the pressure increases the error associated for the calculated conversion increases. The reason for this may be the fact that the kinetic models are not adequate for this case (pressures above the atmospheric one), even using the pressure scale-up factor, or that this pressure scale-up factor is too low. Nevertheless, and up to the author's knowledge, no other factors have been reported in the literature.

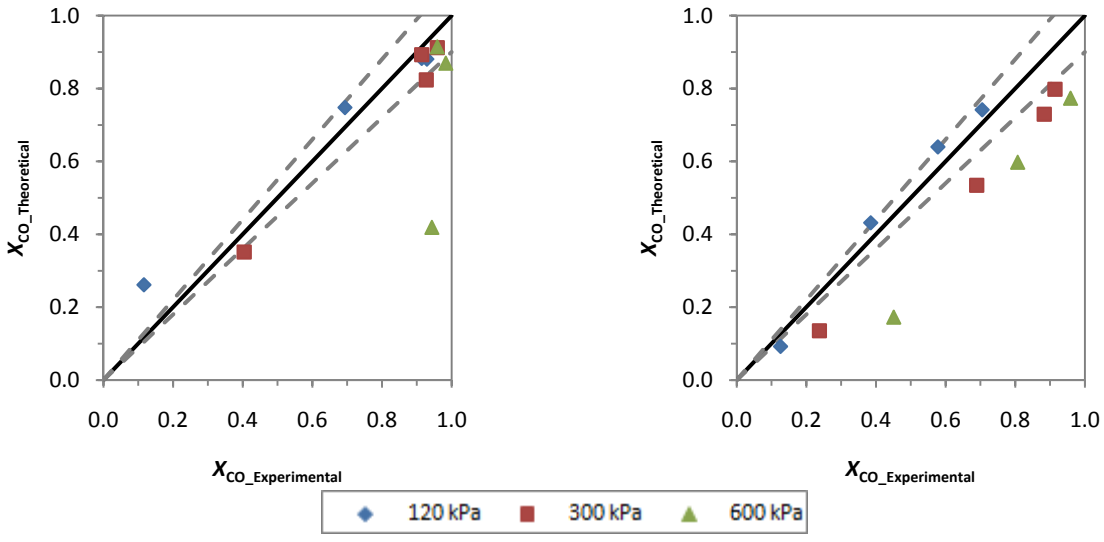

a) Flow Rate: 40 $mL_N \cdot min^{-1}$

b) Flow Rate: 150 $mL_N \cdot min^{-1}$

Figure 28. Parity plots (experimental vs. theoretical CO conversion) using the phenomenological **Model 4.** In both figures the dashed line represents an interval of ±10 % of error.

To study also the effect of temperature in the response of the model, in Figure 29 is represented the CO conversion obtained by Model 4 if different temperatures and pressures along with the experimental data. The largest deviation is at 150 ºC, as consequence of extrapolating the kinetic model for operational conditions very different of which it was determined. Finally, and as shown before, the increase in the flow rate leads to a decrease in the CO conversion (if the mass of catalyst is kept constant), this is not depending of the feed pressure.

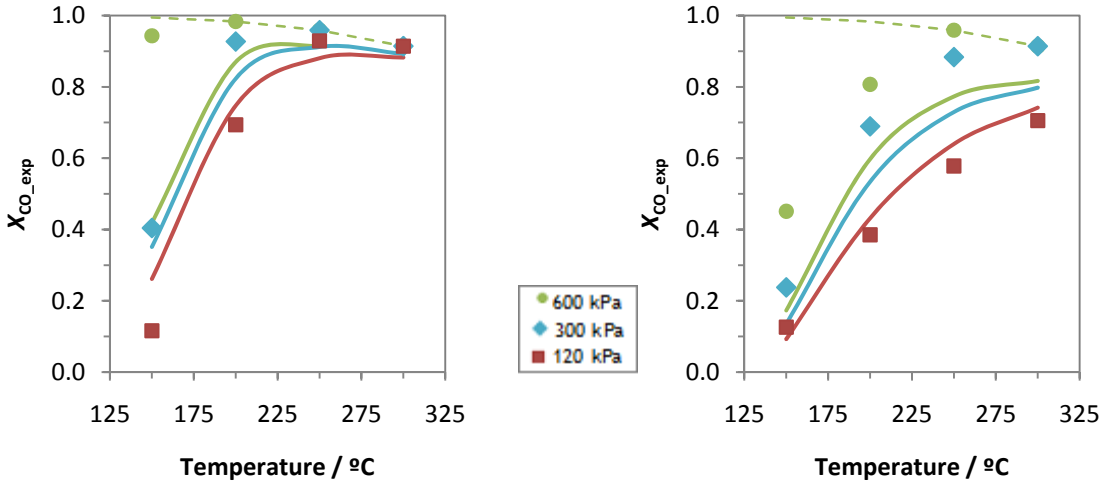

a) Flow Rate: 40 $mL_N \cdot min^{-1}$ b) Flow Rate: 150 $mL_N \cdot min^{-1}$

Figure 29. Effect of the reaction temperature in the CO conversion at different pressures and flow rates. In all figures the point represent the experimental conversion, the continuous line represents the conversion for **Model 4** using the pressure scale-up factor**,** and the dashed lines the equilibrium.

5.2 Membrane Reactor

In this section it was studied the performance reached by a membrane reactor (MR), by assuming the use of a selective hydrogen membrane, able to remove it from the reaction medium. The flow through the membrane was defined by the Sievert's law (cf. section 2.2). For the simulation of the MR the same operating conditions used in section 5.1.1 were employed, i.e. when validating the kinetics and inherently Model 1, with the purpose of comparing the performance of both traditional and membrane reactors (TR and MR) for the assumptions of Model 1 (plug flow and no external mass transfer resistances). A feed pressure of 1 bar was considered in both cases, being null in the permeate for the MR.

Figure 30 shows the predicted conversion 3D plot when varying the contact time and the temperature. It can be seen that the membrane reactor reflects a better conversion when

compared with the traditional reactor in similar operating condition, in all range of temperature and space time values. It is worth noting that the maximum conversion that can theoretically be obtained in the TR, imposed by the equilibrium condition, can be overcome with the MR as a consequence of the hydrogen withdrawal from the reaction system. This seems to occur particularly at higher temperatures and space time values because not only the performance is improved, but also because in these conditions hydrogen permeation is favored (it is a thermal activated process and the residence time of fluid elements is improved in that conditions).

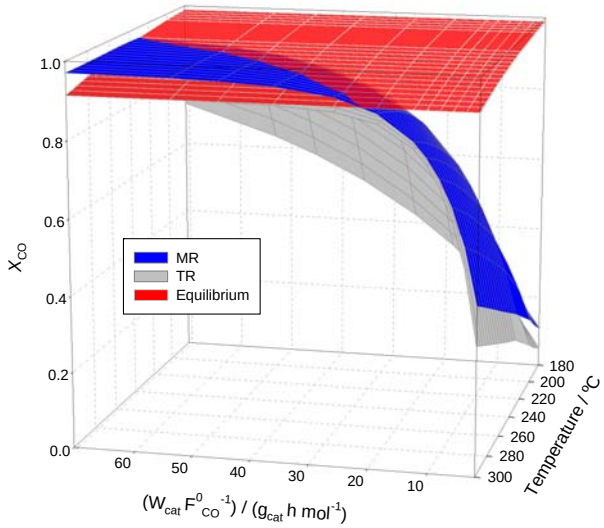

Figure 30. Comparison of the performance the TR and MR for the WGS reaction. Membrane thickness 60 μm.

In Figure 31 are represented the molar fraction profiles along the axial position of a TR and a MR for both CO and H_2. In both cases the CO concentration decreases, as expected, but in the MR goes beyond the equilibrium line (defined based on feed conditions), which is the limit for the TR. Regarding hydrogen, which is also present in the feed (a simulated reformate composition was used), it increases following the expectations in the TR. For the MR, and although being produced through the WGS reaction, after ca. 5 % of the reactor length its concentration starts decreasing, due to the use of the H_2-selective membrane. At the high temperature of the simulation the permeation is enhanced, shifting the reaction in the forward direction, thus allowing to overcome the "thermodynamic barrier" in terms of CO conversion.

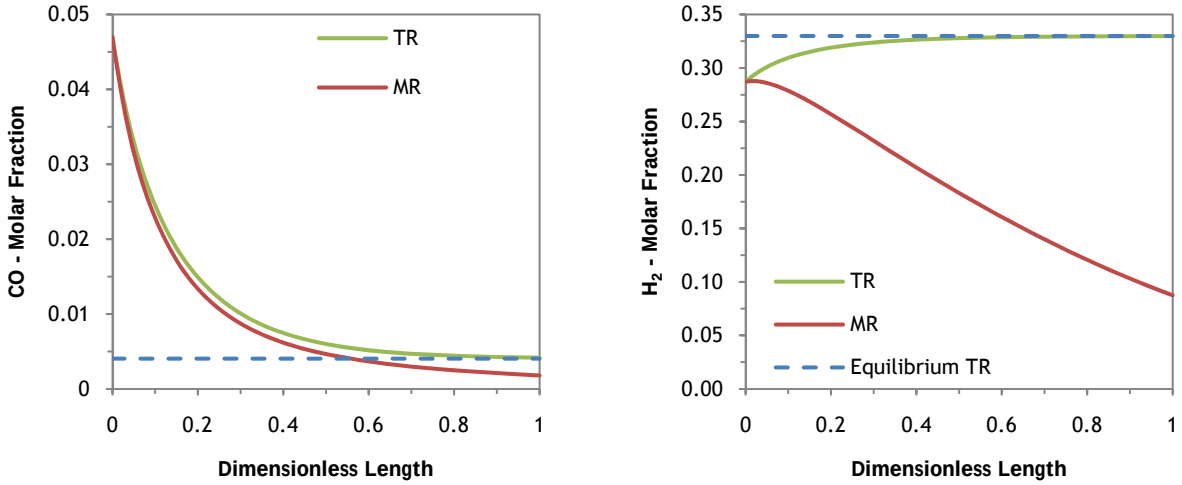

Figure 31. Comparison of molar fraction to CO and H_2 inside the reaction chamber for the TR and MR. At 300 °C and space time of 40 g·h·mol^{-1}.

In case of decreasing the membrane thickness, which would be important in terms of membrane cost saving, the performance is improved, as presented in Figure 32. This can be explained by equation (20), because the flux of hydrogen through the membrane increases while the thickness decreases. Further study is important to be done for lower thicknesses, but taking into account membrane mechanical resistance and feasibility in the synthesis.

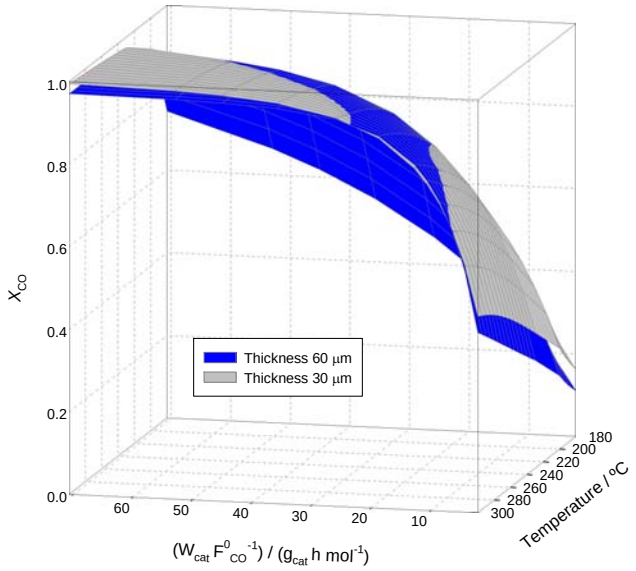

Figure 32. Effect of the membrane thickness in the performance of a WGS MR.

6 Conclusions and Future Work

In this work the water-gas shift (WGS) process was addressed. First of all a composed kinetics over a commercial copper-based catalyst, with a Langmuir-Hinshelwood equation for the lower temperatures and the Redox model for higher temperatures, was validated, showing a good adherence to experimental data.

Following, different phenomenological packed-bed models developed. A parametric study was then carried out, to analyze the effect of different parameters like the space time and Peclet number. Then, experimental work was done to validate the model's predictions (CO conversion in the WGS reaction), in a wide range of operating conditions: temperature between 150 and 300 ºC, pressure from 100 to 600 kPa, flow rate in the range 40 - 150 $mL_N \cdot min^{-1}$ and diverse H_2O/CO ratios in the feed, for a typical reforming stream. It was possible to conclude that:

- For Model 1 (ideal plug flow hypothesis), the fluid flow rate does not affects the CO conversion when the space time is kept constant. For Model 3 (plug flow and external mass transfer resistance), the same variable almost does not affect the WGS reactor performance. However, for the other models this is not true do to the effect of the flow rate in the Peclet number;
- Among all the models tested, the one that provided a better fitting to experimental data was the heterogeneous Model 4, in which external resistances to mass transfer are not negligible and axial dispersion has to be taken into account;
- As expected, and verified either experimentally or theoretically, both the space time and temperature have a positive effect in the CO conversion for a traditional packed-bed reactor, when the WGS reaction is not yet in equilibrium conditions (in the equilibrium the conversion decreases with temperature due to the exothermal nature of the reaction);
- When the H_2O content in the reactor feed increases, keeping constant the other reactants/products concentrations (by adjusting the balance with N_2), the CO conversion increases, following the predictions by the Le Chatelier's principle. However, when the CO concentration in the feed increases, a negative effect in the CO conversion was observed at lower temperatures, attributed to a blocking effect of the active sites by the reaction intermediates. This goes apparently against the Le Chatelier's principle;
- An increase in the feed pressure has a positive effect in the CO conversion, but a good scale-up factor was not found.

Finally, a simple membrane reactor model was developed. It was found that the MR has a better performance when compared (for the same operating conditions) with a TR, as a consequence of the hydrogen permeation through the membrane (shift effect). Besides, under some conditions it is possible to overcome the thermodynamic equilibrium (based on feed conditions), which is the limit for conventional reactors.

Some topics/ideas that could be further explored in future work are the following:

- Determine the kinetic parameters of the rate equations at different pressures, to obtain a better pressure scale-up factor (so that better predictions can be reached in conditions closer to industrial operation);
- Determine the kinetic parameters for different feed compositions (because in real practice the reforming units provide streams with very different compositions, depending on the hydrocarbon used);
- For the modeling studies, and depending on the conditions, eventually consider non-isothermal operation and pressure drop in the bed;
- Validate the MR model proposed against experimental data;
- Develop more elaborated models for the MR (e.g. considering axial dispersion in the packed bed – retentate side – and external resistances to mass transfer, like in Model 4) and perform a parametric study;
- Develop similar studies, but considering a higher temperature (in real practice the WGS reaction is conducted at two different temperature levels).

7 References

Adams, T. A., and Barton, P. I. 2009. A dynamic two-dimensional heterogeneous model for water gas shift reactors. *International Journal of Hydrogen Energy* 34 (21):8877-8891.

Amadeo, N. E., and Laborde, M. A. 1995. Hydrogen production from the low-temperature water-gas shift reaction: Kinetics and simulation of the industrial reactor. *International Journal of Hydrogen Energy* 20 (12):949-956.

Ayastuy, J. L., Gutierrez-Ortiz, M. A., Gonzalez-Marcos, J. A., Aranzabal, A., and Gonzalez-Velasco, J. R. 2004. Kinetics of the Low-Temperature WGS Reaction over a CuO/ZnO/Al2O3 Catalyst. *Industrial & Engineering Chemistry Research* 44 (1):41-50.

Baade, W. F., Parekh, U. N., and Raman, V. S. 2001. Hydrogen In *Encyclopedia of Chemical Technology*, edited by I. John Wiley & Sons.

Basile, A., Paturzo, L., and Lagana, F. 2001. The partial oxidation of methane to syngas in a palladium membrane reactor: simulation and experimental studies. *Catalysis Today* 67 (1-3):65-75.

Basile, A., Gallucci, F., and Paturzo, L. 2005. Hydrogen production from methanol by oxidative steam reforming carried out in a membrane reactor. *Catalysis Today* 104 (2-4):251-259.

Bond, G. C. 1974. *Heterogeneous catalysis principles and applications*. Oxford: Clarendon Press.

Boutikos, P., and Nikolakis, V. 2010. A simulation study of the effect of operating and design parameters on the performance of a water gas shift membrane reactor. *Journal of Membrane Science* 350 (1-2):378-386.

Choi, Y., and Stenger, H. G. 2003. Water gas shift reaction kinetics and reactor modeling for fuel cell grade hydrogen. *Journal of Power Sources* 124 (2):432-439.

Figueiredo, J. L., Ribeiro, F. R., Orfão, J. J. d. M., Lemos, F., and Guisnet, M. 2007. *Catálise heterogénea*. 2ª rev. e actualizada ed. Lisboa: Fundação Calouste Gulbenkian. Serviço de Educação e Bolsas.

Francesconi, J. A., Mussati, M. C., and Aguirre, P. A. 2007. Analysis of design variables for water-gas-shift reactors by model-based optimization. *Journal of Power Sources* 173 (1):467-477.

Froment, G. F., and Bischoff, K. B. 1990. *Chemical Reactor Analysis and Design*. 2nd ed. New York: John Wiley.

Ghenciu, A. F. 2002. Review of fuel processing catalysts for hydrogen production in PEM fuel cell systems. *Current Opinion in Solid State & Materials Science* 6 (5):389-399.

Itoh, N., and Xu, W. C. 1993. Selective Hydrogenation of Phenol to Cyclohexanone Using Palladium-Based Membranes as Catalysts. *Applied Catalysis a-General* 107 (1):83-100.

Koffler, S. A., Hudson, J. B., and Ansell, G. S. 1969. Hydrogen permeation through alpha-palladium. *Trans. Metall. Soc. AIME* 245:1735-1740.

Ladebeck, J. R., and Wang, J. P. 2003. Fuel Cell Technology and Applications. In *Handbook of Fuel Cells*, edited by I. John Wiley & Sons. England.

Levenspiel, O. 1999. *Chemical reaction engineering*. 3rd ed. New York: John Wiley & Sons.

Lukyanov, B. N., Andreev, D. V., and Parmon, V. N. 2009. Catalytic reactors with hydrogen membrane separation. *Chemical Engineering Journal* 154 (1-3):258-266.

Membrane Technology in the chemical industry. 2001. Weinheim: Wiley-VCH.

Mendes, D., Garcia, H., Silva, V. B., Mendes, A., and Madeira, L. M. 2009. Comparison of Nanosized Gold-Based and Copper-Based Catalysts for the Low-Temperature Water−Gas Shift Reaction. *Industrial & Engineering Chemistry Research* 48 (1):430-439.

Mendes, D., Chibante, V., Mendes, A., and Madeira, L. M. 2010a. Determination of the Low-Temperature Water-Gas Shift Reaction Kinetics using a Cu-based Catalyst. *submitted*.

Mendes, D., Mendes, A., Madeira, L. M., Iulianelli, A., Sousa, J. M., and Basile, A. 2010b. The water-gas shift reaction: from conventional catalytic systems to Pd-based membrane reactors - a review. *Asia-Pacific Journal of Chemical Engineering* 5 (1):111-137.

Mond, L., and Langer, C. 1888. Improvements in Obtaining Hydrogen. British Patent 12608.

Padró, C. E. G., and Keller, J. O. 2005. Hydrogen Energy. In *Encyclopedia of Chemical Technology*, edited by I. John Wiley & Sons.

Pereira, B. D. S. 2008. *Uso de reactores de membrana na reacção de "Water-Gas Shift" para aplicação em células de combustível*. Porto: Tese de Mestrado Integrado, FEUP.

Perry's chemical engineers' handbook. 1997. 7th ed ed. New York: McGraw Hill.

Rautenbach, R., and Albrecht, R. 1989. *Membrane processes*. Chichester: John Wiley and Sons.

Rhodes, C., Hutchings, G. J., and Ward, A. M. 1995. Water-gas shift reaction: finding the mechanistic boundary. *Catalysis Today* 23 (1):43-58.

Singh, C. P. P., and Saraf, D. N. 1980. Simulation of Low-Temperature Water-Gas Shift Reactor. *Industrial & Engineering Chemistry Process Design and Development* 19 (3):393-396.

Tosti, S., Basile, A., Bettinali, L., Borgognoni, F., Chiaravalloti, F., and Gallucci, F. 2006. Long-term tests of Pd-Ag thin wall permeator tube. *Journal of Membrane Science* 284 (1-2):393-397.

Appendix 1 – Phenomenological Models

In this appendix the equations for each phenomenological model proposed in chapter 3 are deducted. In first place it was considered a traditional packed-bed reactor (TR), in which the products remain in reaction section. In the second case, one product (H_2) was retired from the reaction medium by the wall of the packed reactor while the reaction shifts (hydrogen-selective membrane reactor).

A general mass balance in all cases can be written as follows:

$$ACCUMULATION_i = IN_i - OUT_i - PERMEATION_i + GERATION_i \quad \text{(A1.1)}$$

where $ACCUMULATION_i$ is the rate of accumulation for species *i*, IN_i is the input flow rate, OUT_i is the output rate flow, $PERMEATION_i$ is the rate flow of permeation, and $GERATION_i$ is the rate of generation by chemical reaction.

In this study it was considered the system in steady-state, and then the term that refers to accumulation does not exist. Therefore, the general balance for a traditional packed-bed reactor becomes:

$$IN_i = OUT_i - GERATION_i \quad \text{(A1.2)}$$

Obviously, the permeation term only appears in the membrane reactor:

$$IN_i = OUT_i + PERMEATION_i - GERATION_i \quad \text{(A1.3)}$$

A1.1 Traditional Packed-Bed Reactor

In this section two types of reactor models are considered; the first case (pseudo-homogeneous model) considers that there are gradients, both in terms of temperature and concentration, between the main stream and the catalyst surface, i.e. it does not account explicitly to the presence of the catalyst. In the second case, it was assumed separately the catalyst and fluid phase (heterogeneous models). In both cases 1-dimensional models have been assumed, and the main assumptions were:

1. Gases have an ideal behavior;
2. Negligible pressure drop across the bed;
3. Isothermal operation;
4. Reaction takes place only on the catalyst surface;
5. Negligible mass and heat-transfer resistances within the catalyst particle (internal limitations).

A1.1.1 Pseudo-homogeneous one-dimensional models

In this model, it was also assumed negligible the resistances between the catalyst surface and the bulk gas phase, i.e., the external limitations. Considering a differential volume element, for the axial position *z* and respecting to a reactor element with length dz, the material balance may be written for species *i* as follows:

$$(\varepsilon A)\varphi_i|_z = (\varepsilon A)\varphi_i|_{z+dz} + (\vartheta_i r_{\mathrm{CO}})\rho_p(1-\varepsilon)A\mathrm{d}z \tag{A1.4}$$

where ε represents the bed void bed fraction, A is the cross section area of the tubular reactor, φ_i is the molar flow of the species per unit area (or mass flux), ϑ_i is the stoichiometric coefficient for species *i* (negative for reagents and positive for products), $-r_{CO}$ is the rate of consumption of CO (in this study CO is always the limiting reagent), and ρ_p is the particle density.

The product of the particle density, with the occupied bed fraction, results in the bed density $\left(\rho_b = \rho_p(1-\varepsilon)\right)$. Then, in limit when $\mathrm{d}z \to 0$, the material balance for each species *i* comes:

$$\varepsilon\frac{\mathrm{d}\varphi|_i}{\mathrm{d}z} = -(\vartheta_i r_{\mathrm{CO}})\rho_b \tag{A1.5}$$

Now, two possibilities for the flow have been considered; in Model 1, it was only considered a convective contribution, while in Model 2 the flow has a contribution by both convection and diffusion.

MODEL 1

When it is only considered that the molar flow by unit area (φ_i) has a convective contribution:

$$\varphi_i = u_i C_{i\_b} \tag{A1.6}$$

where u_i stands for the interstitial velocity and C_{i_b} for the concentration of species *i* in the bulk. Because in this case (pseudo-homogeneous model) it is not considered any difference between the fluid and the solid phases, it can be assumed negligible the concentration gradient among the bulk stream and the catalyst surface for each species.

The interstitial velocity in the previous equation can be defined as a function of the superficial velocity: $u_i = {}^{u_o}/_{\varepsilon}$.

Due to the stoichiometry of the WGS reaction, the number of moles remains constant while the reaction proceeds (i.e. along the tubular reactor). Because it was assumed negligible the pressure drop across the bed, the superficial velocity can be considered as constant. Then, substituting equation (A1.6) into equation (A1.5), the mass balance for species *i* comes:

$$u_o \frac{\mathrm{d}C_i}{\mathrm{d}z} = -(\vartheta_i r_{\mathrm{CO}})\rho_b \tag{A1.7}$$

For ideal gases:

$$P\,V = n\,R\,T \tag{A1.8}$$

where P is the pressure, V represents the volume, n_i is the mol number, R is ideal gas constant and T is the temperature. Then, the concentration of a particular species *i* can be written as:

$$C_i = {}^{p_i}/_{R\,T} \tag{A1.9}$$

Substituting equation (A1.9) into (A1.7) yields:

$$\frac{dp_i}{dz} = -\vartheta_i r_{\mathrm{CO}} \rho_b \frac{RT}{u_o} \tag{A1.10}$$

To solve this first-order differential equation one boundary condition must be used, for instance the partial pressure of each component at the inlet of the reactor, which is known:

$$p_i|_{z=0} = p_i^0 \tag{A1.11}$$

By introducing the dimensionless parameters $y_i = \frac{p_i}{P_t}$ (molar fraction) and $\bar{z} = \frac{z}{L}$ (dimensionless length) in equation (A1.10), where P_t is the total pressure in reactor section, z is the axial position and L is the packed-bed reactor length, the mass balance for the component *i* comes as follows:

$$\frac{P_t}{L}\frac{\mathrm{d}y_i}{\mathrm{d}\bar{z}} = -(\vartheta_i r_{\mathrm{CO}})\rho_b \frac{RT}{u_o} \tag{A1.12}$$

Then,

$$\frac{\mathrm{d}y_i}{\mathrm{d}\bar{z}} = -(\vartheta_i r_{\mathrm{CO}})\rho_b \frac{RT}{P_t}\frac{L}{u_o} = -(\vartheta_i r_{\mathrm{CO}})\rho_b \frac{Q}{F}\frac{L}{u_o} = -(\vartheta_i r_{\mathrm{CO}})\rho_b \frac{Q}{F}\frac{L}{Q/A} = -(\vartheta_i r_{\mathrm{CO}})\frac{W_{cat}}{F} \tag{A1.13}$$

where Q is the total volumetric flow rate, F is the total molar flow rate, ρ_b the bed density, L the length of the packed-bed reactor, u_o is the superficial velocity, $-r_{\mathrm{CO}}$ is the rate of consumption of CO, and ϑ_i is the stoichiometric coefficient for species *i*. In this expression appears an important parameter, the space time $\left(W_{cat}/F\right)$, which represents the inverse of the ratio between fluid flow rate and the catalyst mass. Finally, the dimensionless equation for species *i*, by Model 1 is the following:

$$\frac{\mathrm{d}y_i}{\mathrm{d}\bar{z}} = -(\vartheta_i r_{\mathrm{CO}})\frac{W_{cat}}{F} \tag{A1.14}$$

To solve the previous first-order differential equation, the following boundary conditions applies (because it is known the molar fraction for each component at the reactor inlet):

$$y_i|_{z=0} = y_i^0 \tag{A1.15}$$

Solution Strategy by Model 1

For the WGS reaction the systems of equations was solved:

$$\frac{\mathrm{d}y_{\mathrm{CO}}}{\mathrm{d}\bar{z}} = -(-r_{\mathrm{CO}})\frac{W_{cat}}{F}; \qquad y_{\mathrm{CO}}|_{\bar{z}=0} = {y_{\mathrm{CO}}}^0 \quad \text{a}$$

$$\frac{dy_{\mathrm{H_2O}}}{d\bar{z}} = -(-r_{CO})\frac{W_{cat}}{F}; \qquad y_{\mathrm{H_2O}}\big|_{\bar{z}=0} = {y_{\mathrm{H_2O}}}^0 \quad \text{b}$$

$$\frac{dy_{\mathrm{CO_2}}}{d\bar{z}} = -(r_{CO})\frac{W_{cat}}{F}; \qquad y_{CO_2}\big|_{\bar{z}=0} = {y_{\mathrm{CO_2}}}^0 \quad \text{c} \tag{A1.16}$$

$$\frac{dy_{\mathrm{H_2}}}{d\bar{z}} = -(r_{CO})\frac{W_{cat}}{F}; \qquad y_{\mathrm{H_2}}\big|_{\bar{z}=0} = {y_{\mathrm{H_2}}}^0 \quad \text{d}$$

$$\frac{dy_{\mathrm{N_2}}}{d\bar{z}} = 0; \qquad y_{\mathrm{N_2}}\big|_{\bar{z}=0} = {y_{\mathrm{N_2}}}^0 \quad \text{e}$$

It worth to note that $-r_{\mathrm{CO}} = -r_{\mathrm{H_2O}} = r_{\mathrm{CO_2}} = r_{\mathrm{H_2}}$. In this study three different kinetic rate equations will be used. For the particular case of the Langmuir-Hinshelwood 1, as shows in section 2.1.3, one has:

$$-r_{\mathrm{CO}} = \frac{k\left(p_{\mathrm{CO}}p_{\mathrm{H_2O}} - \frac{p_{\mathrm{CO_2}}p_{\mathrm{H_2}}}{K_p}\right)}{\left(1 + K_{\mathrm{CO}}p_{\mathrm{CO}} + K_{\mathrm{H_2O}}p_{\mathrm{H_2O}} + K_{\mathrm{H_2}}p_{\mathrm{H_2}} + K_{\mathrm{CO_2}}p_{\mathrm{CO_2}}\right)^2} \tag{12}$$

Because the kinetic rate equations must be written as a function of the molar fractions, from the ideal gas law:

$$-r_{\mathrm{CO}} = \frac{kP_t{}^2\left(y_{\mathrm{CO}}y_{\mathrm{H_2O}} - \frac{y_{\mathrm{CO_2}}y_{\mathrm{H_2}}}{K_p}\right)}{\left(1 + K_{\mathrm{CO}}P_ty_{\mathrm{CO}} + K_{\mathrm{H_2O}}P_ty_{\mathrm{H_2O}} + K_{\mathrm{H_2}}P_ty_{\mathrm{H_2}} + K_{\mathrm{CO_2}}P_ty_{\mathrm{CO_2}}\right)^2} \tag{12a}$$

Substituting the rate equation in the system of equations (A1.16), it can be solved numerically. This has been done using the Matlab software package via a 4th order Runga-Kutta method. The function *ODE45* was used.

However, this system of equations can be simplified, because all components can be set as a function of CO, i.e.

$$y_{\mathrm{H_2O}} = y_{\mathrm{H_2O}}{}^0 - (y_{\mathrm{CO}}{}^0 - y_{\mathrm{CO}}) \quad \text{a}$$

$$y_{\mathrm{CO_2}} = y_{CO_2}{}^0 + (y_{\mathrm{CO}}{}^0 - y_{\mathrm{CO}}) \quad \text{b} \tag{A1.17}$$

$$y_{\mathrm{H_2}} = y_{\mathrm{H_2}}{}^0 + (y_{\mathrm{CO}}{}^0 - y_{\mathrm{CO}}) \quad \text{c}$$

By replacing equations (A1.17) in the kinetic rate equation, the following first-order differential equation was reached, which is only a function of y_{CO}:

$$\frac{\mathrm{d}y_{\mathrm{CO}}}{\mathrm{d}\bar{z}} = -\left(-r_{\mathrm{CO}f(y_{\mathrm{CO}})}\right)\frac{W_{cat}}{F}; \qquad y_{\mathrm{CO}}|_{\bar{z}=0} = y_{\mathrm{CO}}{}^0 \tag{A1.18}$$

This first-order differential equation (equation (A1.18)) was solved numerically, using the Matlab software package via a 4th order Runga-Kutta.

The result of the differential equation was the molar fraction of CO along the axial positions; however, it is interesting to know the conversion, evaluated at the outlet reactor:

$$X_{\mathrm{CO}} = \frac{y_{\mathrm{CO}}{}^0 - y_{\mathrm{CO}}|_{\bar{z}=1}}{y_{\mathrm{CO}}{}^0} \tag{A1.19}$$

MODEL 2

In this case, the the molar flow (φ_i) has two contribution terms, one by convection and another by diffusion:

$$\varphi = u_i C_{i\_b} - D_{ix} \frac{\mathrm{d}C_{i\_b}}{\mathrm{d}z} \tag{A1.20}$$

where D_{ix} is the dispersion coefficient in the axial direction. As in the previous case, in this model there is any concentration gradient among the bulk stream and the catalyst surface for any species *i*. Therefore the concentration in the bulk is equal to the concentration in the catalyst surface. The interstitial velocity can be defined as a function of the superficial velocity and bed void fraction as $u_i = {u_o}/{\varepsilon}$.

Considering that the pressure is constant along the packed-bed reactor, then the superficial velocity is also constant, and substituting equation (A1.20) into equation (A1.5) the mass balance for the species *i* comes:

$$u_o \frac{\mathrm{d}C_i}{\mathrm{d}z} - \varepsilon D_{ix} \frac{\mathrm{d}^2 C_i}{\mathrm{d}z^2} = -(\vartheta_i r_{\mathrm{CO}})\rho_b \tag{A1.21}$$

By the ideal gas law, substituting equation (A1.9) into (A1.22):

$$\frac{u_o}{RT} \frac{\mathrm{d}p_i}{\mathrm{d}z} - \frac{\varepsilon D_{ix}}{RT} \frac{\mathrm{d}^2 p_i}{\mathrm{d}z^2} = -(\vartheta_i r_{\mathrm{CO}})\rho_b \tag{A1.22}$$

Then,

$$\frac{\mathrm{d}^2 p_i}{\mathrm{d}z^2} = \frac{u_o}{\varepsilon D_{ix}} \frac{\mathrm{d}p_i}{\mathrm{d}z} + (\vartheta_i r_{\mathrm{CO}})\rho_b \frac{RT}{\varepsilon D_{ix}} \tag{A1.23}$$

To solve this second-order differential equation, two boundary conditions are necessary. The first condition is the Danckwerts one, and the other boundary condition results from the fact that at the reactor outlet there is no reaction (so the derivative of the partial pressure for each component is null):

$$p_i|_{z=0^-} = p_i|_{z=0^+} - \frac{\varepsilon D_{ix}}{u_o} \frac{\mathrm{d}p_i}{\mathrm{d}z}$$

$$\left.\frac{\mathrm{d}p_i}{\mathrm{d}z}\right|_{z=L} = 0 \tag{A1.24}$$

Similar to the strategy used in Model 1, the following dimensionless parameters were introduced in equation (A1.22): $y_i = \frac{p_i}{P_t}$ (molar fraction) and $\bar{z} = \frac{z}{L}$ (dimensionless length):

$$\frac{P_t}{L^2}\frac{\mathrm{d}^2 y_i}{\mathrm{d}\bar{z}^2} = \frac{u_0}{\varepsilon D_{ix}}\frac{P_t}{L}\frac{\mathrm{d}y_i}{\mathrm{d}\bar{z}} + (\vartheta_i r_{\mathrm{CO}})\rho_b \frac{RT}{\varepsilon D_{ix}} \tag{A1.25}$$

Reordering,

$$\frac{\mathrm{d}^2 y_i}{\mathrm{d}\bar{z}^2} = \frac{u_0 L}{\varepsilon D_{ix}}\frac{\mathrm{d}y_i}{\mathrm{d}\bar{z}} + (\vartheta_i r_{\mathrm{CO}})\rho_b \frac{RT}{P_t}\frac{L^2}{\varepsilon D_{ix}} \tag{A1.26}$$

Putting in evidence both parameters, space time and Peclet number $\left({W_{cat}}/{F^0}\,;\ Pe_m = \frac{u_0 L}{\varepsilon\, D_{ax}}\right)$:

$$\frac{\mathrm{d}^2 y_i}{\mathrm{d}\bar{z}^2} = \frac{u_0 L}{\varepsilon D_{ix}}\frac{\mathrm{d}y_i}{\mathrm{d}\bar{z}} + (\vartheta_i r_{\mathrm{CO}})\rho_b \frac{Q}{F}\frac{L}{{Q}/{A}}\frac{u_0 L}{\varepsilon D_{ix}} \tag{A1.27}$$

Finally, the pseudo-homogeneous Model 2 equation keeps as:

$$\frac{\mathrm{d}^2 y_i}{\mathrm{d}\bar{z}^2} = Pe_m\left(\frac{\mathrm{d}y_i}{\mathrm{d}\bar{z}} + (\vartheta_i r_{\mathrm{CO}})\frac{W_{cat}}{F^0}\right) \tag{A1.28}$$

In previous equations appears a new parameter, the Peclet number, which relates the rate of fluid transport by convection and the rate of diffusion. To solve the previous second-order differential equation, two boundary conditions are needed. As above mentioned:

$$y_i|_{\bar{z}=0^-} = y_i|_{\bar{z}=0^+} - \frac{1}{Pe_m}\frac{\mathrm{d}y_i}{\mathrm{d}\bar{z}}\bigg|_{\bar{z}=0} \quad \text{a}$$

$$\frac{\mathrm{d}y_i}{\mathrm{d}\bar{z}}\bigg|_{\bar{z}=L} = 0 \quad \text{b} \tag{A1.29}$$

It is noteworthy that, when Pe_m is too high, Model 2 becomes Model 1. In fact:

$$\frac{1}{Pe_m}\frac{\mathrm{d}^2 y_i}{\mathrm{d}\bar{z}^2} = \frac{\mathrm{d}y_i}{\mathrm{d}\bar{z}} + (\vartheta_i r_{\mathrm{CO}})\frac{W_{cat}}{F^0} \tag{A1.30}$$

And when $Pe_m \to \infty$, this equations tends to equation (A1.14)

Solution Strategy for Model 2

This case the system of equations can be simplified to one single differential equation, by replacing the kinetic rate equation as a function of only one component:

$$\frac{\mathrm{d}^2 y_{CO}}{\mathrm{d}\bar{z}^2} = Pe_m\left(\frac{\mathrm{d}y_{CO}}{\mathrm{d}\bar{z}} + \left(-r_{\mathrm{CO}\,f(\mathrm{CO})}\right)\frac{W_{cat}}{F^0}\right);\ y_{\mathrm{CO}}|_{\bar{z}=0^-} = y_{\mathrm{CO}}|_{\bar{z}=0^+} - \frac{1}{Pe_m}\frac{\mathrm{d}y_{\mathrm{CO}}}{\mathrm{d}\bar{z}}\Big|_{\bar{z}=0}\ and\ \frac{\mathrm{d}y_{\mathrm{CO}}}{\mathrm{d}\bar{z}}\Big|_{\bar{z}=1} = 0 \qquad \text{(A1.31)}$$

However, the boundary conditions for this equation are expressed at the inlet and outlet of the reactor; then, to solve it is necessary to suppose one condition (at the inlet or outlet), and after solving it one must verify if the other condition was satisfied – if this was not the case, another condition has to be supposed in a iterative way.

At inlet it can be supposed the value for $\frac{\mathrm{d}y_{\mathrm{CO}}}{\mathrm{d}\bar{z}}\Big|_{\bar{z}=0}$, while at the outlet one can suppose the value for $y_{\mathrm{CO}}|_{\bar{z}=1}$. It was considered more simple to assume a value for the molar fraction at the exit, because this value cannot be higher than the value obtained in equilibrium, and as a first estimated it can be used the result of the molar fraction obtained by Model 1. On the other hand the value for the first derivate at the inlet is not easy to suppose, and for this reason in can be difficult to obtain the solution in the iterative process.

To solve the second-order differential equation, a change in the variables was done $\left(\overline{y_{\mathrm{CO}}} = \mathrm{d}y\mathrm{CO}\mathrm{d}z\right.$ to convert the system into one of first-order differential equations, as presented bellow:

$$\overline{y_{\mathrm{CO}}} = \frac{\mathrm{d}y_{\mathrm{CO}}}{\mathrm{d}\bar{z}} \qquad \text{a}$$

$$\frac{\mathrm{d}\overline{y_{\mathrm{CO}}}}{\mathrm{d}\bar{z}} = Pe_m\left(\overline{y_{\mathrm{CO}}} + \left(-r_{\mathrm{CO}\,f(\mathrm{CO})}\right)\frac{W_{cat}}{F^0}\right) \qquad \text{b} \qquad \text{(A1.32)}$$

Boundary Conditions: $\overline{y_{\mathrm{CO}}}|_{\bar{z}=1} = 0$ and $y_{\mathrm{CO}}|_{\bar{z}=0^-} = y_{\mathrm{CO}}|_{\bar{z}=0^+} - \frac{1}{Pe_m}\overline{y_{\mathrm{CO}}}|_{\bar{z}=0}$ c

Finally, this problem was resolved using the function *ODE15s*. For the iterative process the *fminsearch* function was used, in which the final value obtained for the molar fraction at the inlet must satisfy the real conditions within a certain tolerance, i.e. $\left|{y_{\mathrm{CO}}}^0 - {y_{\mathrm{CO}}}^0{}_{\mathrm{calculated}}\right| < 10^{-10}$.

It to noteworthy that, as the system was resolved by end conditions, another change in the variables was done, where $\overline{\mathrm{z}'} = 1 - \bar{\mathrm{z}}$. Then, the system was solved in the boundary condition $\overline{\mathrm{z}'} = 0$, that represents $\bar{\mathrm{z}} = 1$.

Again the conversion of CO was calculated by equation (A1.19). The Peclet number is not constant in the axial positions, because the dispersion coefficient changes with the composition along the reactor (to known how to calculate these properties, please refer to Appendix 1). This effect was considered in the solution of the concentration profiles.

A1.1.2 Heterogeneous one-dimensional models

In this case the two phases were considered separately, and then the mass balances cannot be expressed as in equation (A1.4) - a mass balance for each phase must be done. Considering a differential volume element, for the axial position *z* and respecting to a reactor element with length dz, the mass balances for each species *i* may be written as follows:

For the Fluid:

$$(\varepsilon A)\varphi_i|_z = (\varepsilon A)\varphi_i|_{z+\mathrm{d}z} + k_{f_{i,m}} a_v \Delta C_i A \mathrm{d}z \tag{A1.33}$$

For the Solid:

$$k_{f_{i,m}} a_v \Delta C_i = \left(\vartheta_i r_{\mathrm{CO}(f(C_s))}\right) \rho_p (1-\varepsilon) \tag{A1.34}$$

where k_f is the mass transfer coefficient, a_v is the total external surface area of catalyst per unit volume and ΔC_i is the driving force. It should be noted that, for this case, the rate of reaction is dependent upon the concentration on the catalyst surface, and the driving force is the difference of concentration between the bulk and catalyst surface; for the reagents: $\Delta C_i = C_{i\_b} - C_{i\_s} > 0$.

In the limit when $dz \rightarrow 0$, the mass balance for each species *i* in the fluid phase comes:

$$\varepsilon \frac{\mathrm{d}\varphi|_i}{\mathrm{d}z} = -k_{f_{i,m}} a_v \left(C_{i\_b} - C_{i\_s}\right) \tag{A1.35}$$

As in the previous models, two considerations for the contribution of flow have been done. In Model 3 the flow has only a contribution by convection, while in Model 4 is considered a contribution by both convection and diffusion. In these heterogeneous models any resistances within the solid phase are considered (internal resistances are negligible). Therefore the mass balances in the solid phase are equal for the two models.

MODEL 3

This model can be define as the basic model of the heterogeneous category, because is just considers the convective contribution to the molar fux (φ_i) (plug-flow, as in Model 1). Substituting equation (A1.6) into equation (A1.35), the mass balance for Model 3 stands as:

For the Fluid:

$$u_o \frac{\mathrm{d}C_{i\_b}}{\mathrm{d}z} = -k_{f_{i,m}} a_v \left(C_{i\_b} - C_{i\_s}\right) \tag{A1.36}$$

For the Solid:

$$k_{f_{i,m}} a_v \left(C_{i\_b} - C_{i\_s}\right) = \left(\vartheta_i r_{\mathrm{CO}(f(C_s))}\right) \rho_b \tag{A1.37}$$

For ideal gases, substituting equation (A1.9) into (A1.36) and (A1.37):

For the Fluid:

$$\begin{aligned} \frac{u_o}{RT}\frac{\mathrm{d}p_{i\_b}}{\mathrm{d}z} &= -\frac{k_{f_{i,m}} a_v}{RT}\left(p_{i\_b} - p_{i\_s}\right) \\ \frac{\mathrm{d}p_{i\_b}}{\mathrm{d}z} &= -\frac{k_{f_{i,m}} a_v}{u_0}\left(p_{i\_b} - p_{i\_s}\right) \end{aligned} \tag{A1.38}$$

For the Solid:

$$\frac{k_{f_{i,m}} a_v}{RT}\left(p_{i\_b} - p_{i\_s}\right) = \left(\vartheta_i r_{\mathrm{CO}(f(P_s))}\right) \rho_b \tag{A1.39}$$

Applying a similar strategy used for Models 1 and 2, it was introduced the dimensionless parameters $y_i = \frac{p_i}{P_t}$ (molar fraction) and; $\bar{z} = \frac{z}{L}$ (dimensionless length) in equations (A1.38) and (A1.39), resulting:

For the Fluid:

$$\begin{aligned} \frac{P_t}{L}\frac{dy_{i\_b}}{d\bar{z}} &= -\frac{k_{f_{i,m}} a_v}{u_0} P_t \left(y_{i\_b} - y_{i\_s}\right) \\ \frac{dy_{i\_b}}{d\bar{z}} &= -k_{f_{i,m}} a_v \frac{L}{u_o}\left(y_{i\_b} - y_{i\_s}\right) \end{aligned} \tag{A1.40}$$

For the Solid:

$$\begin{aligned} k_{f_{i,m}} a_v \frac{P_t}{RT}\left(y_{i\_b} - y_{i\_s}\right) - \left(\vartheta_i r_{\mathrm{CO}(f(y_s))}\right) \rho_b &= 0 \\ k_{f_{i,m}} a_v \left(y_{i\_b} - y_{i\_s}\right) - \left(\vartheta_i r_{\mathrm{CO}(f(y_s))}\right) \rho_b \frac{RT}{P_t} &= 0 \end{aligned} \tag{A1.41}$$

To solve this system, one boundary condition is necessary for the first-order differential equation (A1.42)) while the algebraic one is used to calculate the surface catalyst concentration (based on the bulk concentration).

$$y_{i\_b}\big|_{\bar{z}=0} = y_i^0 \tag{A1.42}$$

Solution strategy for Model 3

Here, one has a combination of differential and algebraic equations, because the concentration in the catalyst surface is different from that in the bulk. Therefore, the system was composed by first-order differential equations (for fluid phase) and algebraic equations (condition in the surface catalyst). The system for Model 3 is as follows:

$$\frac{\mathrm{d}y_{CO\_b}}{\mathrm{d}\bar{z}} = -k_{f_{CO,m}} a_v \frac{L}{u_o}\left(y_{\mathrm{CO}\_b} - y_{\mathrm{CO}\_s}\right); \qquad \mathrm{y_{CO\_b}}\big|_{\bar{\mathrm{z}}=0} = \mathrm{y_{CO}}^0 \qquad \text{a.1}$$

$$k_{f_{CO,m}} a_v\left(y_{\mathrm{CO}\_b} - y_{\mathrm{CO}\_s}\right) - \left(-r_{\mathrm{CO}(f(y_s))}\right)\rho_b \frac{RT}{P_t} = 0 \qquad \text{a.2}$$

$$\frac{\mathrm{d}y_{\mathrm{H_2O}\_b}}{\mathrm{d}\bar{z}} = -k_{f_{H_2O,m}} a_v \frac{L}{u_o}\left(y_{\mathrm{H_2O}\_b} - y_{\mathrm{H_2O}\_s}\right); \qquad \mathrm{y_{H_2O\_b}}\big|_{\bar{\mathrm{z}}=0} = \mathrm{y_{H_2O}}^0 \qquad \text{b.1}$$

$$k_{f_{H_2O,m}} a_v\left(y_{\mathrm{H_2O}\_b} - y_{\mathrm{H_2O}\_s}\right) - \left(-r_{\mathrm{CO}(f(y_s))}\right)\rho_b \frac{RT}{P_t} = 0 \qquad \text{b.2}$$

$$\frac{\mathrm{d}y_{\mathrm{CO_2}\_b}}{\mathrm{d}\bar{z}} = -k_{f_{CO_2,m}} a_v \frac{L}{u_o}\left(y_{\mathrm{CO_2}\_b} - y_{\mathrm{CO_2}\_s}\right); \qquad \mathrm{y_{CO_2\_b}}\big|_{\bar{\mathrm{z}}=0} = \mathrm{y_{CO_2}}^0 \qquad \text{c.1}$$

$$k_{f_{CO_2,m}} a_v\left(y_{\mathrm{CO_2}\_b} - y_{\mathrm{CO_2}\_s}\right) - \left(r_{\mathrm{CO}(f(y_s))}\right)\frac{\rho_b}{P_t} = 0 \qquad \text{c.2}$$

$$\frac{\mathrm{d}y_{\mathrm{H_2}\_b}}{\mathrm{d}\bar{z}} = -k_{f_{H_2,m}} a_v \frac{L}{u_o}\left(y_{\mathrm{H_2}\_b} - y_{\mathrm{H_2}\_s}\right); \qquad \mathrm{y_{H_2\_b}}\big|_{\bar{\mathrm{z}}=0} = \mathrm{y_{H_2}}^0 \qquad \text{d.1}$$

$$k_{f_{H_2,m}} a_v\left(y_{\mathrm{H_2}\_b} - y_{\mathrm{H_2}\_s}\right) - \left(r_{\mathrm{CO}(f(y_s))}\right)\frac{\rho_b}{P_t} = 0 \qquad \text{d.2}$$

(A1.43)

To solve the previous system, it was not possible to simplify it as in previous models (in a function that only depends on the CO molar fraction), because for this particular case, the molar concentration of all specie in the catalyst surface (where reaction occurs) is not known (and are different from the concentrations in the bulk).

The numerical solution was obtained using the Matlab software package with the *ODE15s* function. However, the problem must be solved as a differential-algebraic equation system, so the problem has the form of $My' = f(t, y)$, where M is a singular constant mass matrix.

$$M = \begin{bmatrix} 1&0&0&0&0&0&0&0 \\ 0&1&0&0&0&0&0&0 \\ 0&0&1&0&0&0&0&0 \\ 0&0&0&1&0&0&0&0 \\ 0&0&0&0&0&0&0&0 \\ 0&0&0&0&0&0&0&0 \\ 0&0&0&0&0&0&0&0 \\ 0&0&0&0&0&0&0&0 \end{bmatrix}; y' = \begin{bmatrix} k_{f_{CO,m}} a_v \, L/u_0 \left(y_{\mathrm{CO_b}} - y_{\mathrm{CO}_s}\right) \\ k_{f_{H_2O,m}} a_v \, L/u_0 \left(y_{\mathrm{H_2O}_b} - y_{H_2O_s}\right) \\ k_{f_{CO_2,m}} a_v \, L/u_0 \left(y_{CO_{2\mathrm{b}}} - y_{CO_{2\mathrm{s}}}\right) \\ k_{f_{H_2,m}} a_v \, L/u_0 \left(y_{H_{2_b}} - y_{H_{2_s}}\right) \\ k_{f_{CO,m}} a_v \, L/u_0 \left(y_{\mathrm{CO_b}} - y_{\mathrm{CO}_s}\right) - \left(-r_{\mathrm{CO}(f(y_s))}\right) \rho_b / P_t \\ k_{f_{H_2O,m}} a_v \, L/u_0 \left(y_{\mathrm{H_2O}_b} - y_{H_2O_s}\right) - \left(-r_{\mathrm{CO}(f(y_s))}\right) \rho_b / P_t \\ k_{f_{CO_2,m}} a_v \, L/u_0 \left(y_{CO_{2\mathrm{b}}} - y_{CO_{2\mathrm{s}}}\right) - \left(r_{\mathrm{CO}(f(y_s))}\right) \rho_b / P_t \\ k_{f_{H_2,m}} a_v \, L/u_0 \left(y_{H_{2_b}} - y_{H_{2_s}}\right) - \left(r_{\mathrm{CO}(f(y_s))}\right) \rho_b / P_t \end{bmatrix}; y|_{\bar{z}=0} = \begin{bmatrix} {y_{\mathrm{CO}}}^0 \\ {y_{\mathrm{H_2O}}}^0 \\ {y_{\mathrm{CO_2}}}^0 \\ {y_{\mathrm{H_2}}}^0 \\ 0 \\ 0 \\ 0 \\ 0 \end{bmatrix}$$

The result of the solved differential-algebraic equations system was the molar fraction of each species along the axial position in each phase. Therefore, the conversion of the reactor can be calculated by:

$$X_{\mathrm{CO}} = \frac{{y_{\mathrm{CO}}}^0 - y_{\mathrm{CO}_b}\big|_{\bar{z}=1}}{{y_{\mathrm{CO}}}^0} \tag{A1.44}$$

MODEL 4

As for Model 2, in this model the molar flux has a term of contribution due to convection and another by diffusion. Therefore, substituting equation (A1.20) into equation (A1.35), the mass balance stands as:

For the Fluid:

$$u_o \frac{\mathrm{d}C_i}{\mathrm{d}z} - \varepsilon D_{ix} \frac{\mathrm{d}^2 C_i}{\mathrm{d}z^2} = -k_{f_{i,m}} a_v \left(C_{i\_b} - C_{i\_s}\right) \tag{A1.45}$$

For the Solid:

$$k_{f_{i,m}} a_v \left(C_{i\_b} - C_{i\_s}\right) = \left(\vartheta_i r_{\mathrm{CO}(f(C_s))}\right) \rho_b \tag{A1.46}$$

For ideal gases, substituting equation (A1.9) into (A1.45) and (A1.46):

For the Fluid:

$$\frac{u_o}{RT} \frac{\mathrm{d}p_i}{\mathrm{d}z} - \frac{\varepsilon D_{ix}}{RT} \frac{\mathrm{d}^2 p_i}{\mathrm{d}z^2} = -\frac{k_{f_{i,m}} a_v}{RT} \left(p_{i\_b} - p_{i\_s}\right) \tag{A1.47}$$

For the Solid:

$$\frac{k_{f_{i,m}} a_v}{RT}\left(p_{i\_b} - p_{i\_s}\right) = \left(\vartheta_i r_{\mathrm{CO}(f(P_s))}\right)\rho_b \tag{A1.48}$$

Introducing the dimensionless parameters $y_i = \frac{p_i}{P_t}$ (molar fraction) and; $\bar{z} = \frac{z}{L}$ (dimensionless length) in the previous equations:

For the Fluid:

$$\begin{aligned} &\frac{P_t}{RT}\frac{u_o}{L}\frac{\mathrm{d}y_i}{\mathrm{d}\bar{z}} - \frac{P_t}{RT}\frac{\varepsilon D_{ix}}{L^2}\frac{\mathrm{d}^2 y_i}{\mathrm{d}\bar{z}^2} = -k_{f_{i,m}} a_v \frac{P_t}{RT}\left(y_{i\_b} - y_{i\_s}\right) && \text{a} \\ &\frac{\mathrm{d}^2 y_i}{\mathrm{d}\bar{z}^2} = Pe_m \frac{\mathrm{d}y_i}{\mathrm{d}\bar{z}} + \frac{k_{f_{i,m}} a_v}{\varepsilon D_{ix}}\left(y_{i\_b} - y_{i\_s}\right) && \text{b} \end{aligned} \tag{A1.49}$$

For the Solid:

$$k_{f_{i,m}} a_v\left(y_{i\_b} - y_{i\_s}\right) - \left(\vartheta_i r_{\mathrm{CO}(f(y_s))}\right)\rho_b \frac{RT}{P_t} = 0 \tag{A1.50}$$

To solve the previous system of second-order differential equations (and algebraic equations), it is necessary to establish two boundary conditions. As above, the first conditions known is in the inlet of the reactor which is given by the Danckwert's BC, and the other can be deduced form the fact that there is no reaction at the outlet of the reactor, i.e.:

$$\begin{aligned} &y_{i\_b}\big|_{\bar{z}=0^-} = y_{i\_b}\big|_{\bar{z}=0^+} - \frac{1}{Pe_m}\frac{\mathrm{d}y_{i\_b}}{\mathrm{d}\bar{z}}\bigg|_{\bar{z}=0} && \text{a} \\ &\frac{\mathrm{d}y_{i\_b}}{\mathrm{d}\bar{z}}\bigg|_{\bar{z}=L} = 0 && \text{b} \end{aligned} \tag{A1.51}$$

Solution strategy for Model 4

Until now, this model was the more complex to solve, because it involves a second-order differential equation (which can be converted into two first-order differential equations) with an algebraic equation for each species involved in the reaction. Then, the solution becomes to be an integration of the strategy used in Models 3 and 2.

For the fluid phase the second-order differential equations were converted in first-order differential equations (as done in Model 2):

$$\begin{aligned} &\overline{y_{i\_b}} = \frac{\mathrm{d}y_{i\_b}}{\mathrm{d}\bar{z}} && \text{a} \\ &\frac{\mathrm{d}\overline{y_{i\_b}}}{\mathrm{d}\bar{z}} = Pe_m \frac{\mathrm{d}y_{i\_b}}{\mathrm{d}z} + \frac{k_{f_{i,m}} a_v}{\varepsilon D_{ix}} y_{i\_b} - y_{i\_s} && \text{b} \end{aligned} \tag{A1.52}$$

But, as in Model 4 the solid phase is considered separately, and the molar fraction in the catalyst surface is not known in advance. Then it is necessary to use the following equation (A1.53), which involves the reaction on the surface for each species:

$$k_{f_{i,m}} a_v \left(y_{i\_b} - y_{i\_s}\right) - \left(\vartheta_i r_{\mathrm{CO}(f(y_s))}\right) \rho_b \frac{RT}{P_t} = 0 \qquad \text{(A1.53)}$$

This system is composed by a total of 12 equations. It was not possible to simplify it for three equations that depend only on the molar fraction of CO (as in Model 2), because for this particular case the molar concentration of all specie on the catalyst surface (where reaction occurs) is not known (as in Model 3). The numerical solution was again obtained using the Matlab software package with the *ODE15s* function. However, the problem must be resolved as a differential-algebraic equation system, so the problem has the form of $My' = f(t, y)$, where M is a singular constant mass matrix. This particular case was solved using the function *ODE15s*, where it was assumed a molar fraction of each species at the reactor outlet, as first estimated it was assumed the value obtained for the same conditions in Model 3. For the iterative process the *fminsearch* function was used, in which the value obtained for the molar fraction at the inlet must satisfy the real value within a certain tolerance, i.e. $\sum\left|y_i{}^0 - yi0\mathrm{calculated}\right| < 10-10$.

Similar to Model 2, as the system was solved by end conditions, a change of variable was done, where $\bar{z}' = 1 - \bar{z}$. Then the system was solved in the boundary condition $\bar{z}' = 0$, that represents $\bar{z} = 1$. As before, the conversion of CO can be calculated by equation (A1.44).

A1.2 Membrane Reactor

When the reaction occurs inside a chamber in which the wall is a membrane, all conditions become different from the case of a traditional packed-bed reactor, principally by the fact that occurs simultaneously reaction and separation. Differently from the traditional reactor, in this section one type of model was employed; it was only considered a pseudo-homogeneous one-dimensional. The only component that permeates through the membrane was hydrogen. The principal assumptions in the model were:

1. Gases have an ideal behavior;
2. Isothermal operation;
3. Reaction takes place only on the catalyst surface;
4. Negligible mass and heat-transfer resistances within the catalyst particle (internal limitations);
5. The flux of hydrogen through the membrane was defined by Sieverts' law.

The mass balance for this case is as follows (for each species):

$$(\varepsilon_b^R A^R)\varphi_i^R|_z = (\varepsilon_b^R A^R)\varphi_i^R|_{z+dz} - \varepsilon_b^R 2\pi r^M F_i^M \mathrm{d}z + (\vartheta_i r_{\mathrm{CO}})\rho_p(1-\varepsilon_b^R)A^R \mathrm{d}z \quad \text{(A1.54)}$$

where ε_b^R represents the bed void fraction, A^R is the cross section area of the tubular reactor, ${\varphi_i}^R$ is the molar flow of species *i* per unit of surface area (or mass flux) in the retentate, r^M is the ratio of the tubular reactor, F_i^M is the permeation flow of species *i*.

In the limit, when $dz \to 0$, the following differential equation is obtained for each species *i*:

$$\varepsilon_b^R \frac{\mathrm{d}\varphi_i^R}{\mathrm{d}z} = -(\vartheta_i r_{\mathrm{CO}})\rho_p(1-\varepsilon) + \frac{\varepsilon_b^R 2\pi r^M F_i^M}{A^R} \quad \text{(A1.55)}$$

Considering an ideal model, where the flow has only a convective contribution:

$$\frac{\mathrm{d}(u_o C_i)}{\mathrm{d}z} = -(\vartheta_i r_{\mathrm{CO}})\rho_b + \frac{\varepsilon_b^R 2\pi r^M F_i^M}{A^R} \quad \text{(A1.56)}$$

In this case the superficial velocity is not constant along the bed-packed reactor, then:

$$u_o \frac{\mathrm{d}C_i}{\mathrm{d}z} + C_i \frac{\mathrm{d}u_o}{\mathrm{d}z} = -(\vartheta_i r_{\mathrm{CO}})\rho_b + \frac{\varepsilon_b^R 2\pi r^M F_i^M}{A^R} \quad \text{(A1.57)}$$

By the ideal gases law:

$$\frac{u_o}{RT}\frac{\mathrm{d}p_i}{\mathrm{d}z} + \frac{p_i}{RT}\frac{\mathrm{d}u_o}{\mathrm{d}z} = -(\vartheta_i r_{\mathrm{CO}})\rho_b + \frac{\varepsilon_b^R 2\pi r^M F_i^M}{A^R} \quad \text{(A1.58)}$$

Putting in evidence $\frac{dp_i}{dz}$

$$\frac{\mathrm{d}p_i}{\mathrm{d}z} = -\frac{p_i}{u_o}\frac{\mathrm{d}u_o}{\mathrm{d}z} - (\vartheta_i r_{\mathrm{CO}})\frac{\rho_b}{u_o} + \frac{\varepsilon_b^R 2\pi r^M F_i^M}{A^R}\frac{RT}{u_o} \quad \text{(A1.59)}$$

Now, the global balance for the retante:

$$\frac{\mathrm{d}P}{\mathrm{d}z} = -\frac{P}{u_o}\frac{\mathrm{d}u_o}{\mathrm{d}z} - \sum(\vartheta_i r_{\mathrm{CO}})\frac{\rho_b}{u_o} + \sum\frac{\varepsilon_b^R 2\pi r^M F_i^M}{A^R}\frac{RT}{u_o} \quad \text{(A1.60)}$$

By the supposition, the global balance looks like:

$$\frac{\mathrm{d}u_o}{\mathrm{d}z} = -\frac{\varepsilon_b^R 2\pi r^M F_{H_2}^M}{A^R}\frac{RT}{u_o} \quad \text{(A1.61)}$$

Appendix 2 – Physical Properties

In this appendix are presented the equations used to calculate the physical properties of the mixture/gases involved in the system.

Mixture viscosity

The viscosity of the gas phase mixtures are estimated according with the procedure proposed by Francesconi et al. (2007):

$$\mu = \sum_{i=1}^{Ns} \frac{y_i \mu_i}{\sum_{j=1}^{Ns} y_i \sqrt{M_j/M_i}} \tag{A2.1}$$

where μ is the viscosity of the mixture, y_i is the molar fraction of species *i*, μ_i is the viscosity of species *i* at a given temperature, and M_i is the corresponding molar weight. N_s stands for the number of components in the mixture.

The viscosity of each species was calculated by the following equation:

$$\mu_i = \frac{AT^B}{1 + C/T + D/T^2} \tag{A2.2}$$

where T is the absolute temperature and the constant A, B, C are in presented in Table A2.1. The viscosity is given in unit: $\mathrm{N{\cdot}s{\cdot}m^2}$

Table A2.1 Gas phase viscosity constant for selected species; (source Adams and Barton, 2009).

Species	A	B	C	D
CO	1.1127×10^{-6}	0.5338	94.6	0
CO_2	2.148×10^{-6}	0.46	290	0
H_2	1.797×10^{-7}	0.685	-0.59	140
H_2O	1.7096×10^{-8}	1.1146	0	0
N_2	6.5592×10^{-7}	0.6081	54.714	0

Diffusivities

The fluid dispersion coefficient in the axial direction was calculated by equation (A2.3) (Mendes et al., 2010a):

$$D_{ax} = 0.73 D_{\mathrm{CO},mix} + \frac{0.5\, u_o d_p}{1 + 9.49 \frac{D_{\mathrm{CO},mix}}{u_o d_p}} \tag{A2.3}$$

where $D_{CO,mix}$ is the bulk diffusivity of CO in the gas mixture, u_o is the superficial velocity and d_p is the particle diameter. The bulk diffusivity of CO was determined by the Wilke Method:

$$D_{\mathrm{CO},mix} = \frac{1 - y_{\mathrm{CO}}}{\sum_{i \neq \mathrm{CO}}^{n} \frac{y_i}{\frac{0.01013 T^{1.75} \left(\frac{1}{M_{\mathrm{CO}}} + \frac{1}{M_i}\right)^{0.5}}{P\left({v_{\mathrm{CO}}}^{1/3} + {v_i}^{1/3}\right)^2}}} \tag{A2.4}$$

where y_i represents the molar fraction of species *i*, T is the absolute temperature, M_i is the molar mass of species *i*, and v_i is diffusion volume of molecule *i*, and n is the number of components.

For the range of temperatures and pressures used in this study, gas phase diffusivities ($D_{i,j}$) were estimated through published correlations. Binary diffusivities for the species considered are estimated by the parameters presented in Table A2.2 (Adams and Barton, 2009) and the equations mentioned therein. This diffusivity was used in the calculation of mass transfer coefficient.

Table A2.2 Binary gas diffusivities for component pairs; source: (Adams and Barton, 2009).

Pair	A	B	C	D	E	F	eq
H_2-CO	15.39 x 10^{-3}	1.548	0.316 x 10^{8}	1	-2.80	1067	a
H_2-CO_2	3.14 x 10^{-5}	1.75	-	0	11.7	0	a
H_2-H_2O	-	1.020	-	-	-	-	b
H_2-N_2	6.007 x 10^{-3}	-0.99311	-	-	-	-	c
CO-CO_2	3.15 x 10^{-5}	1.57	-	0	113.6	0	a
CO-H_2O	0.187 x 10^{-5}	2.072	-	0	0	0	a
CO-N_2	0	0.322	-	-	-	-	c
CO_2-H_2O	9.24 x 10^{-5}	1.5	-	0	307.9	0	a
CO_2-N_2	3.15 x 10^{-5}	1.57	-	0	113.6	0	a
H_2O-N_2	0.187 x 10^{-5}	2.072	-	0	0	0	a

The equations referred in Table A2.2 are the following:

$$D_{i,j} = \frac{AT^B}{P} ln\left(\frac{C}{T}\right)^{-2D} exp\left(-\frac{E}{T} - \frac{F}{T^2}\right) \quad \text{a}$$

$$D_{i,j} = \frac{B}{P} \quad \text{b}$$

$$D_{i,j} = \frac{AT + B}{P} \quad \text{c}$$

It is worth to note that $D_{i,j} = D_{j,i}$. In the previous equations *P* represents the total pressure, and A, B, C, D, E and F are the parameters in Table A2.2, while a, b, c are the equation that it be used to calculated the binary gas diffusivities.

Mass transfer coefficients

The mass transfer coefficients between the bulk gas phase and the catalyst surface can be estimated by a correlation expressed in terms of the Colburn factor analogy (*Perry's chemical engineers' handbook*, 1997; Mendes et al., 2010a):

$$k_{f_{i,m}} = 0.4548\left(\frac{\rho M D_{i,m}}{\mu}\right)^{2/3}\left(\frac{G}{\rho M \varepsilon}\right)\left(\frac{\mu}{d_p G}\right)^{0.4069} \quad \text{(A2.5)}$$

where ρ is the molar density of the mixture, M is the mole-averaged molecular weight, μ is the viscosity of the mixture, ε is the void bed, d_p is the catalyst diameter and G the molar flux.